In Situ Studies of Surface Mobility on Noble Metal Model Catalysts Using STM and XPS at Ambient Pressure

by

Derek Robert Butcher

A dissertation submitted in partial satisfaction of the

Requirements for the degree of

Doctor of Philosophy

in

Chemistry

in the

Graduate Division

of the

University of California, Berkeley

Committee in charge:

Professor Gabor A. Somorjai, Chair
Professor Herbert L. Strauss
Professor Kyriakos Komvopoulos

Fall 2010

In Situ Studies of Surface Mobility on Noble Metal Model Catalysts Using STM and XPS at Ambient Pressure

Copyright © 2010

by

D. R. Butcher

Abstract

In Situ Studies of Surface Mobility on Noble Metal Model Catalysts Using STM and XPS at Ambient Pressure

by

Derek Robert Butcher

Doctor of Philosophy in Chemistry

University of California, Berkeley

Professor Gabor A. Somorjai, Chair
Professor Herbert L. Strauss
Professor Kyriakos Komvopoulos

High Pressure Scanning Tunneling Microscopy (HP-STM) and Ambient Pressure X-ray Photoelectron Spectroscopy were used to study the structural properties and catalytic behavior of noble metal surfaces at high pressure. HP-STM was used to study the structural rearrangement of the top most atomic surface layer of the metal surfaces in response to changes in gas pressure and reactive conditions. AP-XPS was applied to single crystal and nanoparticle systems to monitor changes in the chemical composition of the surface layer in response to changing gas conditions.

STM studies on the Pt(100) crystal face showed the lifting of the Pt(100)-hex surface reconstruction in the presence of CO, H_2, and Benzene. The gas adsorption and subsequent charge transfer relieves the surface strain caused by the low coordination number of the (100) surface atoms allowing the formation of a (1x1) surface structure commensurate with the bulk terminated crystal structure. The surface phase change causes a transformation of the surface layer from hexagonal packing geometry to a four-fold symmetric surface which is rich in atomic defects. Lifting the hex reconstruction at room temperature resulted in a surface structure decorated with 2-3 nm Pt adatom islands with a high density of step edge sites. Annealing the surface at a modest temperature (150 ˚C) in the presence of a high pressure of CO or H_2 increased the surface diffusion of the Pt atoms causing the adatom islands to aggregate reducing the surface concentration of low coordination defect sites.

Ethylene hydrogenation was studied on the Pt(100) surface using HP-STM. At low pressure, the lifting of the hex reconstruction was observed in the STM images. Increasing the ethylene pressure to 1 Torr, was found to regenerate the hexagonally symmetric reconstructed phase. At room temperature ethylene undergoes a structural rearrangement to form ethylidyne.

Ethylidyne preferentially binds at the three-fold hollow sites, which are present on the Pt(100) hex reconstructed phase, but not the (100)-(1x1) surface. The increase in ethylene pressure caused the adsorbate interactions to dominate the crystal morphology and imposed a surface layer structure that matched the ethylidyne binding geometry. The STM results also showed that the surface was reversibly deformed during imaging due to increases in Pt mobility at high pressure.

The size dependence on the activity and surface chemistry of Rh nanoparticles was studied using AP-XPS. The activity was found to increase with particle size. The XPS spectra show that in reaction conditions the particle surface has an oxide layer which is chemically distinct from the surface structure formed by heating in oxygen alone. This surface oxide which is stabilized in the catalytically active CO oxidation conditions was found to be more prevalent on the smaller nanoparticles.

The reaction-induced surface segregation behavior of bimetallic noble metal nanoparticles was observed with APXPS. Monodisperse 15 nm RhPd and PdPt nanoparticles were synthesized with well controlled Rh/Pd and Pd/Pt compositions. *In-situ* XPS studies showed that at 300 ˚C in the presence of an oxidizing environment (100 mTorr NO or O_2) the surface concentration of the more easily oxidized element (Rh in RhPd and Pd in PdPt) was increased. Switching the gas environment to more reducing conditions (100 mTorr NO and 100 mTorr CO) caused the surface enrichment of the element with the lowest surface energy in its metallic state. Using *in-situ* characterization, the redox chemistry and the surface composition of bimetallic nanoparticle samples were monitored in reactive conditions. The particle surfaces were shown to reversibly restructure in response to the gas environment at high temperature.

The oxidation behavior of the Pt(110) surface was studied using surface sensitive *in-situ* characterization by APXPS and STM. In the presence of 500 mTorr O_2 and temperatures between 25 and 200 ˚C, subsurface oxygen was detected in the surface layer. STM images show that these conditions were found to cause a roughened surface decorated with 1 nm islands. The formation of this surface oxide is a high pressure phenomenon and was not detected in 50 mTorr O_2. After forming the surface oxide at high pressure, its chemical activity was measured through the reaction with CO at low pressure while continuously monitoring the oxygen species with XPS. The subsurface oxygen was removed by CO oxidation at a comparable rate to the chemisorbed oxygen at 2 ˚C. Repeating the experiment at -3 ˚C reduced the reaction rate, but not the relative activity of the two chemical species suggesting that neither species is significantly more active for the CO oxidation reaction.

These studies use molecular level surface characterization in the presence of gases to show the structural changes induced by gas adsorption at high pressure. The *in-situ* results show that both the adsorbed gases and the metal surface are dynamic layers which change in structure in response to changing reaction environments.

Table of Contents

List of Figures

Acknowledgements

I would first like to thank my Advisor Professor Gabor Somorjai for allowing me this opportunity to work in his research group. He has been a constant source of advice and encouragement and I have learned a great deal from him in my time here. It has been both tremendously rewarding and a privilege to work in his group. I would also like to thank Miquel Salmeron for all his advice and help as well as welcoming me to work alongside his research group.

I am grateful for the wonderful community of friends and colleagues that I have worked with in my time in Berkeley. I owe much of what I have learned during graduate school to discussions with those who generously shared their time. I would like to thank all the members of the Somorjai and Salmeron research groups. Specifically, I would like to thank Max Montano for his patience as he worked with me in my first year. Chris Kliewer, Russ Renzas, George Holinga, and I began graduate school in the fall of 2005 and their friendships over the years have helped make graduate school a period that I am reluctant to see end. I would also like to thank Mike Grass, Feng Tao, and Zhi Liu, who have been great to work with as well as good friends.

This work was supported by the Director, Office of Science, Office of Basic Energy Sciences, of the U.S. Department of Energy under Contract DE-AC02-05CH11231.

Chapter 1. Introduction

Global energy use is arguably the most pressing concern facing society in the 21st century. The accumulation of greenhouse gases from the use of fossil fuels is changing the composition of the earth's atmosphere with unknown repercussions to the global climate. Additionally, the political and economic power balances in modern society are inextricably tied to energy. According to a 2002 DOE report, the Petroleum and Coal Products industry and the Chemicals Industry are the largest energy consumers in the U.S. [1]. Chemical reactions on metal catalysts are fundamental to these industries and as such constitute an important component of any effort to transition to sustainable energy practices. Additionally, improvements in catalytic activity and selectivity can increase energy efficiency and reduce the production of unwanted chemical byproducts with economic and environmental benefits. The widespread use by the energy and chemicals industries of catalytic processes occurring on metal surfaces at high pressures and temperatures motivates studies aimed at improving the understanding of these processes on a fundamental level. This thesis is comprised of studies of the dynamic processes occurring on well-defined catalytically active noble metal surfaces using molecular level characterization techniques chosen for their ability to study changes in surface behavior with increasing pressure and temperature.

Surface science is by nature an interdisciplinary field due to the broad interest in understanding and engineering the properties of materials on the nanometer scale including, but by no means limited to, heterogeneous catalysts. The increase in surface to volume ratio at these small sizes forces a larger proportion of the material to be confined to the interface causing the surface properties to dominate the behavior of the materials. The study of interfaces on the molecular level presents a number of experimental difficulties. This has lead to the use of a wide array of surface specific experimental techniques. The experimental limitations of surface specific techniques often necessitate the use of simplified model systems in order to allow accurate characterization. The choice of model systems involves striking a balance between choosing a system complex enough to exhibit interesting behavior yet simple enough to allow an accurate interpretation of the results.

Our approach uses model systems of varying complexity to study surface behavior and catalytic properties. This work looks at small molecule gas phase reactions on noble metal single crystals and nanoparticles to understand the effect of gases on surface structure and catalytic activity. Single crystal faces are utilized to simplify the catalyst structure isolating the study to only the behavior occurring on certain site geometries.

1.1 Single Crystal Model Catalysts

Single crystals are valuable model catalyst surfaces. The single crystal faces are prepared such that the sample has large terraces with minimal surface contaminants. The surface structure of a well prepared low Miller index crystal face is composed of atomically flat terraces separated

by steps (Figure 1.1). The highly ordered surface packing geometry allows the detection of small changes in surface structure. Figure 1.1 shows a diagram of the (111), (100), and (110) surfaces of the face centered cubic (fcc) crystal. The three-fold symmetry of the (111) face is the most densely packed and consequently most stable surface structure. The four-fold symmetric (100) face is a more open surface with a higher coordination number. The surface atoms of the fcc(110) plane have the lowest coordination number of the low Miller index fcc surfaces. Studies of the differences in the surface behavior of the different crystal orientations are used to understand the effects of surface coordination and binding geometry. The role of defect sites (steps and kinks) can also be studied using stepped crystal faces. Since the coordination chemistry and electronic structure are dependent on the geometry of the surface site, single crystals are well defined system to study the effects of these properties on the chemical reactivity and surface dynamics.

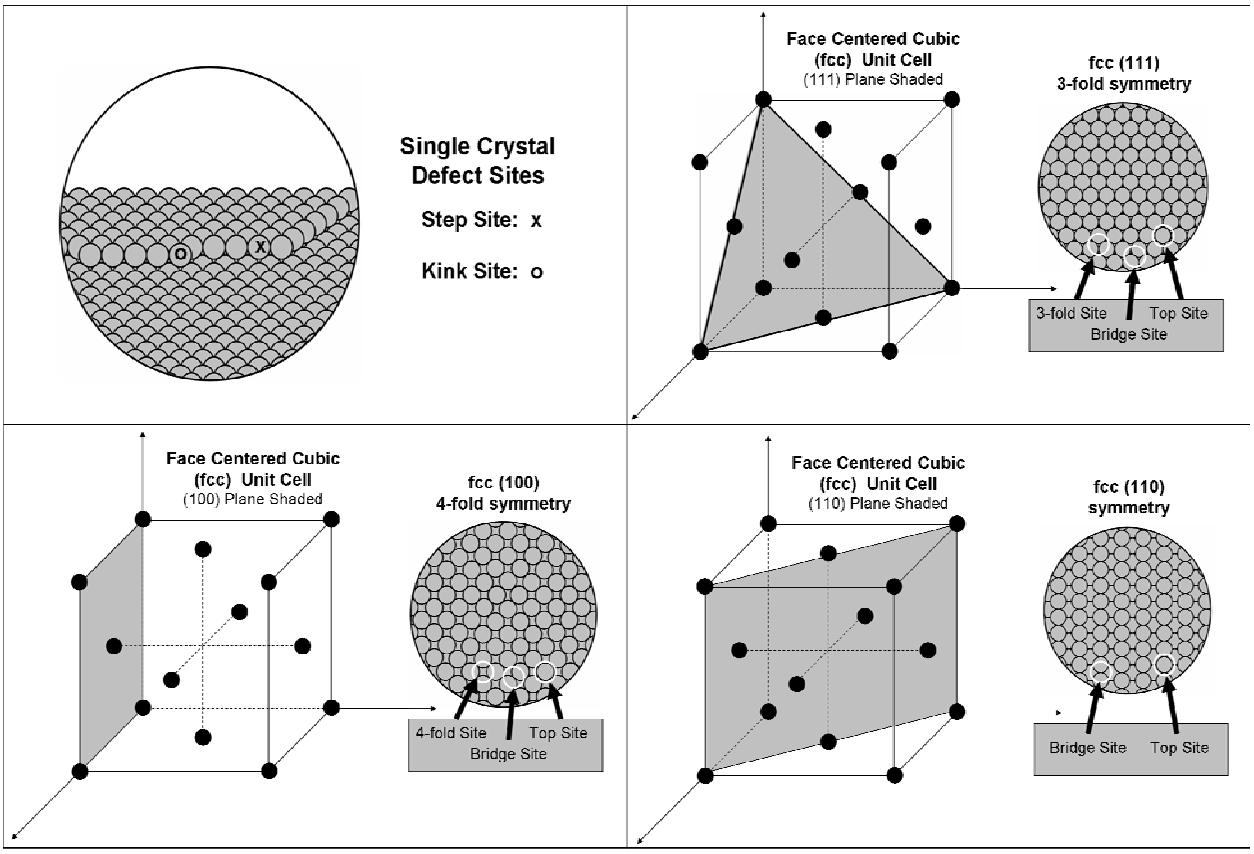

Figure 1.1: Diagrams of flat terraces separated by a singe atom step and the crystal structure of the face centered cubic (111), (100), and (110) surfaces.

1.2 Nanoparticle Model Catalysts

In order to efficiently use catalytic materials, which are often expensive rare earth elements, industrial catalysts relies on high dispersion catalysts with large surface to volume ratios. Figure 1.2 plots the fraction of the atoms on the top surface layer as a function of particle

diameter. These materials have high percentages of step edge and kink sites with low energetic barriers to structural rearrangements. Additionally, the size and composition of the particles affects the electronic properties and catalytic behavior. Colloidal techniques have been developed which can controllably synthesize uniform particles with high reproducibility in order to systematically study the effect of particle size and composition on the chemical properties of the surface.

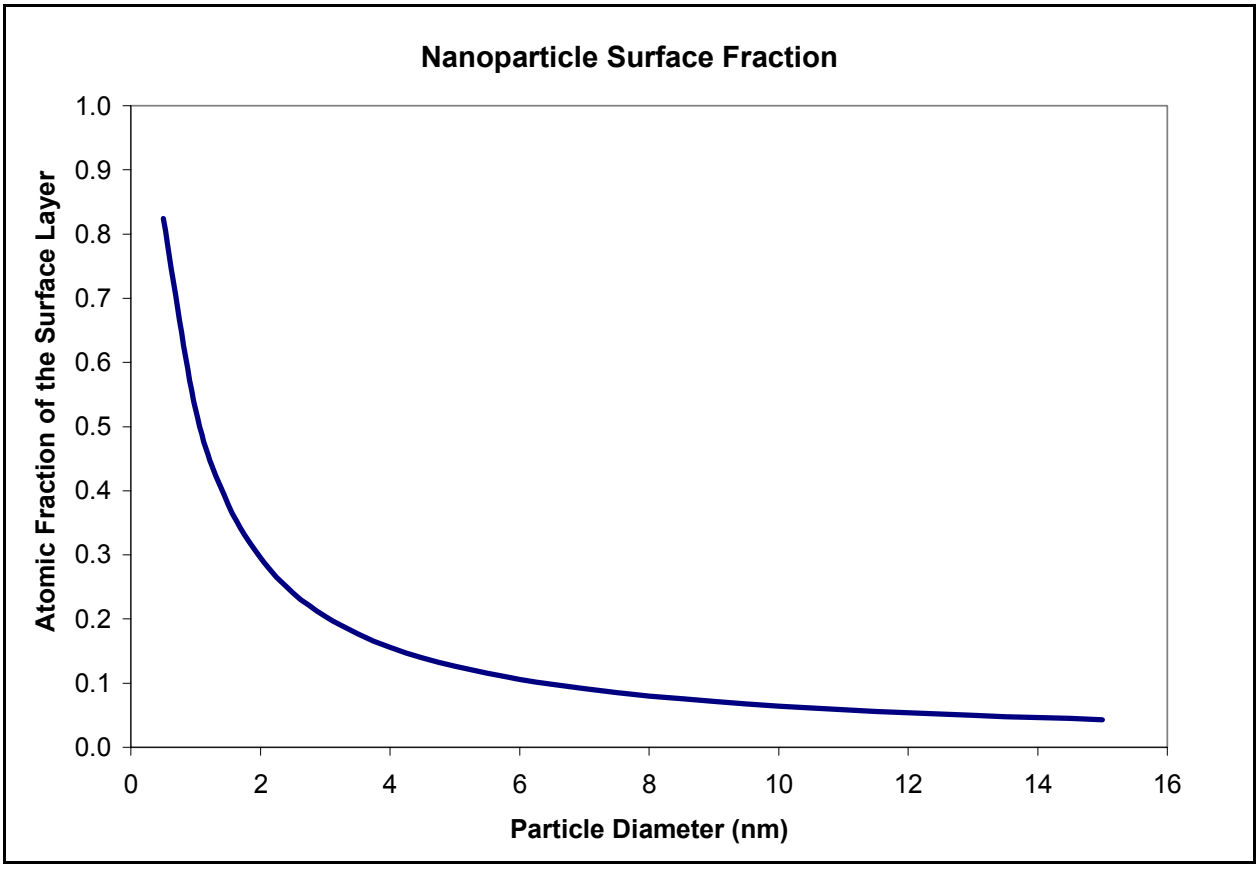

Figure 1.2 The fraction of atoms located in the outermost surface layer as a function of nanoparticle radius for Pt particles assuming a thickness of 0.22 nm per atomic layer.

1.3 *In-Situ* Catalytic Surface Characterization at High Pressure

Heterogeneous catalysis is a dynamic process occurring on the outermost atomic layer of the surface. Under reaction conditions at high temperature and pressure, gas phase reactants and products adsorb, desorb, and defuse across the surface and the metal atoms themselves undergo structural rearrangement. There are experimental obstacles to characterizing the catalyst during reaction conditions. The reaction occurs on the surface, so catalyst characterization is best done with surface sensitive techniques. Molecules undergo chemical rearrangements on the surface, so the adsorbate layer can be made up of a mixture of reactants, intermediates, spectator species, and products. The active intermediates are often a minority species on the surface. This thesis focuses on catalytic surface studies at high pressure using two molecular level *in-situ* techniques:

High Pressure Scanning Tunneling Microscopy (HP-STM) and Ambient Pressure X-ray Photoelectron Spectroscopy (APXPS). STM images the surface topography with atomic resolution and can operate at high pressure. APXPS is a surface specific technique that allows chemical analysis of the surface layer up to a maximum operating pressure of ~5 Torr. These studies investigate the dynamics of catalytic surfaces on the molecular level at high pressure.

References

1. *2002 Manufacturing Energy Data Tables.* [cited; Available from: http://www.eia.doe.gov/emeu/mecs/mecs2002/data02/shelltables.html.

Chapter 2. Theoretical Background

2.1 Surface Processes in Catalysis

A catalyst is material that lowers the activation energy for a reaction without being consumed in the process. In gas phase heterogeneous catalysis, the reactants are gas phase molecules that adsorb on the solid catalyst surface and undergo a chemical reaction with the product molecules then desorbing and returning to the gas phase. This reaction can occur between the adsorbate species or between an adsorbate and a gas phase molecule. The catalyst must have the right chemical properties such that it binds strongly enough to the adsorbates to facilitate the reaction yet weakly enough to allow the product molecule to desorb and free the active site for further reactions.

Adsorption is an exothermic process where the gas phase molecule collides with the surface and binds. When the adsorbate species binds through weak Van der Waals or electrostatic forces this is called physisorption. Chemisorption occurs when the adsorbate forms a chemical bond on the surface. A species can adsorb molecularly binding to the surface intact or dissociatively decomposing on the surface and forming multiple adsorbates. The likelihood for adsorption is quantified the sticking coefficient defined as the probability of an incident particle to adsorb on a clean surface. In the presence of a constant gas pressure, the sticking probability will decrease as the surface becomes saturated and reaches a constant surface coverage when the rate of adsorption becomes equal to the rate of desorption.

After adsorbing on the catalyst surface adsorbates can react either with other adsorbates or with gas phase molecules if there is sufficient energy to overcome the activation barrier. The product molecule formed in the process can then desorb freeing the active site for future reactions. An adsorbate that binds to a catalytic site and prevents it from hosting a reaction is called a catalytic poison. In order to understand the adsorbed structure, we use *in-situ* characterization of the surface layer. Many industrial processes operate at high temperature and pressure. The high temperature allows activation barriers to be overcome and the high pressure keeps a constant flux of reactant molecules incident on the surface and also may play a role in the excitation of surface processes through collisional energy transfer. This thesis involves the molecular level study of the changes in surface structure and dynamics measured *in-situ* at high pressure.

2.2 Scanning Tunneling Microscopy Basics

Scanning tunneling microscopy (STM) is a remarkable imaging technique capable of atomic resolution on conducive surfaces that was invented by Binnig and Rohrer in the early1980s [1]. A sharp conductive tip is brought within a few Angstroms of a conductive surface using piezoelectric devices to control the motion of the tip. A bias applied between the

tip and the sample induces a tunneling current, which is exponentially dependent on the tip sample distance. This strong distance dependence on the tip sample distance causes the tunneling current to be highly localized to the area on the surface nearest to the apex of the tip. Using an electrical feedback loop, the tip sample distance can be precisely controlled by the piezo tube to maintain a constant tunneling current. Typically STM operates at voltages from 0.1-2 V and 0.1-0.5 nA and tip-sample distances of 1-5 Angstroms. By rastering the tip back and forth across the surface and sweeping out an area, an image can be generating by recording the voltage that was applied to the Z (vertical) piezo in order to maintain a constant tunneling current. The resulting image is similar to a topographic map of the surface, but the signal is representative of the tip-sample tunneling probability and not the true topography.

STM uses electron tunneling to image surfaces with atomic resolution. Tunneling is a quantum mechanical phenomenon. Classically, a particle will not pass through a potential barrier unless its energy is larger than the barrier height. Quantum mechanically, the wave function of the particle decays exponentially within the barrier. As a result the particle can pass through the barrier. The transmission probability (P) of a particle of mass m with an energy less than the barrier height (Φ) decays exponentially as a function of barrier distance (d).

$$P \quad e^{\frac{-2d\sqrt{2m\Phi}}{\hbar}}$$

The high resolution of STM results from the exponential dependence of tunneling on barrier distance. The transmission probability of an electron decreases by more than an order of magnitude when the barrier distance is increased by an angstrom.

When the STM tip is within a few Å of the sample surface, applying a bias (typically 0.1-1V) induces a tunneling current between the tip and the sample. STM typically operates using tunneling currents in the 0.1-1 nA range. The tunneling current is exponentially dependent on the tip-sample distance causing the signal to be highly weighted to the closest point between the tip and the sample. By using a sharp STM tip with a single apex protruding closest to the surface, the tunneling current is representative of the electronic environment in close proximity to that point.

Tersoff and Hamann showed that the STM signal probes the Local Density of States (LDOS) of the surface at the position of the tip [2]. In constant current mode, piezoelectric motors adjust the tip-sample distance using an electronic feedback loop so that the tunneling current remains constant. As the tip is moved across the surface sweeping out an area the signal sent to the piezo is used to map the LDOS of the surface. The resulting images can have resolution on the order of tens of picometers depending on the sharpness of the tip, the stability of the tunnel junction, and the noise level of the instrument.

2.3 X-ray Photoelectron Spectroscopy (XPS) Basics

In XPS, and X-ray photon excites a core level electron that is ejected it from the surface. An energy analyzer measures the flux and the kinetic energy of the resulting photoelectron. The

initial photon energy (hν) is equal to the sum of the kinetic energy of the electron (KE), the binding energy of the core state (BE), and the work function of the detector (φ).

$h\nu = KE + BE + \varphi$

The binding energy of the electron is sensitive to the chemical state of the atom showing detectable chemical shifts on the order of a 0.05-1 meV depending on the local environment. The surface sensitivity of XPS results from the small mean free path of electrons in solids, causing only the photoelectrons at the top few atomic layers of the surface to escape the material before being scattered. The detector is kept at low pressure to reduce the scattering of the photoelectrons in the gas phase. XPS is a powerful surface characterization technique that can quantitatively measure the chemical composition of the surface.

2.4 References

1. Binnig, G., et al., *Surface Studies by Scanning Tunneling Microscopy.* Physical Review Letters, 1982. **49**(1): p. 57.
2. Tersoff, J. and D.R. Hamann, *Theory of the scanning tunneling microscope.* Physical Review B, 1985. **31**(2): p. 805.

Chapter 3. Experimental Techniques

3.1 UHV System

Clean metal surfaces are terminated by undercoordinated atoms which are often susceptible to gas phase adsorption at room temperature. For example, O_2, CO, H_2, NO, and most unsaturated hydrocarbons will readily adsorb on Pt, Rh, and Pd surfaces at room temperature [1]. Ultrahigh Vacuum (UHV) technology allows the preparation of atomically clean surfaces. At atmospheric pressure and room temperature, the mean free path of an oxygen molecule is ~100 nm. Since the mean free path is inversely proportional to pressure, reducing the pressure to 10^{-10} Torr, the base pressure of the apparatus used in our studies, increases the mean free path to $\sim 10^5$ m, which ensures that the gas phase collisions in the chamber are negligible. An important factor in UHV surface science studies is the collision frequency of gas phase particles, which scales linearly with pressure. At 10^{-10} Torr pressure, the average collision frequency is $\sim 10^{-4}$ collisions per surface atom per second or, assuming a sticking coefficient of 1, $\sim 10^4$ seconds to build up one monolayer of adsorbates on the surface. This allows enough time to prepare and maintain reproducible atomically clean surfaces.

The experimental apparatus used in the *in-situ* Scanning Tunneling Microscopy (STM) studies has been described previously [2]. It uses a two chamber design with a sample preparation chamber and a high pressure chamber housing the STM. The sample preparation chamber is equipped with an electron beam heater for crystal heating, an ion gun for Argon sputtering, quadrupole mass spectrometer for gas analysis, and an Auger Electron Spectrometer to analyze the elemental composition of the sample surface. The STM chamber houses an RHK VT-UHV300 STM with a light bulb for heating in the presence of reactant gases and a manifold to introduce gases. Each chamber has a dedicated Ion Pump as well as a shared turbomolecular pump backed by a mechanical pump allowing a base pressure of $\sim 10^{-10}$ Torr. The samples holders and tip exchangers can be moved in and out of the system as well as between the two chambers with a magnetic transfer arm and a wobble stick in the STM chamber. The entire chamber is mounted on a wooden frame and floats on air legs (Newport Laminar Flow Isolators, I-2000 series) for vibrational damping.

During reaction studies, the clean sample is transferred to the STM chamber which is isolated and filled with the desired gas composition. During STM measurement, the turbo pump, and ion gauges are turned off to reduce vibration and electrical noise and the mechanical pump is both turned off and disconnected from the system. During experiments involving sample heating, a manipulator allows the light bulb to be placed directly underneath the sample and is powered by a DC current while a cooling loop connected to the STM stage with a copper braid actively cools with cooling water or liquid nitrogen. The gas composition of the high pressure cell can be measured by a leak valve connecting it to the sample prep chamber for Mass Spec analysis. Additionally the STM tip material is selected such that it is compatible with the reaction gas mixture.

The Ambient Pressure X-ray Photoelectron Spectroscopy Studies were conducted on the three end stations at beamlines 9.3.2 [3, 4] and 11.0.2 [5] at the Advanced Light Source (ALS) at the Lawrence Berkeley National Laboratory (LBNL).

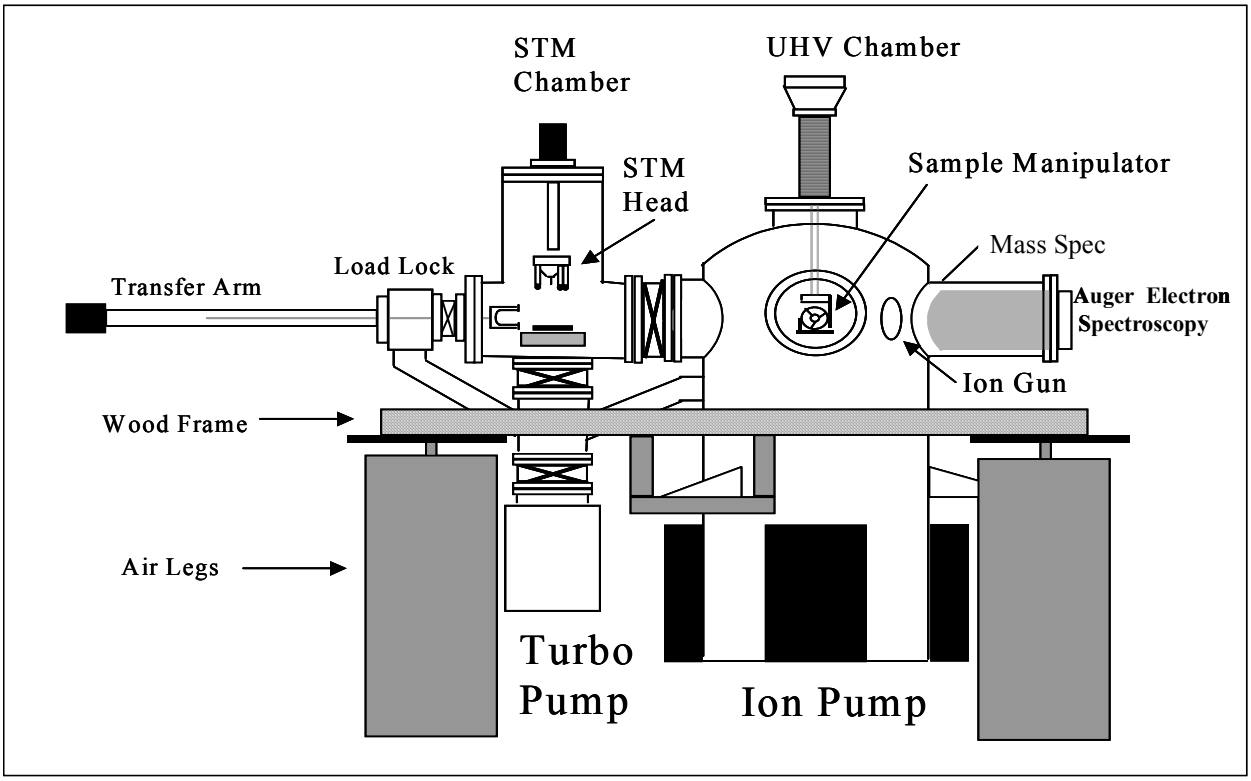

Figure 3.1 Schematic of the high pressure STM apparatus [2].

3.2 Sample cleaning

The single crystal samples are prepared through cycles of Ar^+ sputtering and high temperature annealing. Ion sputtering (Varian ion bombardment gun 981-2043) uses a low pressure (~10^{-5} Torr) of Argon. The argon is ionized and accelerated at the sample with a high voltage to energies typically in the range of 0.5-2 keV at a current of ~20 mA. Since chemical bond energies are on the order of eV, each collision is a destructive event expelling atoms from the surface layer including impurities adsorbed on the surface and exposing a fresh chemically pure surface characteristic of the single crystal. However the surface will be roughened and defect-rich from the ion bombardment. In order to heal these defects, the crystal is annealed at a high temperature (~0.5 $T_{melting\ point}$) using electron beam heating. The high temperature annealing allows the surface atoms to have sufficient energy to overcome the activation energy to diffusion allowing the defects to be healed. The crystal is then slowly cooled (~1 $^{\circ}C\ sec^{-1}$) to ambient temperature. The rate of cooling affects the surface structure with faster cooling rates resulting in smaller terraces and a higher step density. The terraces have the atomic packing geometry of

the oriented single crystal face with the exception of those surfaces which spontaneously reconstruct. The electron beam heater uses a Tungsten filament which has been doped with Thorium to decrease the work function. The wire is heated with a current (2-3 A) giving the valence electrons sufficient kinetic energy to overcome the work function and be accelerated to the sample by a high voltage (1-1.5 kV) bias. The filament is located directly behind the back side of the crystal. In order to allow the temperature to be controlled accurately and minimize the temperature of the sample holder, the sample holder is kept in contact with a copper cooling block cooled by liquid nitrogen. The sample temperature is monitored by a k-type thermocouple which is spot welded to or in physical contact with the crystal face. To help remove carbon impurities on the surface, the sample can be annealed to 500 ˚C in the presence of 10^{-7} Torr O_2. Sample preparation uses cycles of sputtering, oxygen annealing, and high temperature annealing in UHV, until a clean surface is produced.

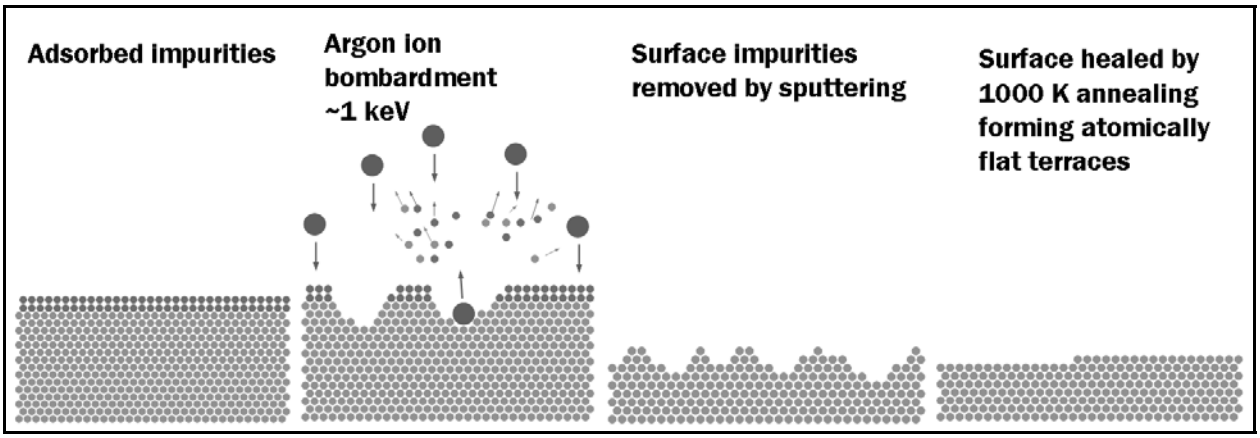

Figure 3.2 Single crystal cleaning. Surface impurities are removed through bombardment of the surface with 1 keV Ar ions producing a roughened, defect-rich surface. High temperature annealing heals the defects producing large flat terraces characteristic of the sample.

3.3 Mass Spectrometry

The Sample preparation chamber is equipped with a Stanford Research Systems RGA 200 mass spectrometer for gas phase analysis. The mass spec uses a filament to ionize gas particles which then pass through a quadrupole mass filter followed by a detector which measures a current from the ions of the specific mass that are selected by the filter. The quadrupole filter uses an RF potential applied to the four rods of the quadrupole to select masses. At a given frequency of oscillation, only a certain M/Z will pass through the filter without colliding with one of the rods and losing its charge. The detector can then measure the current at a given M/Z ratio to quantify the gas composition. The ionization of the gas particles causes molecules to fragment in statistically reproducible mass ratios which can be used to identify the gas composition.

3.4 Auger Electron Spectroscopy (AES)

The elemental composition of the sample surface can be measured using Auger Electron Spectroscopy (Varian) in high vacuum. A high energy (3 keV) electron beam is used to eject core level electrons on the sample resulting in an energetically unstable core hole (Figure 3.3). In a two electron process, the core hole can be filled by the transition of an outer shell electron with the difference in energy transferred to another outer shell electron which is ejected from the atom. The kinetic energy of this Auger electron is not dependent on the energy of the initial high voltage electron source, but rather the difference in energy between the core electron levels of the atom which are specific to the element. The surface specificity of AES is a result of the finite mean free paths of electrons in solids. Only electrons in the top few atomic layers can escape the surface before scattering and de-excitation.

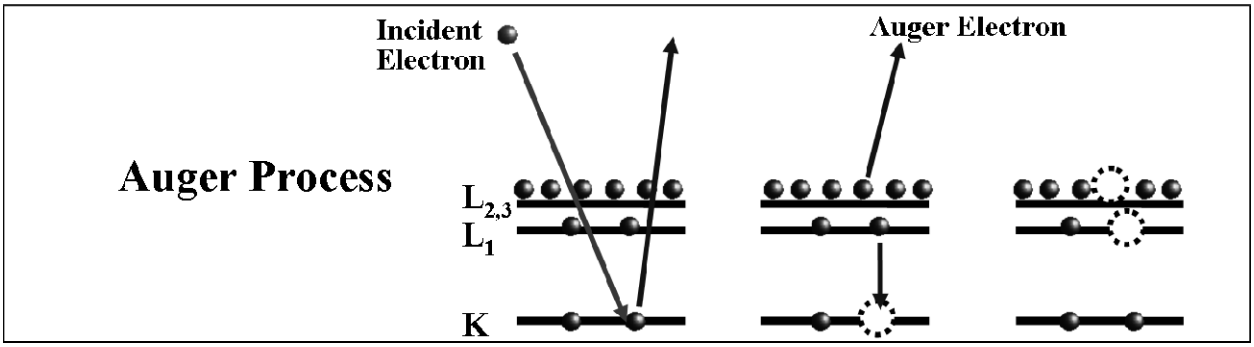

Figure 3.3 Auger process: electron beam causes the ejection of a core electron followed by two electron process where one electron fills the core hole transferring the energy from the relaxation event to the Auger electron which is ejected from the atom.

The emitted electrons pass through a cylindrical mirror analyzer (CMA) and are detected by a photomultiplier tube that amplifies the signal. The CMA is an energy filter that uses an electric field to deflect electrons of a given energy to the detector. A spectrum is produced using the CMA to scan through the desired energy range. Figure 3.4 shows typical Pt Auger spectra before and after crystal cleaning, which removes the carbon impurities from the surface.

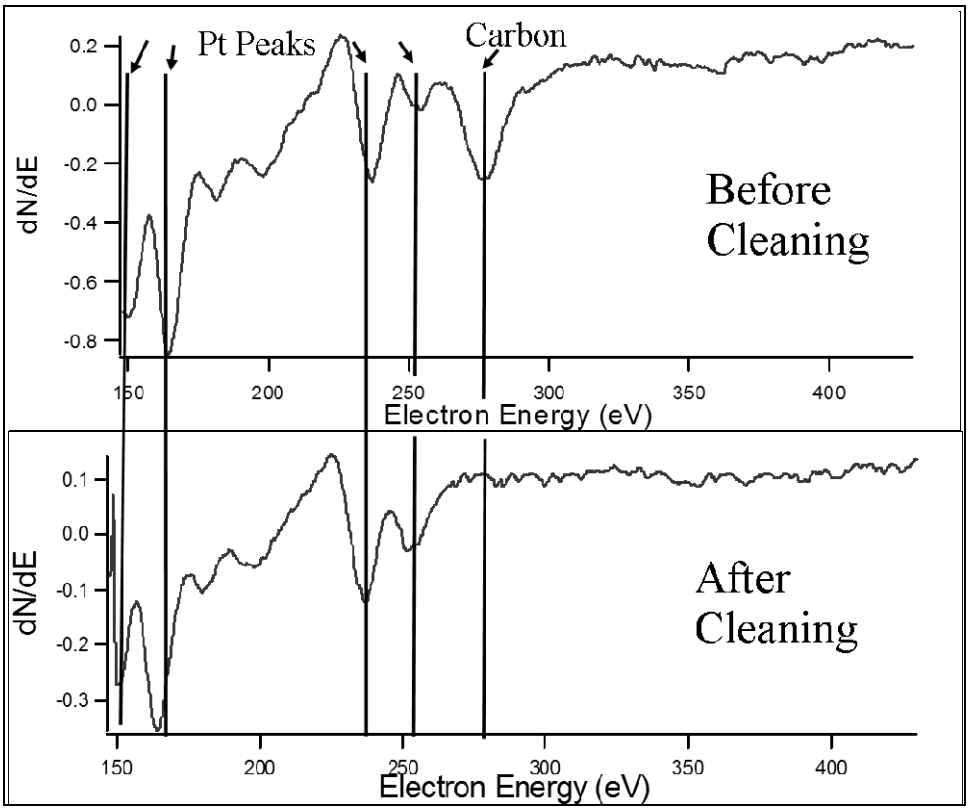

Figure 3.4 Auger spectra of a Pt(111) surface before and after crystal cleaning showing the reduction of the carbon peak after the removal of surface impurities.

3.5 *STM Design*

The STM chamber is equipped with an RHK VT-UHV300 STM. The STM scan head has a "beetle" design pictured in Figure 3.5. The scan head contains 4 piezoelectric tubes. The three outer piezo tubes are terminated by sapphire beads and form the legs of a tripod that stand on the sample holder which is machined with ramps. The central piezo tube holds the STM tip. The microscope approaches the STM tip to the sample surface using the three piezo legs of the tripod to "walk" the scan head down the ramps of the sample holder until a tunneling current is detected between the tip and the sample. Since the vertical displacement of the scan head is limited to the height difference of the ramps (1 mm), the STM tip must be mounted at the proper length within 1 mm to approach the surface without physically contacting it. The coarse motion of the scan head in the x, y, and z directions is performed by the walking motion of the tripod legs, but the fine motion (including image scanning) uses the deflection of the central scan tube and has a maximum range of 500 nm before the coarse motion must be used.

The STM stage rests on flexible Viton loops for vibration damping and holds the sample holder securely with leaf springs. A ceramic feedthrough contains the thermocouple connections to measure the temperature of the sample. A quartz projector light bulb used for crystal heating

is mounted on a manipulator in the center of the sample stage. The light bulb allows the sample to be heated in the presence of reaction gases.

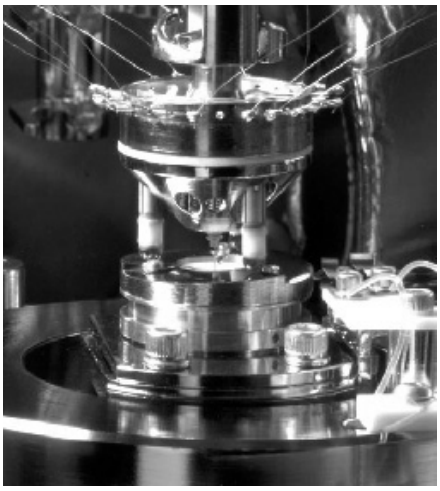

Figure 3.5. RHK VT-UHV300 STM scan head. The scan head has three outer legs that rest on ramps machined into the sample holder. In order for the STM tip to approach the sample, the piezoelectric legs use slip-stick motion to walk down the ramps.

3.6 Sample Transfer

The sample holder and tip exchanger can be moved throughout the system with a magnetic transfer arm and a wobble stick mounted on the STM chamber. Both have forks that slide into grooves machined into the side of the sample holder and tip exchanger. Each has two sets of grooves so that the holders can be passed from one set of forks to another. The transfer arm can move between the load-lock, the STM chamber, and the sample preparation chamber (Figure 3.1). The wobble stick is a hand held manipulator on a flexible bellows that can be used to move the sample holder between the transfer arm and the STM stage.

3.7 Sample Holder

Figure 3.6 shows a diagram of the sample holder. The sample holder has a face plate machined with three ramps 1 mm in height. The STM scan head rests on the face plate and uses the ramps for coarse approach. The main body of the sample holder has grooves allowing it to be held securely by the transfer arm, wobble stick, STM sample stage, and preparation stage manipulator. The interior of the holder is hollow exposing the underside of the sample for efficient heating by the electron beam heater in the preparation chamber and the quartz light bulb in the STM chamber. A ceramic feedthrough passing through the side of the holder houses the two thermocouple wires which are spot welded together with the junction either spot welded directly to the side of the sample or held in contact with the sample by one of the Tantalum clamps. The opposite ends of the of the thermocouple wires extend out from the side of the crystal and are bent in a geometry that they make good electrical contact in both the STM

chamber and the preparation chamber allowing the sample temperature to be measured in both locations. Tantalum strips on the face plate are bent into clips that hold the sample firmly in place. The majority of the sample holder is made of Molybdenum or Tantalum which are inactive for the reactions in these studies.

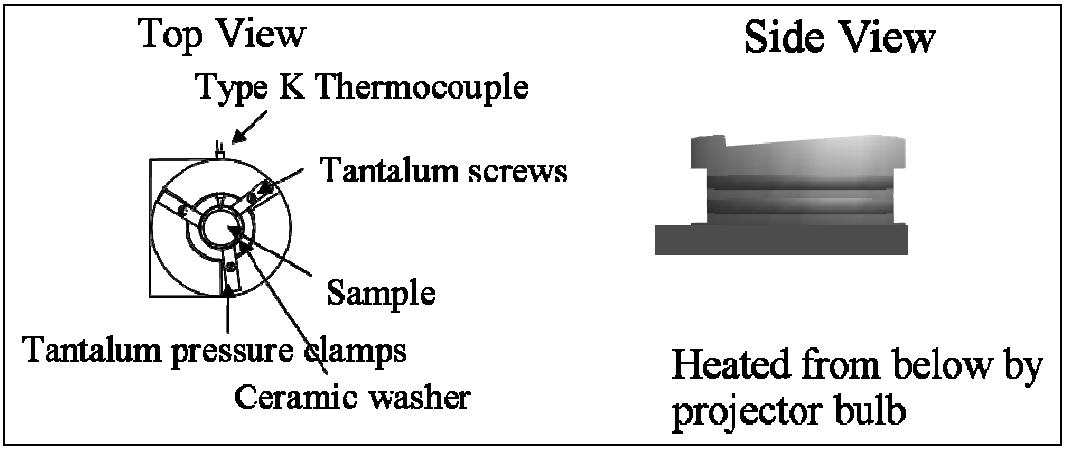

Figure 3.6. Sample holder schematic

3.8 Load-Lock

The system is equipped with a load-lock in order to introduce and remove STM tips and samples while maintaining UHV pressure (Figure 3.1). The load-lock can be isolated, brought up to ambient pressure, and independently pumped to UHV allowing sample and trip transfer without contamination of the UHV environment.

3.9 Tip Preparation

Tungsten STM tips are prepared by electrochemical etching in KOH in a procedure developed by Klein and Schwitzgebel [6]. 0.010" (0.2 mm) diameter W wire was suspended through a small (6 mm diameter) wire loop. The loop was briefly submerged in a solution of ~2 M KOH. The solution was removed, leaving a film of $KOH_{(aq)}$ spanning the loop. Applying a positive DC bias (5-15 V, 1.5 A) on the W wire with respect to the loop, creates an electrochemical cell using the $KOH_{(aq)}$ film as the electrolyte (Figure 3.7). The W tip is slowly etched in the solution. A microscope objective is used to monitor the etching progress. Periodically, the KOH film will pop or solid crystals will become deposited on the W wire. The loop is submerged in DI water to rinse and then $KOH_{(aq)}$ film is refreshed. When the tip diameter becomes small a small cup is placed beneath the tip to catch the wire segment after it etches off to be used as an STM tip. The lower portion of the wire is used because the electrical contact is instantly severed when the tip breaks causing the etching to stop and producing sharper tip apexes. Frequently, the wire is inverted before it severs so that the tip will be the wire segment

that spent most of the etching time at the upper end causing it to have a shorter taper, which seems to more frequently produce stable STM tips. The tip is then rinsed to remove KOH and checked for macroscopic sharpness with an optical microscope.

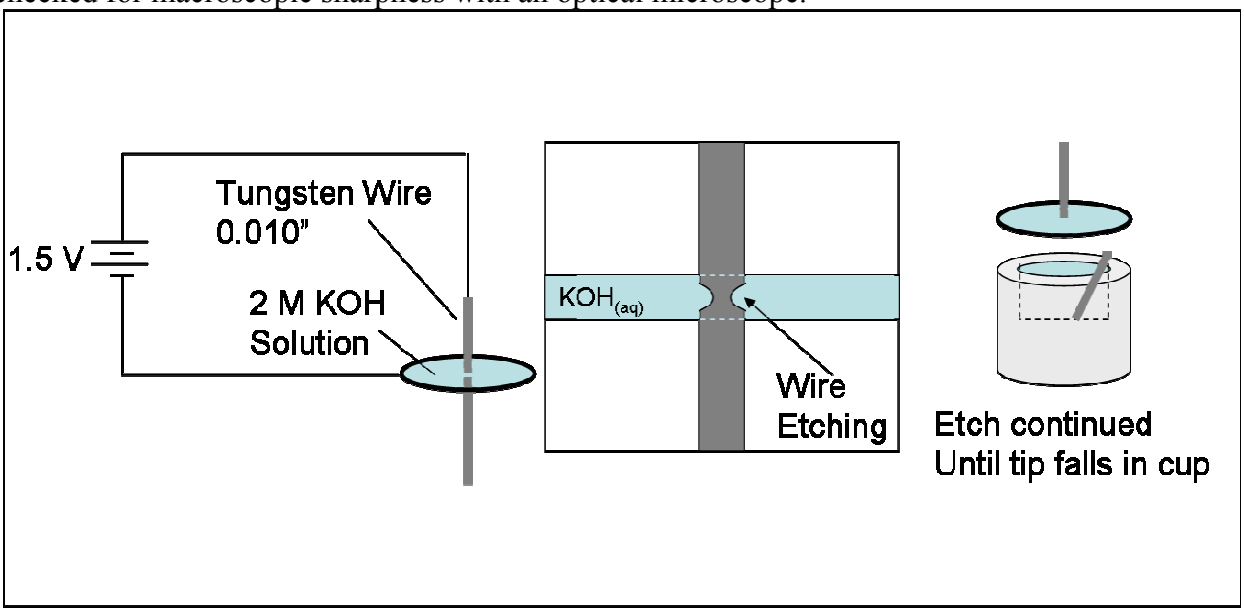

Figure 3.7. Tungsten Tip etching diagram

3.10 Ambient Pressure X-ray Photoelectron Spectroscopy (AP-XPS) apparatus

XPS uses X-rays to excite photoelectrons which are measured by a detector. Before reaching the detector, the electrons pass through a hemispherical analyzer energy which uses an electric field applied between two concentric hemispherical plates to separate electrons by kinetic energy. Once entering the analyzer, the electric field causes the electrons to be accelerated towards the inner spherical plate. At a given field strength, electrons with too much kinetic energy will hit the outer plate and those with too little will hit the inner plate. The electrons that pass through the analyzer are collected by the detector. Since the photoelectrons must travel large distances between the sample surface and the detector, UHV conditions are used to prevent the scattering of the photoelectrons by gas particles.

In order to extend the pressure range of XPS, APXPS uses a differential pumping system with an electrostatic lens [3]. Figure 3.8 contains a cartoon of the experimental geometry. A cone with a small aperture (~0.5-1.0 mm in diameter) is brought within a small distance (0.5-1.5 mm) of the sample surface. The differential pumping allows the chamber outside the cone to be kept at high pressure while pressure inside the cone quickly falls to UHV. This minimizes the path length that the photoelectrons must travel in the presence of high pressure gases and allows the current generation of APXPS systems to operate in the 1-10 Torr range [3-5]. The upper pressure limit limit is caused by gas phase scattering reducing the signal strength until the spectra acquisition time becomes impractical.

The APXPS experiments in these studies were conducted on beamlines 9.3.2 and 11.0.2 a the ALS at LBNL. The synchrotron provides a bright, tunable monochromatic X-ray source. The ability to choose the X-ray energy allows a number of advantages such as control over the kinetic energy of the photoelectrons and with it the sampling depth as well as the ability to select energies to avoid interfering Auger peaks.

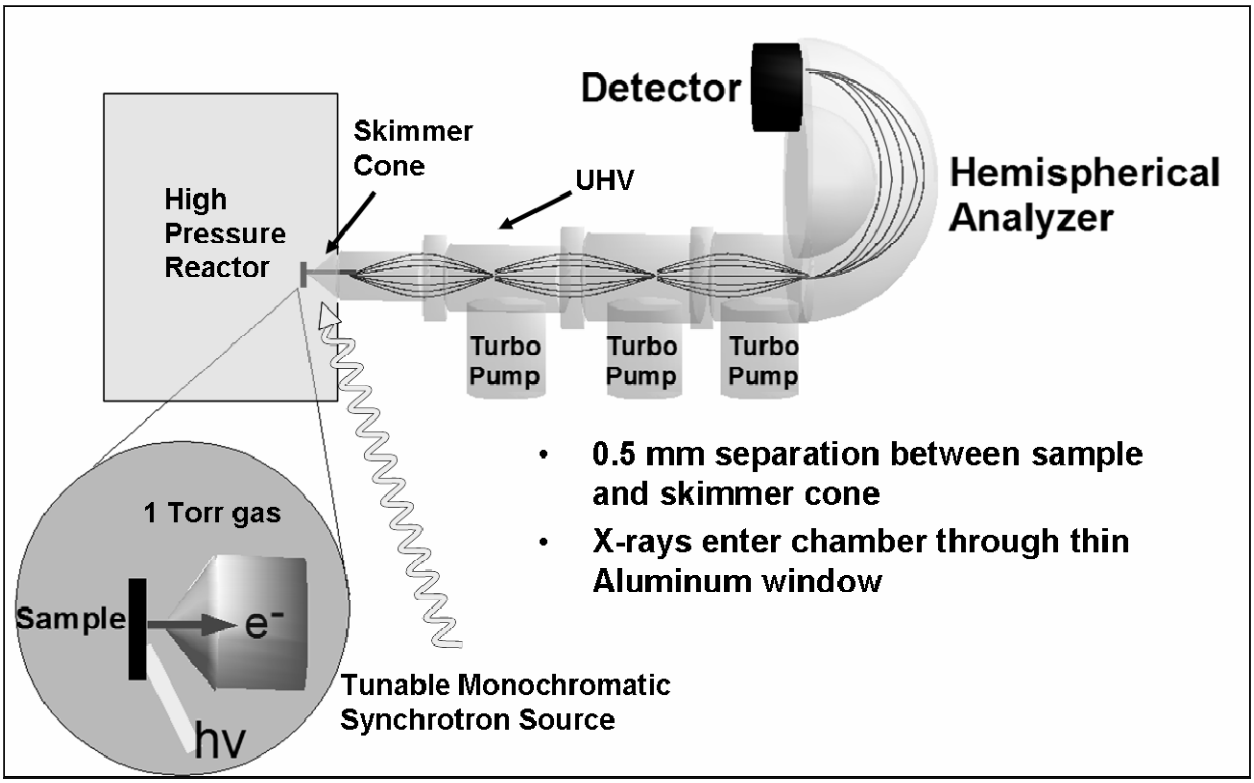

Figure 3.8. Schematic of APXPS experimental setup with differential pumping system and electrostatic lens.

3.11 References

1. Somorjai, G.A., *Introduction to surface chemistry and catalysis*. 1994, New York: Wiley. xxiv, 667.
2. Jensen, J.A., et al., *High pressure, high temperature scanning tunneling microscopy.* Journal of Vacuum Science & Technology B: Microelectronics and Nanometer Structures, 1999. **17**(3): p. 1080-1084.
3. Ogletree, D.F., et al., *A differentially pumped electrostatic lens system for photoemission studies in the millibar range.* Review of Scientific Instruments, 2002. **73**(11): p. 3872-3877.
4. Grass, M.E., et al., *New ambient pressure photoemission endstation at Advanced Light Source beamline 9.3.2.* Review of Scientific Instruments. **81**(5): p. 053106.

5. Bluhm, H., et al., *Soft X-ray microscopy and spectroscopy at the molecular environmental science beamline at the Advanced Light Source.* Journal of Electron Spectroscopy and Related Phenomena, 2006. **150**(2-3): p. 86-104.
6. Klein, M. and G. Schwitzgebel, *An improved lamellae drop-off technique for sharp tip preparation in scanning tunneling microscopy.* Review of Scientific Instruments, 1997. **68**(8): p. 3099-3103.

Chapter 4. Structural Dynamics on an Undercoordinated Surface: *In-situ* STM Studies of the Adsorbate-Induced Restructuring of Pt(100) crystal face by CO, H2, Benzene

4.1 *Abstract*

The adsorbate-induced restructuring of Pt(100) was studied using *in-situ* STM at high pressure. The undercoordinated surface geometry results in a quasihexagonal surface reconstruction on the clean crystal face that was lifted upon adsorption of CO, H_2, or Benzene. When the hex phase was lifted at room temperature, the STM images showed a surface covered by 2-3 nm Pt adatom islands which were a single Pt atom in height. The island structure has a high density of step high energy edge sites, which is a function of island size. Heating in the presence of high pressures of CO or H_2 increases the rate of Pt self-diffusion allowing the surface to form lower energy structures by increasing the island size which minimizes the step edge density. These studies use a highly ordered open crystal face to show the dynamic behavior of metal surface at high pressures and elevated temperatures.

4.2 Introduction

Metallic single crystals are useful model systems in catalytic studies. Examining the behavior of well-ordered atomically flat surfaces with uniform crystal structures allows structural rearrangements arising from small energetic changes to be observed experimentally. The uniformity of oriented single crystals can produce large scale ordering of the surface. This allows the use of STM to study the behavior of catalytic surfaces. STM images the electronic structure of flat surfaces with high resolution. The contrast in the images is similar to a topographic map of the surface. Since STM operates over a wide range of temperature and pressure, it can be used to study the changes in surface topography on flat conductive catalytic surfaces but the interpretation of STM images requires well defined surfaces. Catalysis is a dynamic process and active metal surfaces can undergo changes in the surface structure that are inaccessible to most surface characterization techniques. This study looks at the dynamics observed in the Pt(100) surface layer on an atomic scale in the presence of adsorbing gases.

Cooling the Pt(100) surface to room temperature after preparing a clean surface through Argon sputtering and high temperature annealing cycles produces the Pt(100)-hex reconstructed surface [1-6]. The (100) face of fcc crystals has four-fold symmetry however on Pt the crystal face the surface can rearrange to form a hexagonal structure similar to the (111) crystal face (Figure 4.1). This rearrangement results in a lattice mismatch that causes the surface layer to buckle resulting in periodic corrugated rows. The Pt(100)-hex reconstruction forms because it allows for more highly coordinated surface atoms and reduces the surface energy. A surface atom on the bulk terminated (100) face has a nearest neighbor coordination number of 8 compared with 9 on the (111) face. This hex-reconstruction is thought to exist in only the

topmost atomic layer with the second layer close to the bulk (100) positions with a second layer geometry close to that of the bulk termination [7].

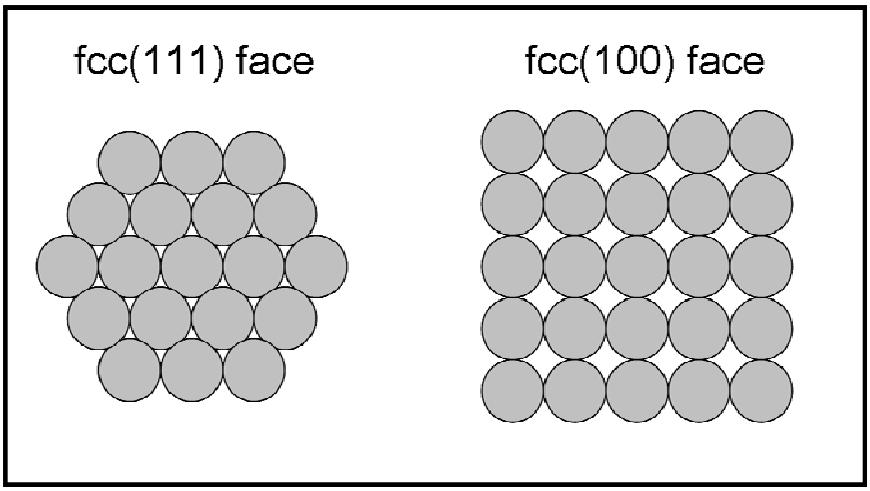

The adsorption of CO has been shown to lift the Pt(100)-hex reconstruction resulting in a (1x1) surface structure [2, 6]. STM images of the CO covered Pt(100) surface show a surface decorated by 2-3 nm islands [6, 8-10]. Since the formation of the Pt(100)-hex reconstruction is a result of the low coordination of Pt(100) surface atoms, the adsorption of CO can relieve this surface strain allowing the Pt surface atoms to return to the bulk terminated (100) positions. The Pt(100)-hex reconstructed surface has a denser atomic packing on the surface layer than the (100) face, causing the extra Pt atoms to be forced out of the terrace forming a partially filled layer of Pt adatom islands. The resulting (1x1) island structure has a high density of step sites.

4.3 Results and Methods

Pt(100)-hex Reconstruction

Cleaning the Pt(100) crystal face through cycles of 10-20 min Argon ion sputtering (1 keV, 20 mA, 10^{-5} Torr Ar pressure), a 5 min oxygen annealing treatment (773 K, 10^{-7} Torr O_2) and lastly a high temperature annealing step (1025 K at 10^{-10} Torr base pressure) produced a clean surface without oxygen or carbon present in the Auger spectra. An STM image of the clean surface is shown in Figure 4.1. This image shows the corrugated structure of the Pt(100)-hex reconstruction. Although the image does not show atomic resolution, the circular dark spots are most likely single Pt atom vacancies. Comparison with previous STM studies with clear single atom resolution confirms that the corrugated structure is the Pt(100)-hex surface [6] [8] [11]. Figure 4.1 also contains the plots of two line scans running perpendicular to the corrugations that are marked A and B. Line scan A (light gray, top plot) shows a periodicity of ~1.3 nm and an amplitude of ~20 pm. Line scan B has a 4 nm period and amplitude of 0.15 pm. The apparent height of a full atomic step was ~250 pm, so the vertical displacement within the terrace on the Pt(100)-hex surface is less than 10% of an atomic step.

Figure 4.2 shows STM images of the partially lifted reconstruction. At room temperature in an atmosphere of 10^{-9} Torr, the collision frequency is substantially low (~1 collision per Pt surface atom per 1000 s to allow a slow accumulation of a CO monolayer. Figure 4.2A is a (200 nm)^2 STM image showing steps and terraces. The terraces contain areas with two morphologies: smooth areas showing the Pt(100)-hex surface and roughened areas showing the lifted island structure. The white box in the center of image A marks the area scanned in image B. Image B (100 nm)^2 allows a closer view of the islands which are 2-3 nm wide and appear slightly elongated. Image C is a close up scan of the flat region in image B where the corrugated rows of the Pt(100)-hex reconstruction are clearly identified. The line scan in 4.2D is the topography on the black line in image C, which shows the same corrugated features as line scan A in Figure 4.1.

CO Adsorption on Pt(100)

Figure 4.3 shows a series of (200 nm)^2 STM images at 298 K and 10^{-9} Torr CO at the same location as the images in Figure 4.2. Panel A has the remaining Pt(100)-hex reconstructed regions outlined in black. Panel B is the same image as A without the outlines. In the series of images from B-H, the regions of Pt(100)-hex morphology are lifted by the low pressure of CO. The images were acquired in succession with each image taking ~1 min. At the end of the series, the entire area is decorated by the island structure showing that the lifting of the hex phase is anisotropic and with domain boundaries that parallel the reconstructed rows.

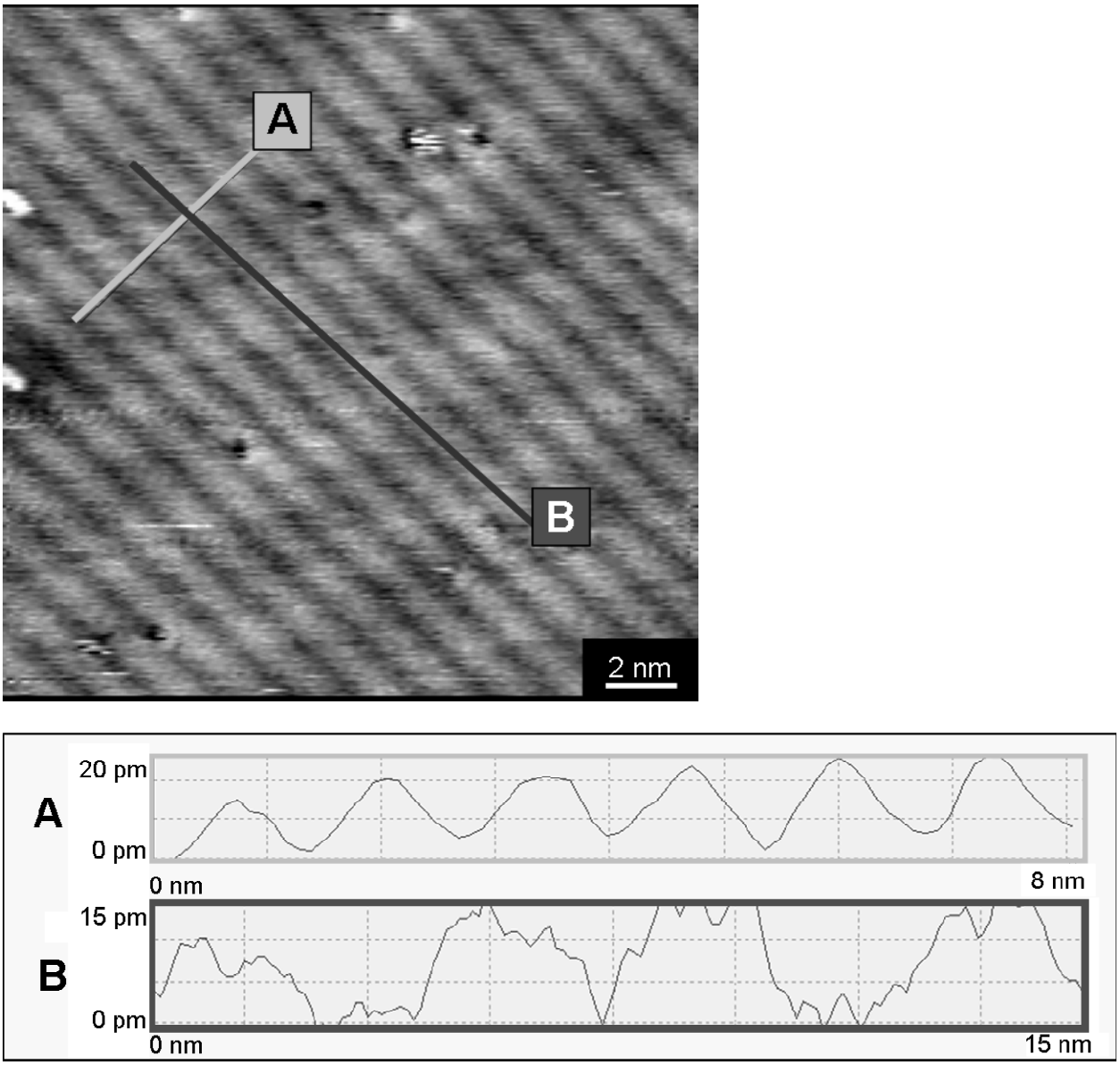

Figure 4.1. $(17\ \text{nm})^2$ STM image of the clean Pt(100) surface. The two lines labeled A and B are the traces plotted above. Line Scan A shows the short range corrugated structure (~1.3 nm period, ~15 pm amplitude) and Line Scan B shows the long range corrugation (~4 nm period, ~20 pm amplitude)

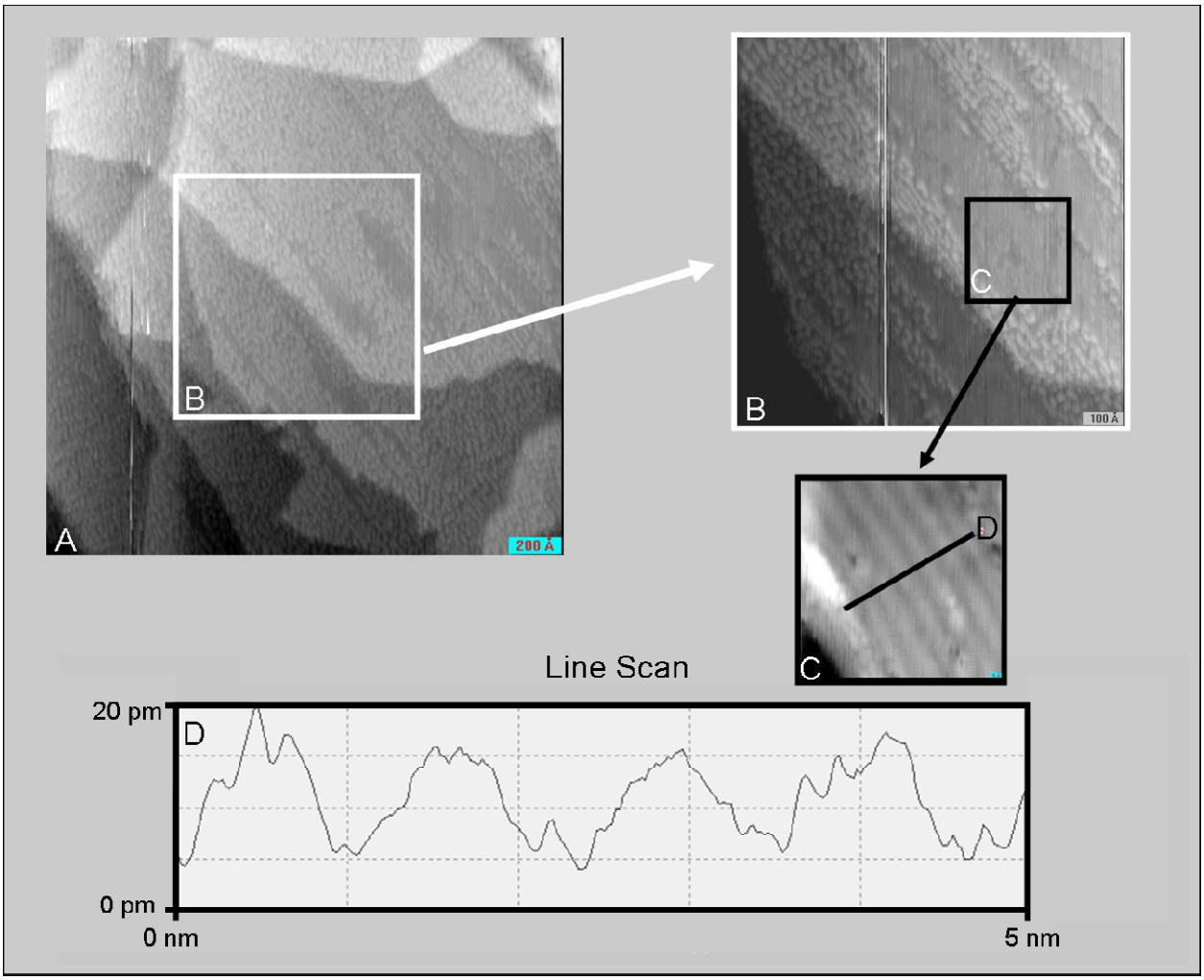

Figure 4.2 At the top left is a $(200\ nm)^2$ image (A) of Pt(100) in 10^{-9} Torr CO. The image contains multiple steps and terraces. Some of the terraces show differences in contrast indicating changes in roughness. B $(100\ nm)^2$ and C $(20\ nm)^2$ show higher magnification images of the same area with the exact image locations marked with white (B) and black (C) borders. In B, there are two surface morphologies: roughened islands and smooth terraces. In C, the smooth terrace is shown to have the corrugated structure of the Pt(100)-hex. A line scan of the corrugated rows is in agreement with Figure 4.1A.

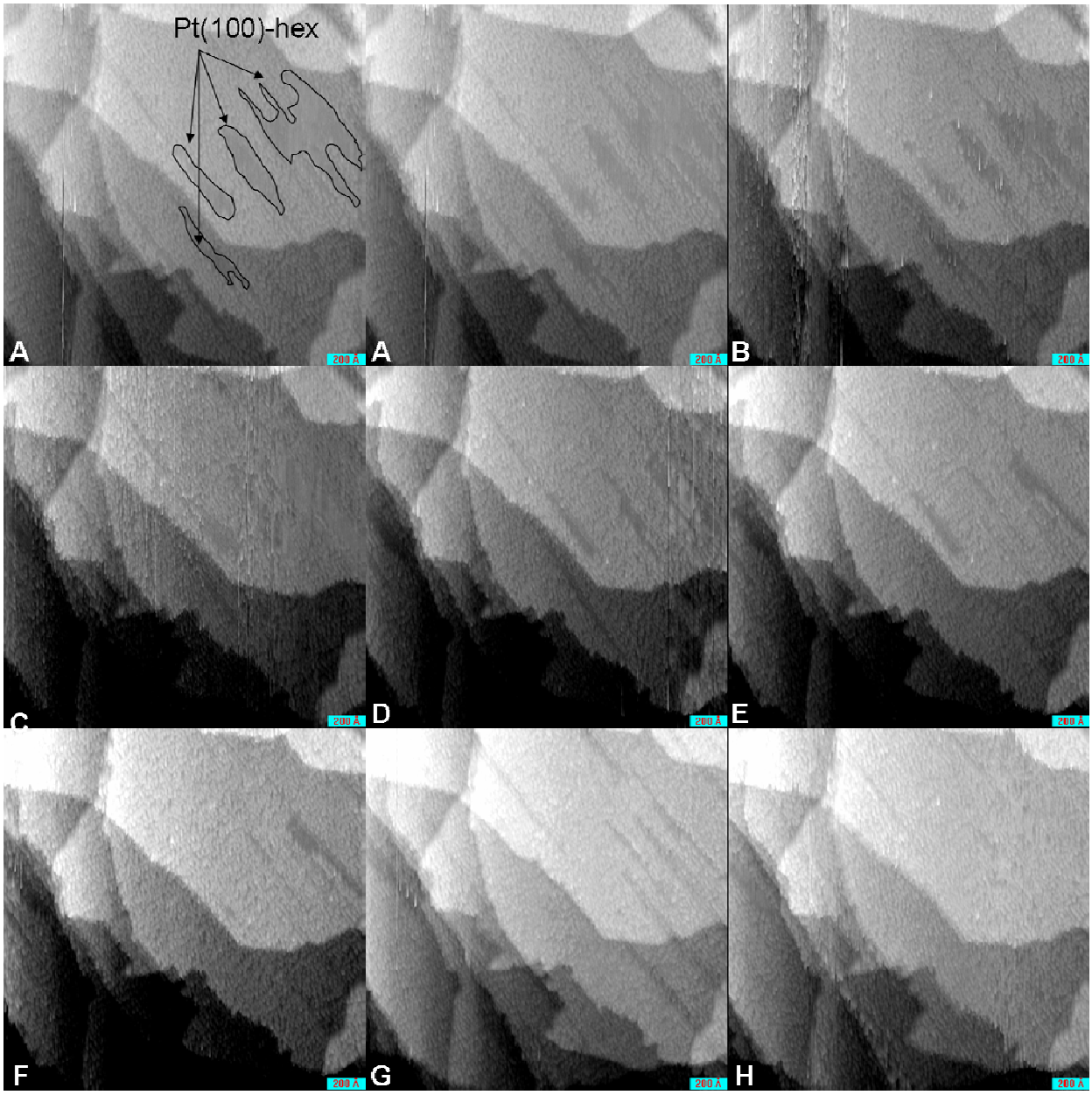

Figure 4.3 Image A is the same $(200\ nm)^2$ STM image shown in Figure 4.2 of the Pt(100) crystal face in 10^{-9} Torr CO. The image contains multiple steps and terraces. Outlined in black are flat sections of the terrace that are shown in 4.2 to be the Pt(100)-hex reconstructed surface. The surrounding area is the lifted (1x1) island structure. Panels B-H contain a series of images taken at 60 s intervals showing the lifting of the remaining hex reconstructed regions.

The room temperature CO exposure resulted in a Pt(100)-(1x1) structure with islands covering ~45% of the surface. Figure 4.4 shows a schematic of the transition from the corrugated Pt(100)-hex phase to the (1x1) structure. This results in ~20% surface coverage of step edges. This is an important point because numerous studies have compared the activities of (111) and (100) faces in order to understand the geometric effects on the reactivity. Without being able to monitor the changes in surface morphology, differences in catalytic activity due to the increase in step sites could be attributed to the geometry of the terraces. Step sites have been shown to have increased activities for certain catalytic processes such as oxygen dissociation [12] and hydrocarbon cracking [13] so the changes in surface activity could be changed considerably by the spontaneous formation of a high concentration of step edges. However there is some controversy about the exact role of step sites in many reactions [14]. Unfortunately few techniques other than STM are capable of detecting changes in step behavior (including the Pt(100) island formation) in the presence of gases and under catalytic conditions. Overcoming the shortage of *in-situ* atomic level surface characterization experiments could help shed light on these questions because step edges can undergo changes such as spontaneous formation, removal by step doubling and island coalescence, and step edge deactivation through selective poisoning. It is known that these processes are induced by gas adsorption at high temperatures however the experimental obstacles to *in-situ* studies have prevented the systematic mapping of the temperature pressure phase space of reactive conditions.

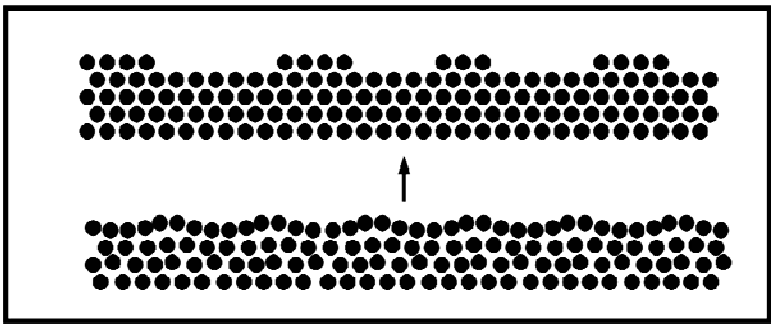

Figure 4.4 Schematic showing the rearrangement of the densely packed corrugated Pt(100)-hex phase (bottom) into the (1x1) phase with the extra Pt atoms promoted to islands (top).

The low pressure (10^{-6} Torr) CO structure on the Pt(100)-(1x1) surface was studied on a different HPSTM system in our laboratory with molecular resolution [10]. The spacing between adjacent CO molecules on the islands was found to be 0.37-0.4 nm. This spacing does not coincide with a nearest neighbor or next nearest neighbor structure with the bulk Pt bond distance being 0.277 nm. DFT calculations attributed the observed expansion of the CO-CO distance to the Coulomb repulsion between adjacent CO adsorbates [10]. The calculations suggested that the expansion was more likely to be caused by a tilting of the CO molecule rather than an expansion of the underlying Pt-Pt distance. CO usually bonds vertically on the Pt surfaces with the Carbon atom down. In the model, the CO tilt angle was largest at the edges of the islands. The expansion of the neighboring CO molecules due to the tilted geometry offers an explanation for the discrepancy between the 45% island coverage and the excess of Pt atoms in the Pt(100)-hex phase of only 20-25%. In a separate experiment the Pt(100) structure at 25 ˚C in a CO pressure of 1 Torr was found to have 2-3 nm islands which is consistent with the low pressure structure.

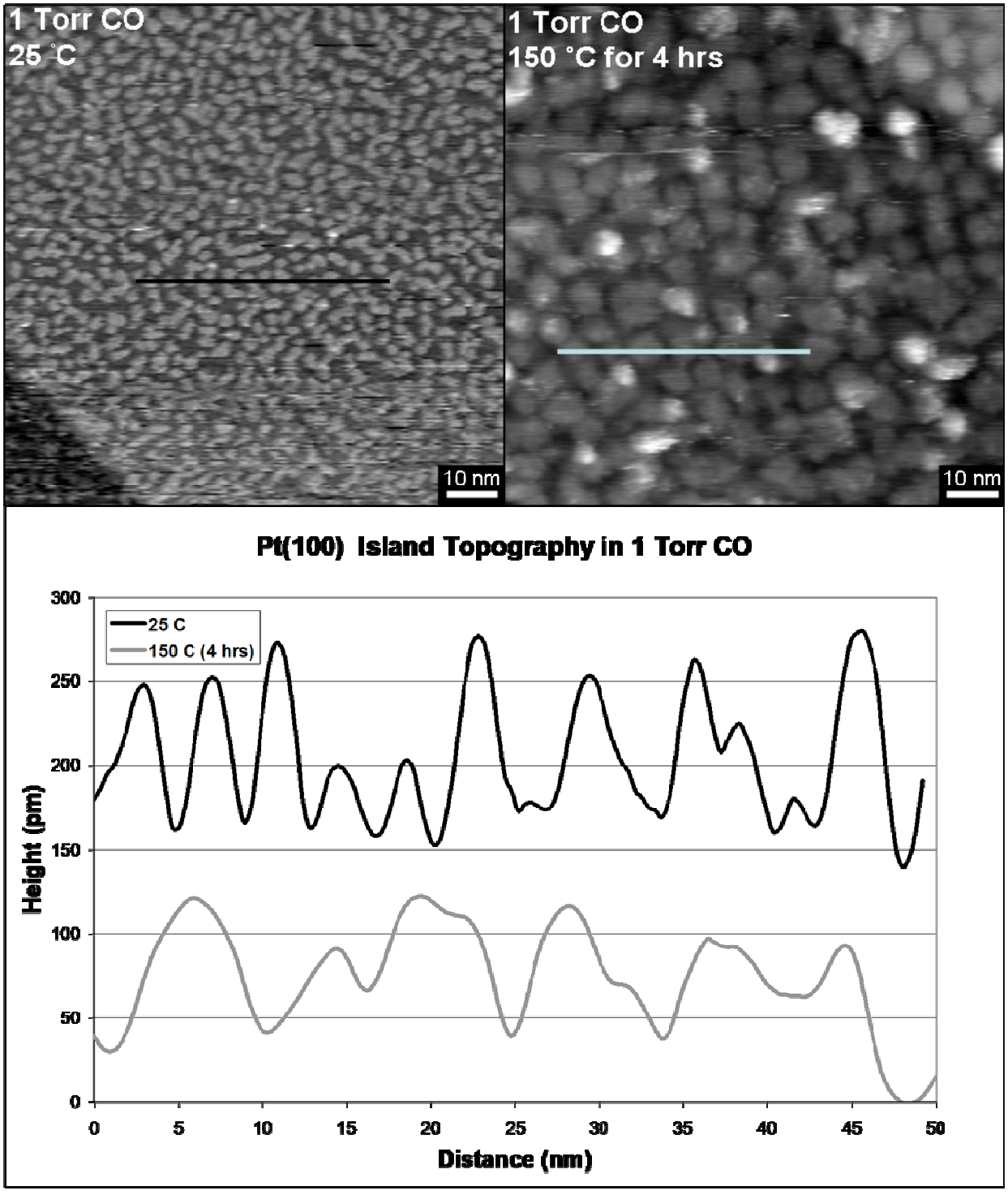

Figure 4.5 $(200\ nm)^2$ STM images of Pt(100) in 1 Torr CO at 25 (left) and 150 ˚C (right). After 4 hrs at 150 ˚C in the presence of 1 Torr CO, the islands which are stable at room temperature coalesce reducing the amount of edge sites on the surface. The images were taken in the presence of CO at the temperatures indicated.

The top left panel of Figure 4.5 contains a $(200\ nm)^2$ STM image of the Pt(100) island structure at 25 ˚C in 1 Torr CO. The image contains a large terrace decorated by 2-3 nm islands. The apparent height of the islands is roughly the same as the step height measured either from terrace to terrace or island to island which is consistent with single Pt atom islands with CO covering the entire surface. When the crystal was annealed at moderate temperatures in CO, the island size increased. The top right panel contains a $(200\ nm)^2$ STM image taken at 150 ˚C in the presence of 1 Torr CO. The image was taken 4 hours into the annealing treatment at which point the Pt islands had widths of 5-10 nm. At the bottom of Figure 4.5 is a comparison between 50 nm line scans from each of the images. The island height does not change, but the width in the 150 ˚C image has increased leading to a ~10 fold increase in area per island, which reduces the density of island edge sites by a factor of ~3. The islands in the 150 ˚C image are mostly a single Pt atomic step in height, with the bright islands showing multilayer clusters. The CO annealing treatment was carried out for 24 hours without significant change in the island size.

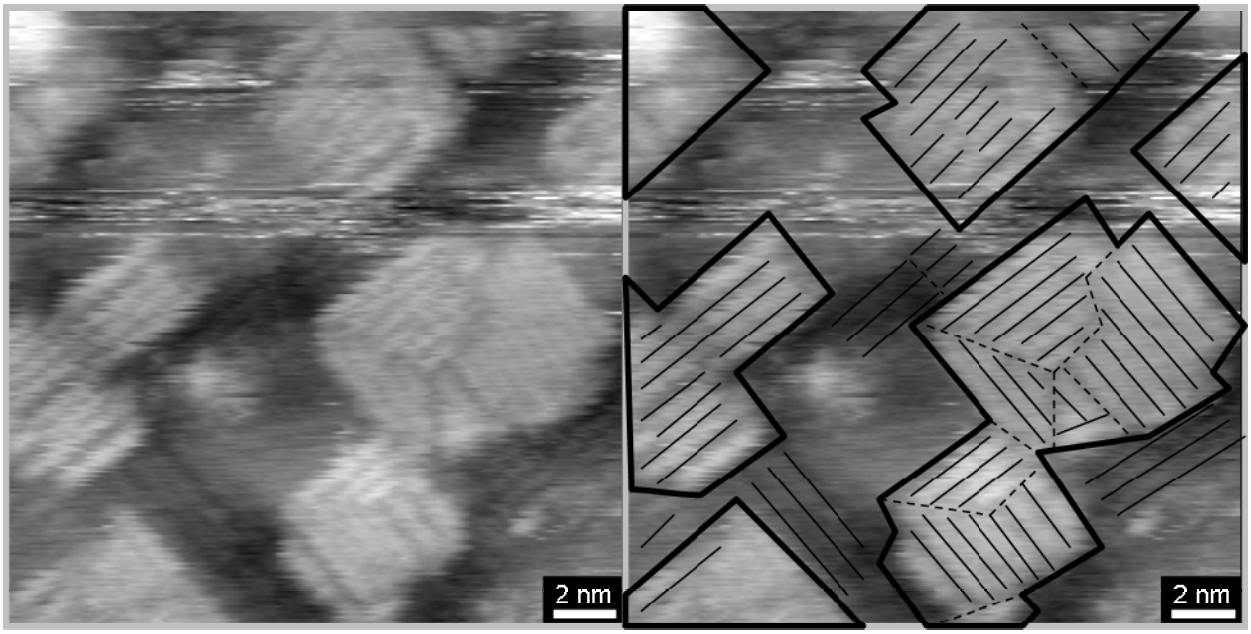

Figure 4.6 $(20\ nm)^2$ STM image of Pt(100) at 150 ˚C in 1 Torr CO. The left and right panels contain the same image. Due the high noise level at these imaging conditions, the ordered features have been outlined in the image on the right with thick solid lines indicating island edges, thin solid lines separating rows of CO molecules, and dashed lines for domain boundaries. Rows of CO molecules are seen on both islands and terraces in one of two perpendicular domains due to the (100) face. The spacing between rows is not uniform and increases at the island edges.

A $(200\ nm)^2$ STM image (Figure 4.6) of the Pt(100) island structure at 150 ˚C in 1 Torr CO resolved features on the islands. The two panels in Figure 4.6 contain the same image with some of the ordered features outlined on the right. Island edges (thick, solid lines), CO adsorbate rows (thin, solid lines), and domain boundaries (thin, dotted lines) are indicated in the right panel. The image shows CO molecules adsorbed in ordered rows. The rows are arranged in perpendicular domains reflecting the (100) symmetry of the crystal face. The width of the rows

is variable with larger row spacing on the edges of the islands. This variable row spacing is likely to be a result of the Coulomb repulsion of adjacent CO molecules. The steric freedom of the edge sites could allow for the CO molecules to tilt away from the neighboring adsorbates, which would explain the observed lattice expansion.

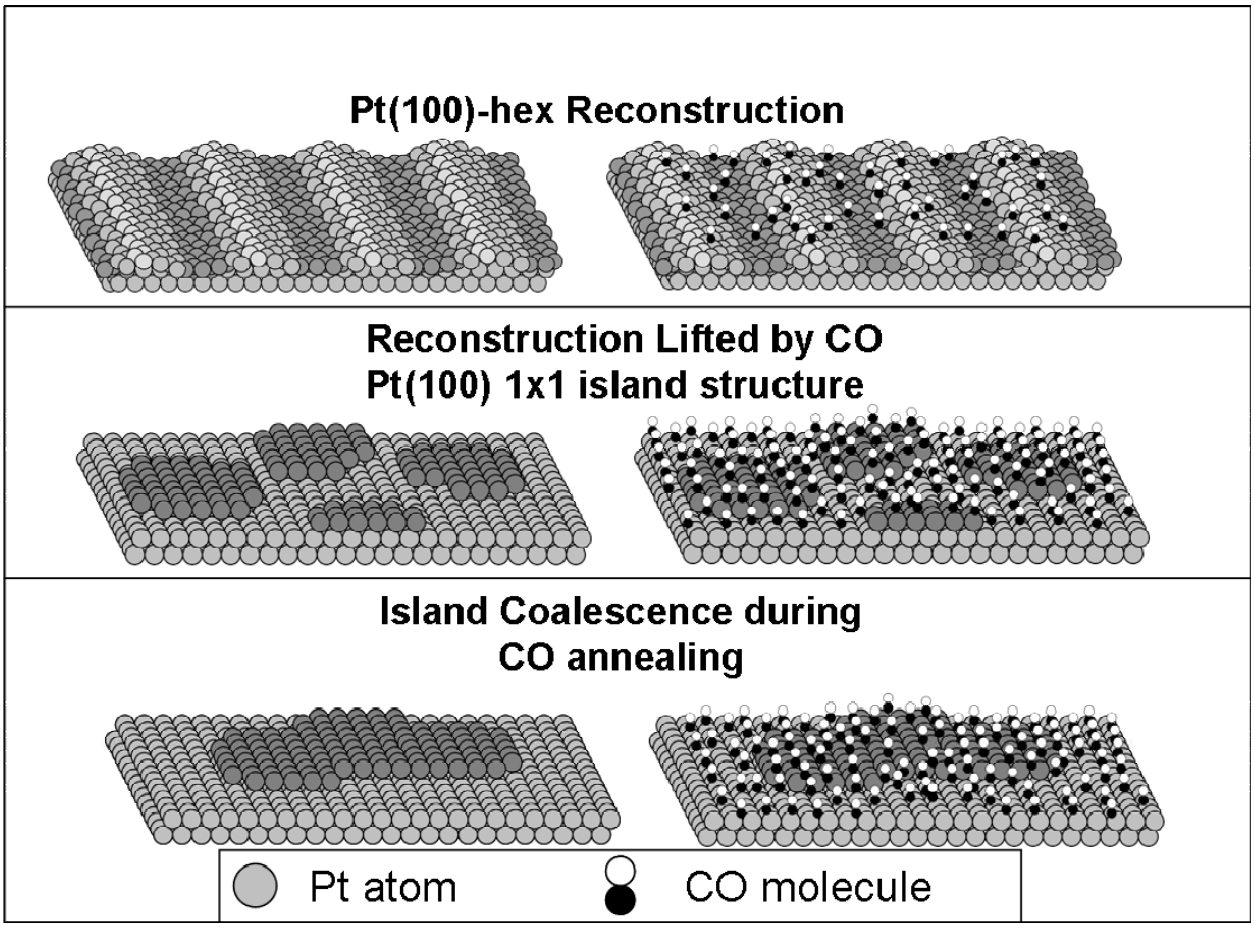

Figure 4.7 Schematic of the surface restructuring on the Pt(100) surface induced by CO adsorption and heating. The gray circles depict the Pt atoms and the black and white circles CO. The drawings show the Pt atoms alone on the left and on the right include CO. The clean surface shows the corrugated Pt(100)-hex structure. When sufficient amounts of CO adsorb on the surface at room temperature, the hex reconstruction is lifted into the (1x1) structure with 2-3 nm adatom islands. Annealing at 150 ˚C caused the islands to agglomerate into 5-10 nm islands.

Figure 4.7 contains diagrams summarizing the morphological changes observed on the Pt(100) surface in the CO adsorption studies. The open structure of the (100) face causes the Pt surface to dramatically restructure to minimize the surface energy. The top diagram shows the corrugated rows of the Pt(100)-hex surface. At room temperature CO exposure lifts the reconstruction into small (2-3 nm) islands. This surface is a kinetically trapped high surface energy surface due to the high density of edge sites. Low temperature (150 ˚C) annealing treatments in the presence of 1 Torr CO allows the Pt surface atoms in the partially filled island layer to become mobile enough for the islands to coalesce minimizing edge sites and forming a lower energy surface structure.

Pt(100) Structure in Hydrogenation Conditions

The focus of the adsorption studies on Pt(100) was to use CO as a model system to understand the behavior resulting from the instability of this open crystal face in the presence of gases so that it could be related to the behavior of the surface under catalytic conditions. CO is a catalytic poison for many hydrogenation reactions, so in order to study the active surface in hydrogenation conditions, it is useful to study whether the structural changes are specific to CO. The Pt(100) surface was studied in the presence of benzene and hydrogen.

Introducing an atmosphere of 1 Torr benzene at room temperature caused the lifting of the Pt(100)-hex surface into the characteristic 2-3 nm Pt adatom islands. Figure 4.8 shows a (9 nm)^2 STM image where molecularly adsorbed benzene appear as 0.5 nm circular features. On the right hand side of Figure 4.8, the locations of the benzene molecules on the tops of the islands are marked with closed circles and those adjacent to the islands marked with open circles. On top of the islands, the benzene molecules are close packed on the surface with regions of hexagonal and square symmetry. At these conditions, the entire surface is covered with benzene, but only the tops of the islands can be resolved clearly, which is likely the result of the finite sharpness of the STM tip.

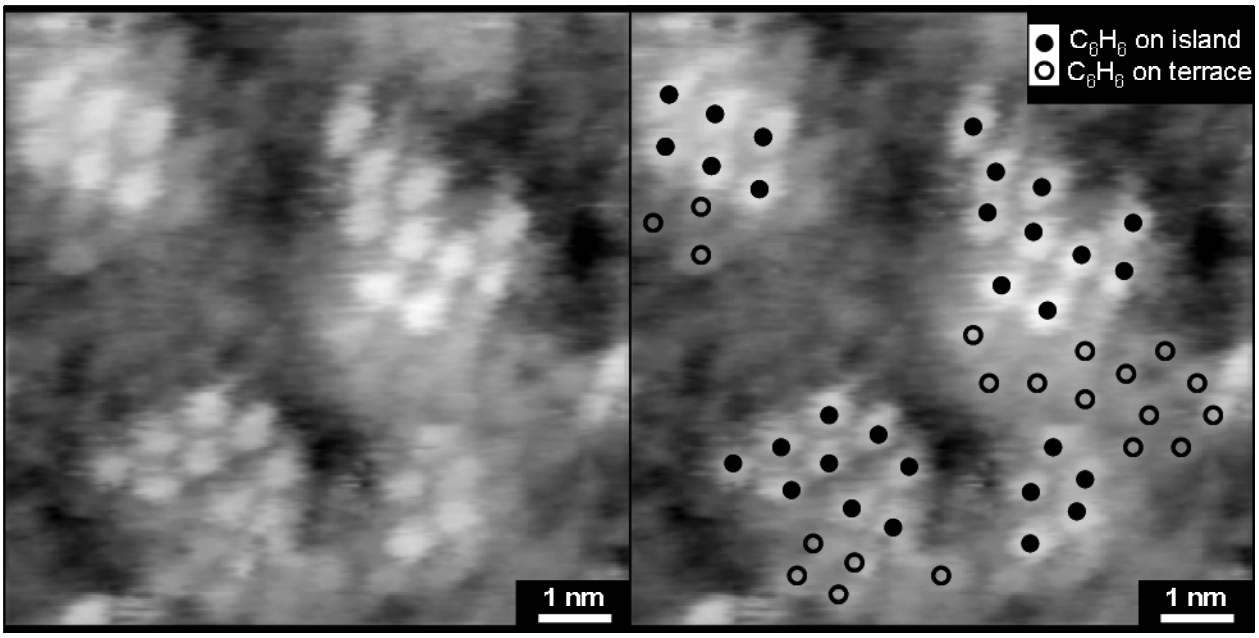

Figure 4.8 (9 nm)^2 STM image of Pt(100) in 1 Torr Benzene at 25 ˚C. The right panel shows the same image with solid circles marking benzene molecules on the top of the Pt adatom islands and open circles marking benzene molecules next to the islands. Benzene lifts the hex reconstruction producing 2-3 nm islands at room temperature and adsorb on the top of the islands in both hexagonal and square close-packed domains.

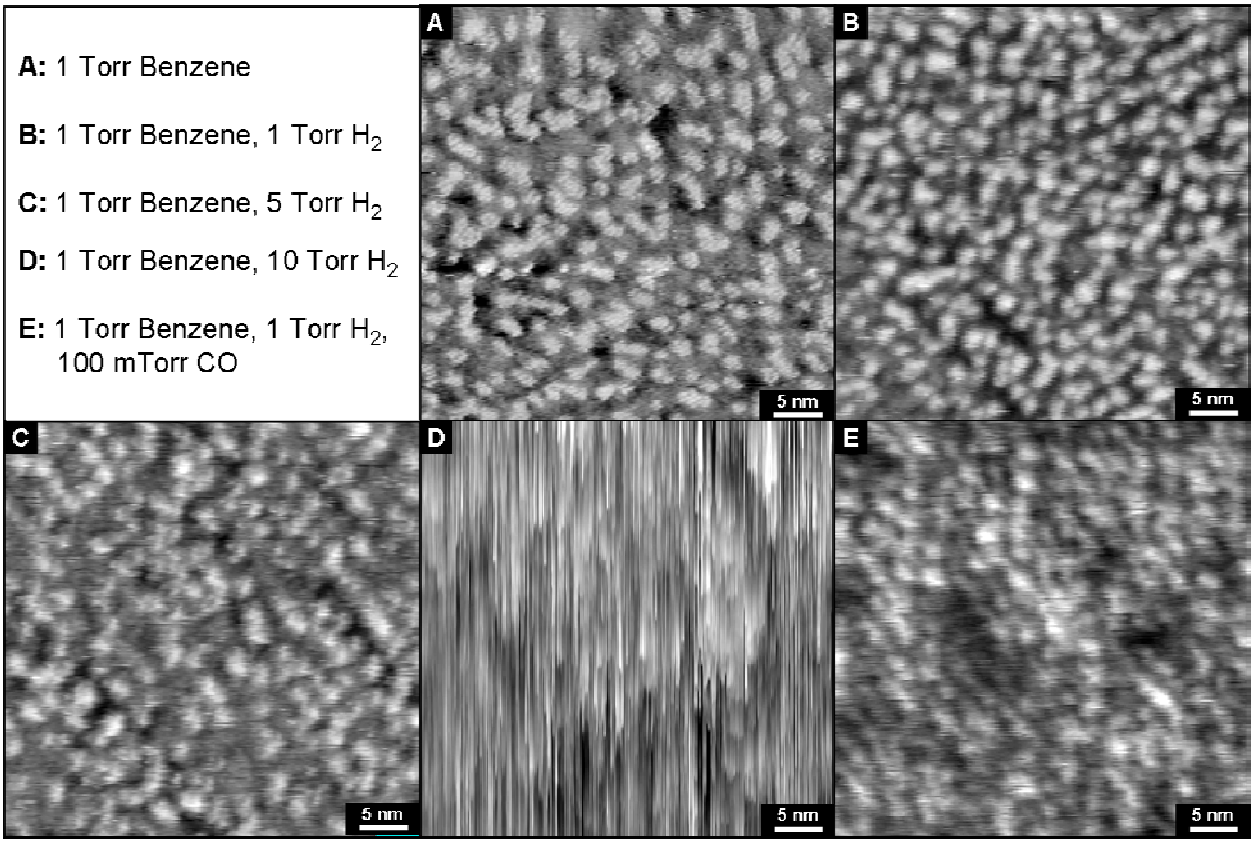

Figure 4.9 $(50\ nm)^2$ STM images taken at 25 ˚C in (A) 1 Torr Benzene, (B) 1 Torr Benzene and 1 Torr H_2, (C) 1 Torr Benzene and 5 Torr H_2, (D) 1 Torr Benzene and 10 Torr H_2, and (E) 1 Torr Benzene, 10 Torr H_2, and 100 mTorr CO. Image A shows the islands of the lifted reconstruction with adsorbed benzene molecules on the tops of the islands. When H_2 is introduced (B-D), the islands remain the individual benzene molecules can no longer be resolved which is attributed to increased adsorbate diffusion induced by coadsorption with hydrogen. At 10 Torr H_2, no features are could be resolved. The introduction of CO (E), a strongly binding hydrogenation poison, stabilizes the adsorbate mobility allowing the adatom islands to be imaged.

Figure 4.9 contains a series of $(50\ nm)^2$ STM images at room temperature. Image A shows the same 1 Torr benzene condition as in Figure 4.8 with the 2-3 nm Pt adatom islands of the lifted reconstruction with resolved benzene molecules on the top of the islands. When 1 Torr of hydrogen (image B) and later 5 Torr hydrogen (image C) is added to the chamber, the islands remain on the Pt(100) crystal face, but no benzene molecules are resolved on the islands. Further increasing the hydrogen pressure to 10 Torr resulted in unstable imaging conditions (image D). In previous *in-situ* STM studies on hydrogenation reactions, the transition from an adsorbed layer to a catalytically active surface was found to coincide with a transition to unstable imaging conditions which have been attributed to a mobile surface layer with diffusion, adsorption, and desorption causing disruptions on the surface area on timescales faster than image acquisition [15-18]. The STM images in figure 4.9 were collected with an STM tip speed of 250 nm/s. When 100 mTorr CO was added to the system (image E), the surface was stabilized and the island structure was clearly present in the images.

This is the first report benzene lifting the Pt(100)-hex reconstruction. It is important to note that the island size is the same as in the case of CO adsorption at room temperature. This agreement in island size along with the observed island sintering at 150 ˚C in CO, suggests that these are kinetically trapped structures with the island size determined by the Pt self-diffusion rate. The STM images in 1 Torr benzene (Figs. 4.8-9) show close packed molecular benzene on the tops of the islands. The benzene molecules show some ordering with aligned benzene rows with hexagonal and square domains. At these conditions benzene is known to be present on the surface in both the chemisorbed and the physisorbed state [19] and the island morphology that divides the surface into small domains is a likely cause of the disordered overlayer detected by previous LEED studies [20].

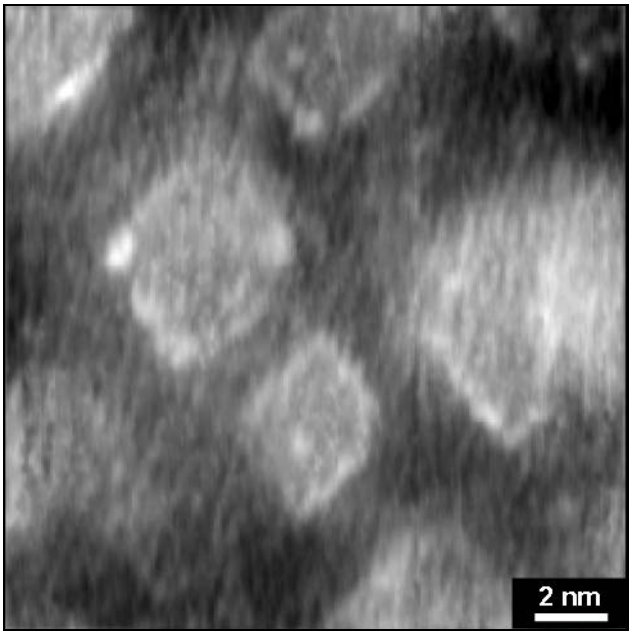

Figure 4.10 (20 nm)^2 STM image of Pt(100) in the presence of 100 Torr H_2 at 150 ˚C for 2 hrs. This H_2 annealing treatment produced 4-8 nm adatom islands with square symmetry matching the underlying Pt(100) face.

The coverage of the partially filled Pt adatom island layer on the lifted Pt(100) surface is constant, so the spacing between islands increases with island size. STM can only measure the region of the surface closest to the tip, so the finite sharpness of the STM tip makes it difficult to image the terraces between closely spaced islands. In an effort to make more of the Pt(100) face accessible to STM imaging, yet remain active for hydrogenation reactions, low temperature hydrogen annealing studies were performed. Figure 4.10 shows a (20 nm)^2 STM image in 100 Torr H_2 and 150 ˚C. After 2 hrs of the H_2 annealing treatment, the islands of the lifted Pt(100)-(1x1) structure were 4-8 nm in width and had a square morphology matching the geometry of the Pt(100) crystal face. Low pressure hydrogen exposure above 100 K is known to lift the Pt(100)-hex reconstruction [21] and hydrogen adsorption has been found to have large effects on the self-diffusion coefficient for Pt [22]. The hydrogen annealing treatment allowed the islands to coalesce forming a more stable structure with fewer edge sites.

4.4 Conclusions

The restructuring behavior of the Pt(100) surface was studied *in-situ* using STM. The room temperature adsorption of CO, Hydrogen, and Benzene was shown to lift the Pt(100)-hex reconstruction resulting in a surface decorated by 2-3 nm Pt adatom islands. The restructuring is caused by adsorbate bonding which relieves surface strain and allows atoms to revert to the bulk terminated crystal sites. However this mass transport occurs as a disruptive phase change in the surface layer which can expose a high density of defect sites such as edges and steps. Annealing the crystal at 150 ˚C in either CO or H_2 allowed the Pt atoms to overcome diffusion barriers and was shown to reduce the density of surface edge sites by increasing the island size. Additionally, close packed adsorption structure of benzene molecules was imaged on the island covered surface. The benzene molecules were resolved at room temperature, but could no longer be resolved in high partial pressures of hydrogen. Similarly the benzene structure could be disrupted by heating to 60 ˚C. The loss of resolution was attributed to increases in the mobility of the surface species which prevented imaging by STM. The surface could be re-stabilized by the introduction of CO, a strongly binding catalytic poison.

The rich surface dynamics observed in these studies on the Pt(100) crystal face shows the utility of single crystals as model catalysts and *in-situ* studies. Few surface characterization techniques other than STM are sensitive to the observed morphological changes observed on the surface which are likely to play a role in its catalytic behavior. The spontaneous formation of a high density of edge sites could explain the selectivity of the Pt(100) surface towards hydrocarbon cracking products [23]. Since active catalysts have mobile surface layers that restructure in response to high temperatures and pressures, *ex-situ* characterization is insufficient to develop an accurate description of catalytic behavior. The Pt(100) surface is a useful model system where the controlled formation and subsequent removal of defect sites can be used to understand the energetics of low coordination sites which are ubiquitous on the high dispersion particles used in industrial catalysis.

4.5 References

1. Hagstrom, S., H.B. Lyon, and G.A. Somorjai, *SURFACE STRUCTURES ON CLEAN PLATINUM (100) SURFACE.* Physical Review Letters, 1965. **15**(11): p. 491-&.
2. Morgan, A.E. and G.A. Somorjai, *LOW ENERGY ELECTRON DIFFRACTION STUDIES OF GAS ADSORPTION ON PLATINUM (100) SINGLE CRYSTAL SURFACE.* Surface Science, 1968. **12**(3): p. 405-&.
3. Morgan, A.E., G.A. Somorjai, and E, *LOW-ENERGY ELECTRON-DIFFRACTION STUDIES OF ADSORPTION OF UNSATURATED HYDROCARBONS AND CARBON MONOXIDE ON PLATINUM (111) AND (100) SINGLE-CRYSTAL SURFACES.* Journal of Chemical Physics, 1969. **51**(8): p. 3309-&.
4. Pirug, G. and H.P. Bonzel, *A low-pressure study of the reduction of NO by H2 on polycrystalline platinum.* Journal of Catalysis, 1977. **50**(1): p. 64-76.
5. Bonzel, H.P., G. Brodén, and G. Pirug, *Structure sensitivity of NO adsorption on a smooth and stepped Pt(100) surface.* Journal of Catalysis, 1978. **53**(1): p. 96-105.
6. Borg, A., et al., *STM STUDIES OF CLEAN, CO-EXPOSED AND O2-EXPOSED PT(100)-HEX-R0.7-DEGREES.* Surface Science, 1994. **306**(1-2): p. 10-20.

7. Ritz, G., et al., *Pt(100) quasihexagonal reconstruction: A comparison between scanning tunneling microscopy data and effective medium theory simulation calculations.* Physical Review B, 1997. **56**(16): p. 10518.
8. Wakisaka, M., et al., *Structural Change and Electrochemical Behavior of Pt(100)-hex-R0.7[degree] Surfaces in Gases and in Solution.* Journal of The Electrochemical Society, 2003. **150**(2): p. E81-E88.
9. Sinsarp, A., et al., *Local tunneling barrier height studies of thermally treated CO and O-covered Pt(100) surfaces.* Japanese Journal of Applied Physics Part 1-Regular Papers Short Notes & Review Papers, 2004. **43**(7B): p. 4659-4662.
10. Tao, F., et al., *Restructuring of hex-Pt(100) under CO Gas Environments: Formation of 2-D Nanoclusters.* Nano Letters, 2009. **9**(5): p. 2167-2171.
11. Ronning, M., et al., *Scanning tunnelling microscopic studies on the adsorption and decomposition of ethene on the reconstructed Pt(100)-hex-R0.7o surface.* Surface Science, 2001. **477**: p. 191-197.
12. John T. Yates, Jr. *Surface chemistry at metallic step defect sites*. 1995: AVS.
13. Vang, R.T., et al., *Controlling the catalytic bond-breaking selectivity of Ni surfaces by step blocking.* Nat Mater, 2005. **4**(2): p. 160-162.
14. Ford, L.P., P. Blowers, and R.I. Masel, *Role of steps and kinks in catalytic activity.* Journal of Vacuum Science & Technology A: Vacuum, Surfaces, and Films, 1999. **17**(4): p. 1705-1709.
15. Tang, D.C., et al., *High Pressure Scanning Tunneling Microscopy Study of CO Poisoning of Ethylene Hydrogenation on Pt(111) and Rh(111) Single Crystals.* J. Phys. Chem. B, 2004. **108**(35): p. 13300-13306.
16. Montano, M., M. Salmeron, and G.A. Somorjai, *STM studies of cyclohexene hydrogenation/dehydrogenation and its poisoning by carbon monoxide on Pt(1 1 1).* Surface Science, 2006. **600**(9): p. 1809-1816.
17. Montano, M., et al., *Hydrogen and Deuterium Exchange on Pt(111) and Its Poisoning by Carbon Monoxide Studied by Surface Sensitive High-Pressure Techniques.* J. Am. Chem. Soc., 2006. **128**(40): p. 13229-13234.
18. Bratlie, K.M., et al., *Sum Frequency Generation Vibrational Spectroscopic and High-Pressure Scanning Tunneling Microscopic Studies of Benzene Hydrogenation on Pt(111).* J. Am. Chem. Soc., 2006. **128**(39): p. 12810-12816.
19. Bratlie, K.M., C.J. Kliewer, and G.A. Somorjai, *Structure Effects of Benzene Hydrogenation Studied with Sum Frequency Generation Vibrational Spectroscopy and Kinetics on Pt(111) and Pt(100) Single-Crystal Surfaces.* The Journal of Physical Chemistry B, 2006. **110**(36): p. 17925-17930.
20. Fischer, T.E., S.R. Kelemen, and H.P. Bonzel, *Adsorption of acetylene and benzene on the Pt(100) surface.* Surface Science, 1977. **64**(1): p. 157-175.
21. Pennemann, B., K. Oster, and K. Wandelt, *Hydrogen adsorption on Pt(100) at low temperatures: work function and thermal desorption data.* Surface Science, 1991. **249**(1-3): p. 35-43.
22. Horch, S., et al., *Enhancement of surface self-diffusion of platinum atoms by adsorbed hydrogen.* Nature, 1999. **398**(6723): p. 134-136.
23. Kliewer, C.J., *In-situ Studies of the Reactions of Bifunctional and Heterocyclic Molecules over Noble Metal Single Crystal and Nanoparticle Catalysts Studied with Kinetics and*

Sum-Frequency Generation Vibrational Spectroscopy, in *Chemistry*. 2010, UC Berkeley: Berkeley. p. 151.

Chapter 5. Adsorbate-Induced Regeneration of the Pt(100) Hex Reconstruction and Enhancement of Pt Surface Mobility

5.1 Abstract

In heterogeneous catalysis on metallic surfaces, the structure of the outermost atomic layer is modified by gas-phase adsorption which makes *in-situ* characterization essential in the understanding of catalyst activity. In the presence of 10^{-6} Torr ethylene at room temperature, the corrugated hexagonally symmetric surface reconstruction is lifted into a (1x1) structure with 2-3 nm Pt islands. At an elevated pressure of 1 Torr ethylene, the hex reconstruction is regenerated under the adsorbate layer. Through this transformation to the hex structure the Pt surface atoms conform to the preferential binding geometry of the adsorbates while at low pressure the surface matches the bulk (100) geometry. The dominance of the adsorbate interactions at high pressure also leads to an increased mobility of the underlying Pt surface atoms which are reversibly deformed by the tip during STM imaging. The mobility is linked to the activity of the surface which can be stabilized through catalytic poisoning.

5.2 Introduction

Ethylene hydrogenation on Platinum single crystals has been studied extensively as a model system in heterogeneous catalysis. Much of this work has been devoted to the understanding of the nature of the adsorbate bonding as it relates to the mechanism for the activation of alkene hydrogenation reactions. This work studies local atomic structural rearrangements of the Pt surface on the (100) crystal face induced by adsorbate interactions at elevated pressures using scanning tunneling microscopy (STM).

The exposed surface atoms on the (100) fcc crystal face have cubic packing symmetry but the clean Pt(100) surface exhibits the Pt(100)-hex surface reconstruction with a more densely packed quasihexagonal surface layer, which is similar in structure to a (111) layer with corrugated rows running in the [011] and [01-1] directions [1-3]. Experiment and theory suggest that the hex phase is confined to the outermost surface layer with the second atomic layer near to the bulk-terminated geometry [4]. The adsorption of CO, O_2, NO, and C_2H_4 have been shown to lift the hex reconstruction resulting in a (1x1) structure where the Pt surface reverts to the four-fold symmetry of the (100) surface [1, 2, 4-7]. High resolution STM studies show periodic corrugated rows on the clean hex-reconstructed surface compared with a roughened surface with 2-3 nm wide islands on the lifted (1x1) structure resulting from the extra Pt atoms in the more densely packed hex phase that are promoted to an incomplete surface layer when the Pt surface reorganizes to the bulk terminated positions [3, 4, 8-10].

It has been shown that upon low pressure dosing at 120 K, ethylene adsorbs molecularly on the Pt(100) surface [7]. This species lies parallel to the surface and physisorbs through the π-bond. However at 300 K, the adsorbed ethylene is present in the form of two majority species

which preferentially bind to 3-fold hollow sites: a di-σ-bonded species ($CH_2\eta$-$CH_2\eta$) and ethylidyne ($\eta\equiv C$-CH_3) which has undergone a partial dehydrogenation [7, 11]. SFG vibrational spectra has shown that ethylidyne and di-σ-bonded ethylene remain on the Pt(100) surface when the pressure is increased to 35 Torr ethylene [11]. Hydrogen molecules are known to adsorb dissociatively on Pt surfaces resulting in H atom adsorbates. At catalytically active temperatures and pressures, the most active catalytic pathway for hydrogenation is thought to involve the π-bonded physisorbed species, which then combines stepwise with two adsorbed hydrogen atoms with the resulting weakly bound ethane product desorbing from the surface [11].

Ethylene has previously been studied on Pt(111) using STM looking at both the adsorption behavior [12, 13] and, in our laboratory, the high pressure hydrogenation reaction [14]. At 160 K, Land et al. imaged ordered structures of di-σ-bonded ethylene [12]. In order to image the ordered ethylidyne structure, the adsorbed ethylene was first heated to 350 K to convert all the adsorbed ethylene to ethylidyne and subsequently cooled to 180 K [12, 13]. Above this temperature, ordered STM images have not been obtained although LEED shows a (2x2) structure [13]. The difficulty in imaging ethylidyne above 180K is likely to be a result of the low barrier for diffusion which was calculated to be (~0.1 eV) over a bridge position between two 3-fold hollow sites [15]. Tang et al. attributed the absence of ordering in the 300K STM images of Pt(111) exposed to hydrogen and ethylene to the rapid diffusion of the mobile adsorbed ethylidyne layer [14]. The transition to disordered STM images caused by adsorbate diffusion has been studied previously [16] and has been identified as characteristic of catalytic activity in the hydrogenation reactions studied by in-situ STM in our laboratory [14, 17, 18].

STM studies by Ronning et al. showed the lifting of the Pt(100) hex reconstruction by ethylene [19]. Exposing the surface to 2 x 10^{-8} Torr ethylene caused the (1x1) structure to develop. Through a series of STM images at exposures from 9 to 72 L, they showed the accumulation of raised lines on the surface that were attributed to the formation of the (1x1) structure. The lifting of the hex reconstruction preferentially began at defect sites and step edges and propagated in lines following the rows of the hex corrugation. After saturation, the surface was heated in vacuum and was found to partially reform the hex surface after desorption/decomposition of the adsorbates at 670 K with a complete transition to the hex surface being observed at 900 K.

Our work builds upon these extensive studies characterizing the structural changes on the surface at low pressure and the chemical composition over a range of pressures by investigating the changes in surface structure surface dynamics induced by the presence of high pressures of ethylene.

5.3 Experiment

The experiments were conducted on a High Pressure Scanning Tunneling Microscope (HP-STM) system that has been described previously [20]. Briefly, a UHV system with a base pressure of 10^{-10} Torr has been designed for reaction studies on single crystals. The Pt(100) crystal is cleaned through repeated cycles of Argon sputtering at 20 mA and 1 keV in a 2 x 10^{-5} Torr Ar followed by 5 min annealing cycle in the presence of 10^{-7} Torr O_2, and an annealing

cycle at 800˚C for 15 min. These sputtering and annealing cycles were repeated until the Auger spectra showed an absence of carbon impurities on the surface. The high pressure chamber houses a VT-300 RHK STM that can be isolated from the UHV environment to allow the introduction of reactant gases. Under scanning conditions, the system is floated on air legs for vibration damping. The STM images were obtained using a Tungsten tip that was electrochemically etched in a 2 M KOH solution [21]. All STM images were acquired using constant current mode.

5.4 Results and Discussion

Regeneration of the Hex Reconstruction at High Pressure

In agreement with previous studies, the STM images of the clean Pt(100) surface show the corrugated structure of the hex reconstruction (Figure 5.1). Although atomic resolution of the clean Pt surface was not obtained, single atom vacancies are clearly visible. Figure 5.2A is a $(50\ nm)^2$ STM image of Pt(100) at 300K in the presence of 10^{-6} Torr C_2H_4.

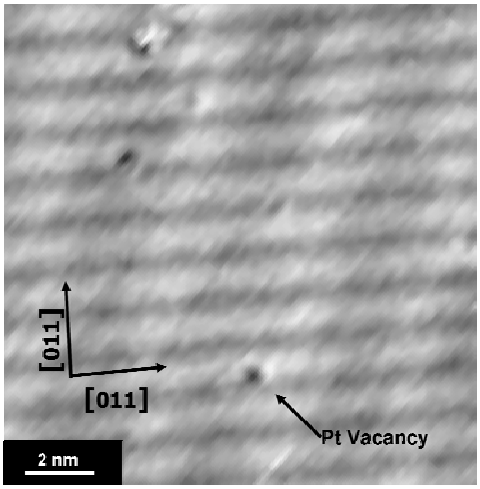

Figure 5.1: $(14\ nm)^2$ Image of clean hex reconstructed Pt(100) surface.

Ethylene adsorption caused a lifting of the hex reconstruction with the image showing the (1x1) island morphology. However, when the surface was exposed to 1 Torr C_2H_4 at 300K, the corrugated surface of the hex reconstruction persisted at this high pressure and was detectable under the adsorbate layer in the STM (Figure 5.2B). An STM image of the clean surface with the corrugated hex reconstruction is overlayed as an inset in Figure 5.2B at the same magnification and orientation as the $(50\ nm)^2$ high pressure image. This is the first report of the regeneration of the hex reconstruction at a high adsorbate pressure. Three 7 nm line scans of the apparent topography in the [011] direction in the STM images are plotted Figure 1C. The corrugation of the surface at 1 Torr ethylene (solid gray line) is in close agreement with the clean hex reconstructed periodicity (dashed gray line) in contrast to the higher topography and larger periodicity structure of the lifted (1x1) morphology at 10^{-6} Torr ethylene (solid black line). The presence of a high pressure of ethylene stabilizes the hexagonal surface phase causing the surface

to exhibit a different structure than that at low pressure which results in the formation of 3-fold hollow sites, the most energetically favorable for the ethylidyne and di-σ-bonded adsorbate species.

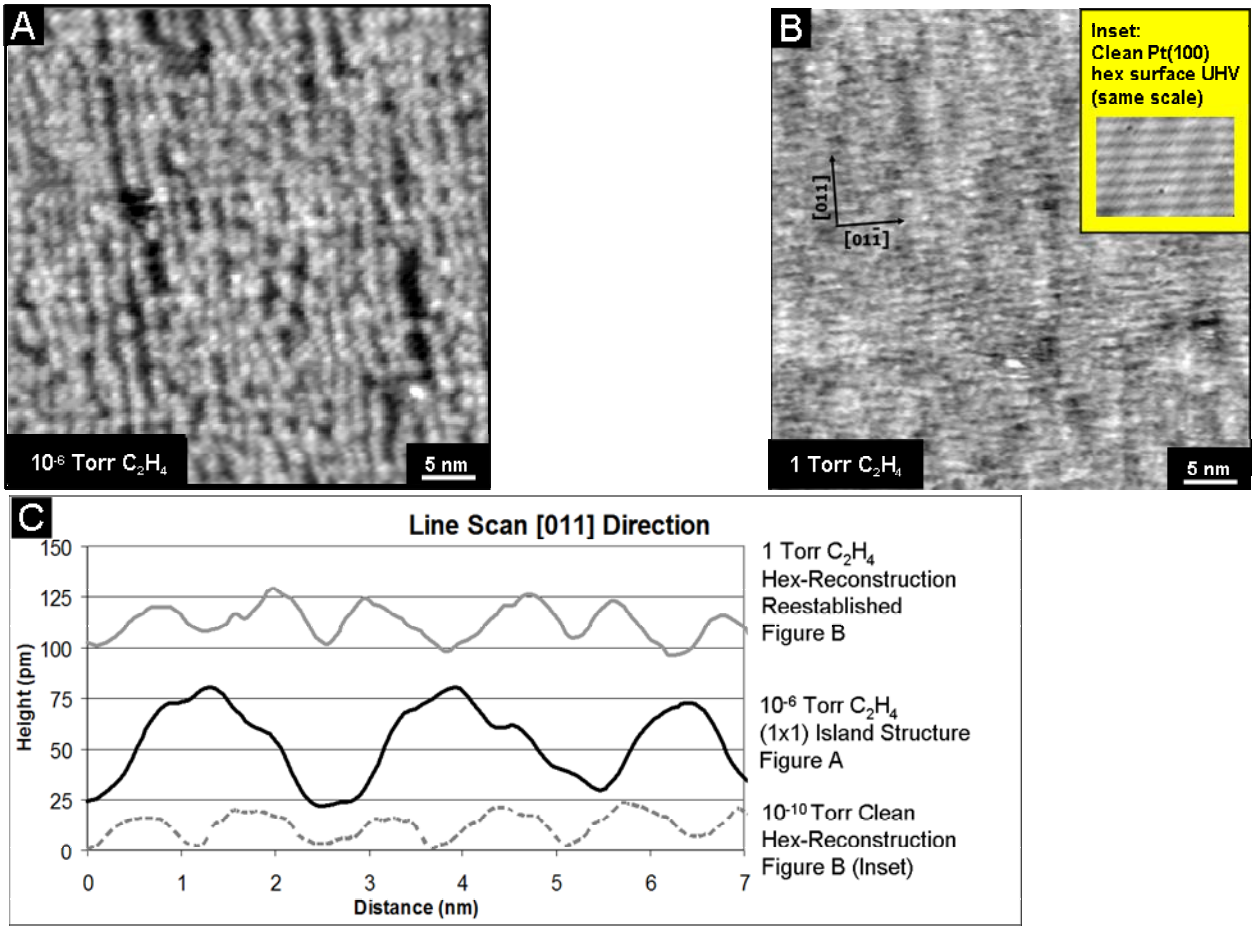

Figure 5.2: A: $(50\ nm)^2$ STM image of Pt(100) at 300 K in 10^{-6} Torr C_2H_4 with (1x1) lifted reconstruction and 2-3 nm Pt islands. B: $(50\ nm)^2$ STM image of Pt(100) at 300 K in 1 Torr C_2H_4. The corrugated rows running in the [011] direction show the regenerated hex-reconstruction (the inset shows the rows of the hex reconstruction on the clean surface at the same scale and orientation for comparison). C: 7 nm line scans of the STM topography on the clean hex surface (dashed), the (1x1) islands in 10^{-6} Torr C_2H_4 (black), and the hex surface reformed in 1 Torr C_2H_4.

Mobility of the Pt Surface at high pressure

At higher magnification, the STM images of the Pt(100) surface in the presence of high pressures of ethylene show that the surface is not static. In a series of three $(10\ nm)^2$ STM images taken at the same location at 300 K in 1 Torr ethylene show distortions in the corrugated rows of the high pressure hex reconstruction Figure 5.3. A defect site shared by the three images has been marked with an X. Figure 5.3A was acquired scanning in the horizontal direction with the images in 5.3B and C scanned vertically. The images show that the rows are reversibly

distorted by the tip interaction as it scans the surface with the corrugated hex reconstruction appearing roughly linear when the tip scans along the row and warped when the tip scans back and forth perpendicular to the rows. The modified structure is reversible since the pattern of the deformations change in consecutive images. The image in Figure 5.3B, where the corrugated rows appear uniform was taken in the same location at the same imaging conditions (+0.4 V and 0.2 nA) with the distortions becoming more apparent with decreasing scan area. This behavior shows that at 1 Torr ethylene the Pt surface layer is a flexible skin with a decreased barrier for diffusion across the Pt surface. The high pressure condition results in an adsorbate layer that appears to weaken the interaction of the top surface layer with the underlying Pt.

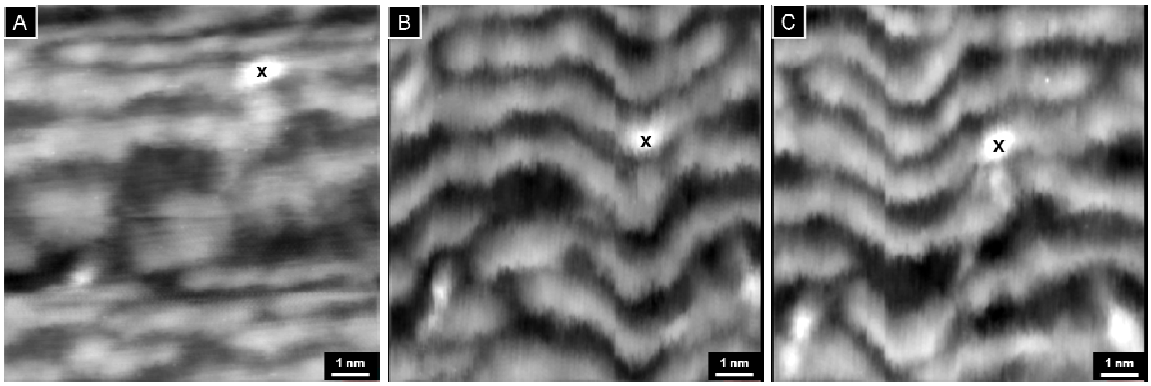

Figure 5.3: $(10\ nm)^2$ STM images scanning in the horizontal direction (A) and the vertical direction (B-C). The three images were taken at 1 Torr C_2H_4 and 300 K in the same location and the X marks a shared defect feature. Figures B and C show the reversible distortions caused by the STM tip dragging Pt surface atoms as it scans perpendicular to the corrugated rows.

When 1 Torr of H_2 was added to the 1 Torr ethylene at 300K, the hydrogenation reaction was active on the Pt(100) surface. The turnover frequency of hydrogenation to ethylene was estimated to be ~5 molecules per Pt site per sec from the decrease in total pressure. In the $(100\ nm)^2$ STM image of Pt(100) in 1 Torr C_2H_4 and 1 Torr H_2 at 300K (Figure 5.4A) no features could be resolved. The inability to resolve the adsorbate layer under active hydrogenation conditions is a known effect that has been attributed to the catalytically active surface layer that is mobile on the timescale of the scan speed in our microscope [14, 17, 18]. When 4 mTorr CO is added to the reaction mixture (Figure 5.4B), the reaction is poisoned and CO lifts the reconstruction into a (1x1) island structure [8-10]. The more strongly binding CO molecule restructures the surface in the presence of Hydrogen and ethylene which are the majority species in the gas phase. These findings are consistent with the view of loosely bound mobile surface as the active catalyst.

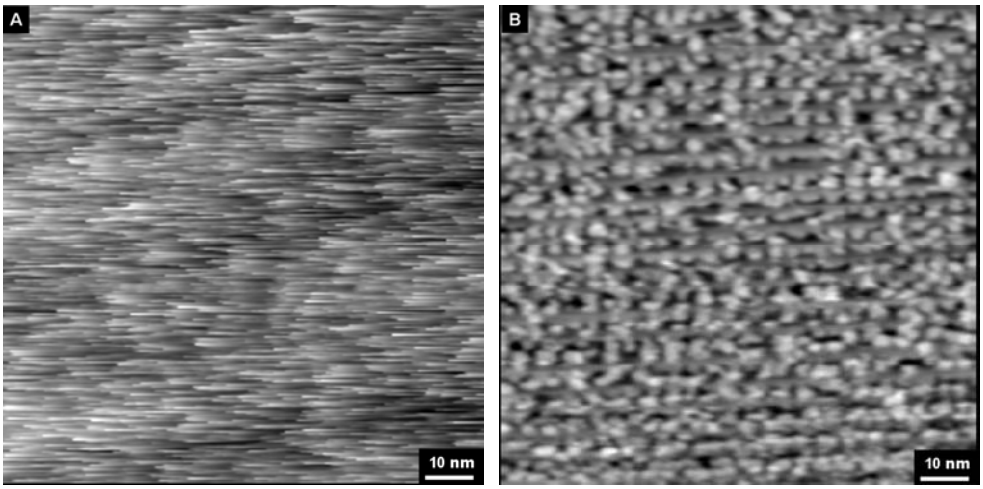

Figure 5.4: A: $(100\ nm)^2$ STM image in 1 Torr C_2H_4 and 1 Torr H_2 at 300 K. The hydrogenation reaction is active and no features are resolved. B: $(100\ nm)^2$ STM image after poisoning by CO taken in the presence of 1 Torr C_2H_4, 1 Torr H_2, and 4 mTorr CO at 300 K. The reaction is poisoned by CO stabilizing the surface layer and lifting the Pt(100) reconstruction resulting in 2-3 nm islands.

Discussion

Adsorption induces structural rearrangements on the Pt(100) crystal face. A low pressure ethylene caused a lifting of the hex reconstruction to the (1x1) structure. As the pressure of ethylene was increased to 1 Torr, the STM images show corrugated rows with a periodicity and amplitude consistent with the hex reconstruction reforming at high pressure. This behavior is an example of the catalyst surface being modified by adsorption to conform to the preferred geometry of the ethylidyne and di-σ-ethylene adsorbates. The STM images of the high pressure structure revealed that the Pt surface layer was mobile during imaging as it was reversibly deformed by the STM tip. These results suggest that at high pressure the adsorbate layer causes the Pt surface atoms to be more mobile. When 1 Torr H_2 was added the surface was active for the ethylene hydrogenation reaction resulting in an active surface that could not be imaged on the timescale of our STM although atomic steps were present in images with large scan areas. The addition of CO which binds strongly to the Pt surface poisoned this reaction and lifted the reconstruction forming 2-3 nm Pt islands.

Imaging the surface of the catalyst *in-situ*, was essential in the observation of these changes in the Pt surface. The surface phase transformation was induced by an increase in ethylene pressure, so it is clear that pressure plays a role in the catalyst surface structure. However, the ability of CO to reverse these changes shows that the adsorbate binding strength and geometry are also important factors. At 300K, ethylene preferentially adsorbs at three fold hollow sites in the form of ethylidyne and the di-σ-bonded species, where as CO will bind at both top and bridge sites. Since the three fold hollow sites are not present on the bulk terminated Pt(100) surface, the formation of the hex reconstruction can be explained by the bonding energetics of the ethylene adsorbate species. The surface rearrangement to conform to the

adsorbates creates a mismatch with the crystal structure resulting in a decreased barrier for lateral diffusion of the Pt surface layer. Since CO binds at top and bridge sites which are present on the (1x1) structure, its introduction stabilized the surface while still in the presence of high pressures of ethylene and Hydrogen.

5.5 Summary and Conclusions

Adsorption induces structural rearrangements on the Pt(100) crystal face. At low pressure ethylene caused a lifting of the hex reconstruction to the (1x1) structure. As the pressure of ethylene was increased to 1 Torr, the STM images show corrugated rows with a periodicity and amplitude consistent with the hex reconstruction reforming at high pressure. This behavior is an example of the catalyst surface being modified by adsorption to conform to the preferred geometry of the ethylidyne and di-σ-ethylene adsorbates. The STM images of the high pressure structure revealed that the top-most Pt layer was mobile during imaging as it was reversibly deformed by the STM tip. These results suggest that at high pressure the adsorbate layer causes the Pt surface atoms to be more mobile. When 1 Torr H_2 was added the surface was active for the ethylene hydrogenation reaction resulting in an active surface that could not be imaged on the timescale of our STM. The addition of 4 mTorr CO poisoned this reaction and lifted the reconstruction forming 2-3 nm Pt islands.

These results show in-situ STM to be a valuable tool to study morphological changes in the surface structure in the presence of gases. This study's finding of the structural rearrangement to the hex phase at elevated pressures of ethylene is a Pressure Gap phenomenon where the dynamic high pressure surface behavior is only accessible to in-situ techniques capable of operating in the presence of gases.

5.6 References

1. Hagstrom, S., H.B. Lyon, and G.A. Somorjai, *SURFACE STRUCTURES ON CLEAN PLATINUM (100) SURFACE.* Physical Review Letters, 1965. **15**(11): p. 491-&.
2. Bonzel, H.P., G. Brodén, and G. Pirug, *Structure sensitivity of NO adsorption on a smooth and stepped Pt(100) surface.* Journal of Catalysis, 1978. **53**(1): p. 96-105.
3. Borg, A., et al., *STM STUDIES OF CLEAN, CO-EXPOSED AND O2-EXPOSED PT(100)-HEX-R0.7-DEGREES.* Surface Science, 1994. **306**(1-2): p. 10-20.
4. Ritz, G., et al., *Pt(100) quasihexagonal reconstruction: A comparison between scanning tunneling microscopy data and effective medium theory simulation calculations.* Physical Review B, 1997. **56**(16): p. 10518.
5. Morgan, A.E. and G.A. Somorjai, *LOW ENERGY ELECTRON DIFFRACTION STUDIES OF GAS ADSORPTION ON PLATINUM (100) SINGLE CRYSTAL SURFACE.* Surface Science, 1968. **12**(3): p. 405-&.
6. Behm, R.J., et al., *The interaction of CO and Pt(100). I. Mechanism of adsorption and Pt phase transition.* The Journal of Chemical Physics, 1983. **78**(12): p. 7437-7447.
7. Hatzikos, G.H. and R.I. Masel, *Structure sensitivity of ethylene adsorption on Pt(100): Evidence for vinylidene formation on (1×1) Pt(100).* Surface Science, 1987. **185**(3): p. 479-494.

8. Sinsarp, A., et al., *Local tunneling barrier height studies of thermally treated CO and O-covered Pt(100) surfaces.* Japanese Journal of Applied Physics Part 1-Regular Papers Short Notes & Review Papers, 2004. **43**(7B): p. 4659-4662.
9. Tao, F., et al., *Restructuring of hex-Pt(100) under CO Gas Environments: Formation of 2-D Nanoclusters.* Nano Letters, 2009. **9**(5): p. 2167-2171.
10. Wakisaka, M., et al., *Structural Change and Electrochemical Behavior of Pt(100)-hex-R0.7[degree] Surfaces in Gases and in Solution.* Journal of The Electrochemical Society, 2003. **150**(2): p. E81-E88.
11. McCrea, K.R. and G.A. Somorjai, *SFG-surface vibrational spectroscopy studies of structure sensitivity and insensitivity in catalytic reactions: cyclohexene dehydrogenation and ethylene hydrogenation on Pt (1 1 1) and Pt (1 0 0) crystal surfaces.* Journal of Molecular Catalysis A: Chemical, 2000. **163**(1-2): p. 43-53.
12. Land, T.A., et al., *STM investigation of the adsorption and temperature dependent reactions of ethylene on Pt(111).* Applied Physics A: Materials Science & Processing, 1991. **53**(5): p. 414-417.
13. Land, T.A., et al., *Direct observation of surface reactions by scanning tunneling microscopy: Ethylene --> ethylidyne --> carbon particles --> graphite on Pt(111).* The Journal of Chemical Physics, 1992. **97**(9): p. 6774-6783.
14. Tang, D.C., et al., *High Pressure Scanning Tunneling Microscopy Study of CO Poisoning of Ethylene Hydrogenation on Pt(111) and Rh(111) Single Crystals.* J. Phys. Chem. B, 2004. **108**(35): p. 13300-13306.
15. Nomikou, Z., M.A. Van Hove, and G.A. Somorjai, *Molecular Modeling of Ethylidyne Adsorption and Diffusion on Pt(111).* Langmuir, 1996. **12**(5): p. 1251-1256.
16. Dunphy, J.C., et al., *Scanning-tunneling-microscopy study of the surface diffusion of sulfur on Re(0001).* Physical Review B, 1993. **47**(4): p. 2320.
17. Montano, M., et al., *Hydrogen and Deuterium Exchange on Pt(111) and Its Poisoning by Carbon Monoxide Studied by Surface Sensitive High-Pressure Techniques.* J. Am. Chem. Soc., 2006. **128**(40): p. 13229-13234.
18. Montano, M., M. Salmeron, and G.A. Somorjai, *STM studies of cyclohexene hydrogenation/dehydrogenation and its poisoning by carbon monoxide on Pt(1 1 1).* Surface Science, 2006. **600**(9): p. 1809-1816.
19. Ronning, M., et al., *Scanning tunnelling microscopic studies on the adsorption and decomposition of ethene on the reconstructed Pt(100)-hex-R0.7o surface.* Surface Science, 2001. **477**: p. 191-197.
20. McIntyre, B.J., et al., *A VARIABLE PRESSURE TEMPERATURE SCANNING TUNNELING MICROSCOPE FOR SURFACE SCIENCE AND CATALYSIS STUDIES.* Review of Scientific Instruments, 1993. **64**(3): p. 687-691.
21. Klein, M. and G. Schwitzgebel, *An improved lamellae drop-off technique for sharp tip preparation in scanning tunneling microscopy.* Review of Scientific Instruments, 1997. **68**(8): p. 3099-3103.

Chapter 6. Identification of a Reaction Stabilized Surface Oxide using *In-Situ* Ambient Pressure XPS to study the Size Dependence of CO Oxidation on Monodisperse Rh Nanoparticle Catalysts

6.1 Abstract

A surface oxide phase established under reactive conditions for CO oxidation which is chemically distinct from the oxide formed by heating in oxygen alone was identified using APXPS *in-situ* characterization on Rh nanoparticles. Rh nanoparticles in the size range of 2-11 nm were synthesized with monodisperse size distributions to study the effect of catalyst size on activity. This reaction stabilized surface oxide was found to be more prevalent on Rh nanoparticles of smaller size which were found to be more active for CO oxidation.

6.2 Introduction

CO oxidation is one of the most studied reactions in heterogeneous catalysis. The oxidation of CO to CO_2 is useful for the removal CO from exhausts and fuels [1], which can be desirable since it is an environmental and catalytic poison. The reaction is also of scientific interest as a test case to study the surface properties of catalysts in one of the simplest oxidizing reactions. Pt group metals are effective catalysts for CO oxidation. This study investigates the size dependence of CO oxidation on Rh nanoparticles and uses *in-situ* APXPS to study the surface in reactive conditions.

Nanoparticles are extensively used in industrial catalysis. These high surface area systems maximize the exposure to the gas phase by the increase in surface to volume ratio. In addition the properties of materials can change when their sizes are reduced to nanometer scales. In some cases nanoparticles have been found to show activity at lower temperature than the bulk materials [2, 3]. The structure of the nanoparticle surface has a high concentration of low coordination sites (step edges and kink sites), which have been shown to affect catalytic activity [4]. Additionally the size of nanoparticles is known to affect the electronic properties of the metals [5]. Understanding these factors motivates studies of the effect of size-dependence on catalytic behavior.

In order to study size dependent nanoparticle properties, it is necessary to develop syntheses with precise control of particle size. Nanoparticles are unstable structures with a high degree of surface strain. Evidence of this instability can be seen in the tendency of particles to sinter combining to form larger particles in high temperature reactions. The synthesis of metallic nanoparticles takes place by a solution phase reduction of metallic salts and requires stabilizing agents to keep the particles separated in the solution phase. Careful manipulation of the synthetic parameters can yield uniform samples with low size dispersion. These particles can then be deposited on supports producing a series of samples for size-dependence studies.

6.3 Experiment

Rh nanoparticles on 2D supports were studied with the Ambient Pressure X-ray Photoelectron Spectroscopy at beamline 11.0.2 of the Advanced Light Source at Lawrence Berkeley National Laboratory. The details of this system have been published previously [6]. APXPS makes use of a differentially pumped electron analyzer with an electrostatic lens that allows the measurement of photoelectrons from surfaces in the presence of gases (Figure 6.1). The effective operating range of this system is from UHV to a few Torr. The high pressure limit is due to the attenuation of the signal caused by adsorption and scattering of the photoelectrons by gas phase molecules. In photoelectron spectroscopy, an X-ray source is used to excite core level electrons which are ejected from the surface. XPS is a highly surface sensitive technique due to the short inelastic mean free path of (0-1 keV) photoelectrons in solids. The X-ray source passes deep within the sample however only those photoelectrons generated within a few atomic layers of the surface will escape and reach the detector without being scattered. These photoelectrons are then measured by an electron energy analyzer. Although the core level electrons are not involved in chemical bonding their binding energies are sensitive to the chemical environment of their surroundings. The photon energy for all spectra was chosen to excite photoelectrons with a kinetic energy of about 200 eV taking advantage of the tunable X-rays from the synchrotron light source. Constraining the photoelectrons to a single energy region ensures a consistent sampling depth in the experiments. In order to have consistent comparable binding energy measurements, the XPS spectra obtained from polymer capped metal nanoparticle samples deposited on silicon wafers must first be calibrated. The binding energy was normalized by shifting the maximum of the PVP C1s spectra to the reported value of 285.4 eV for PVP [7].

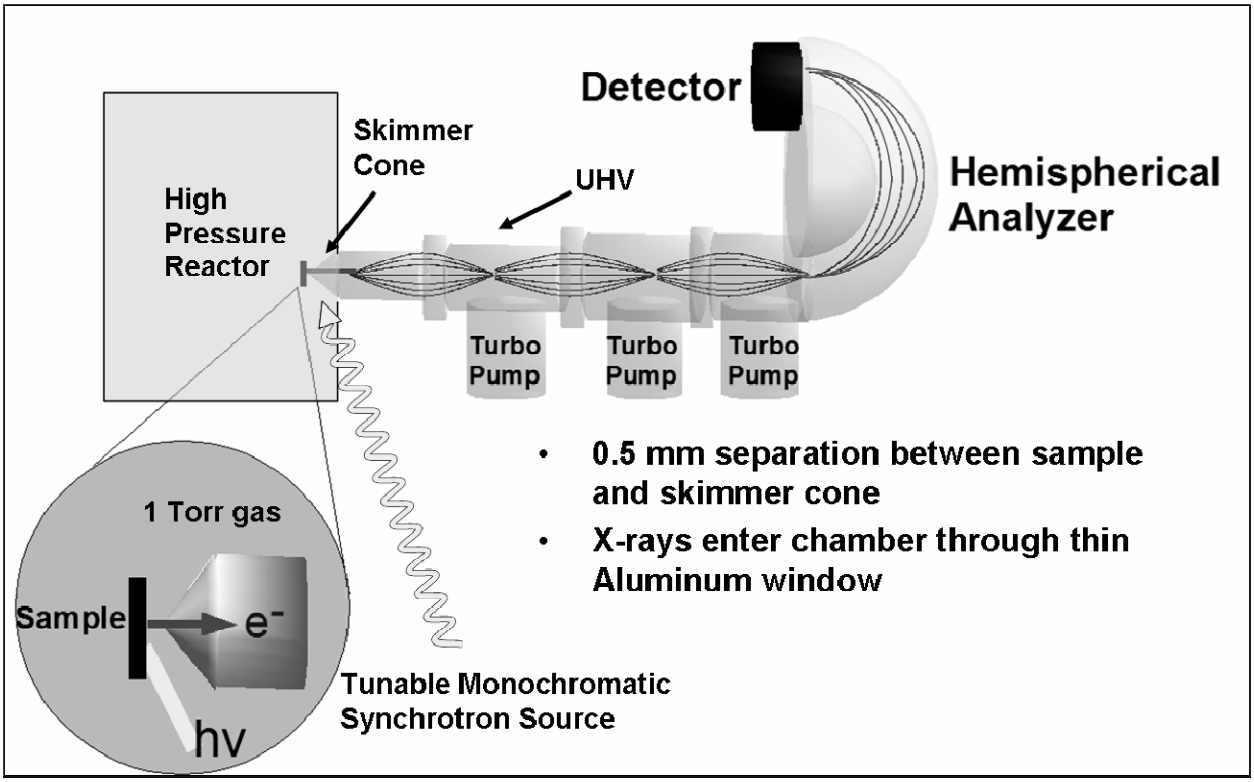

Figure 6.1 Schematic of the experimental setup for APXPS reaction chamber and differentially pumped analyzer.

6.4 Results and Discussion

A strategy expanding on the one step polyol synthesis for size controlled Rhodium nanoparticles [8] was developed using sodium citrate to extend the size range down to the 2 nm regime [9]. Poly(vinylpyrrolidone) (PVP) capped Rh nanoparticles were synthesized with diameters of: 1.9 ± 0.3, 2.5 ± 0.4, 3.6 ± 0.5, 7.1 ± 0.5, and 10.7 ± 0.9 nm. Monolayer films were prepared using the Langmuir-Blodgett technique. Figure 6.2 shows TEM images of the 1.9 and 7.1 nm Rh particles.

CO oxidation reactions were performed on the Rh nanoparticle samples deposited on silicon wafers in a flow reactor. The surface area of the samples was estimated from TEM and/or SEM images. Assuming the particles to be roughly spherical, the total Rh surface area was estimated to be four times the area in the images. The density of Rh atoms on that surface area was then estimated to be the same as the packing density on the Rh(111) crystal face. All the catalytic activity of the particles is reported as a turn over frequency relative to a Rh foil sample and was corrected for the estimated particle surface area. Although there may be errors in the calculated particle surface areas which will affect the magnitude of the reported turn over frequencies, the overall trends should be accurate because the area calculation was consistent for each of the samples.

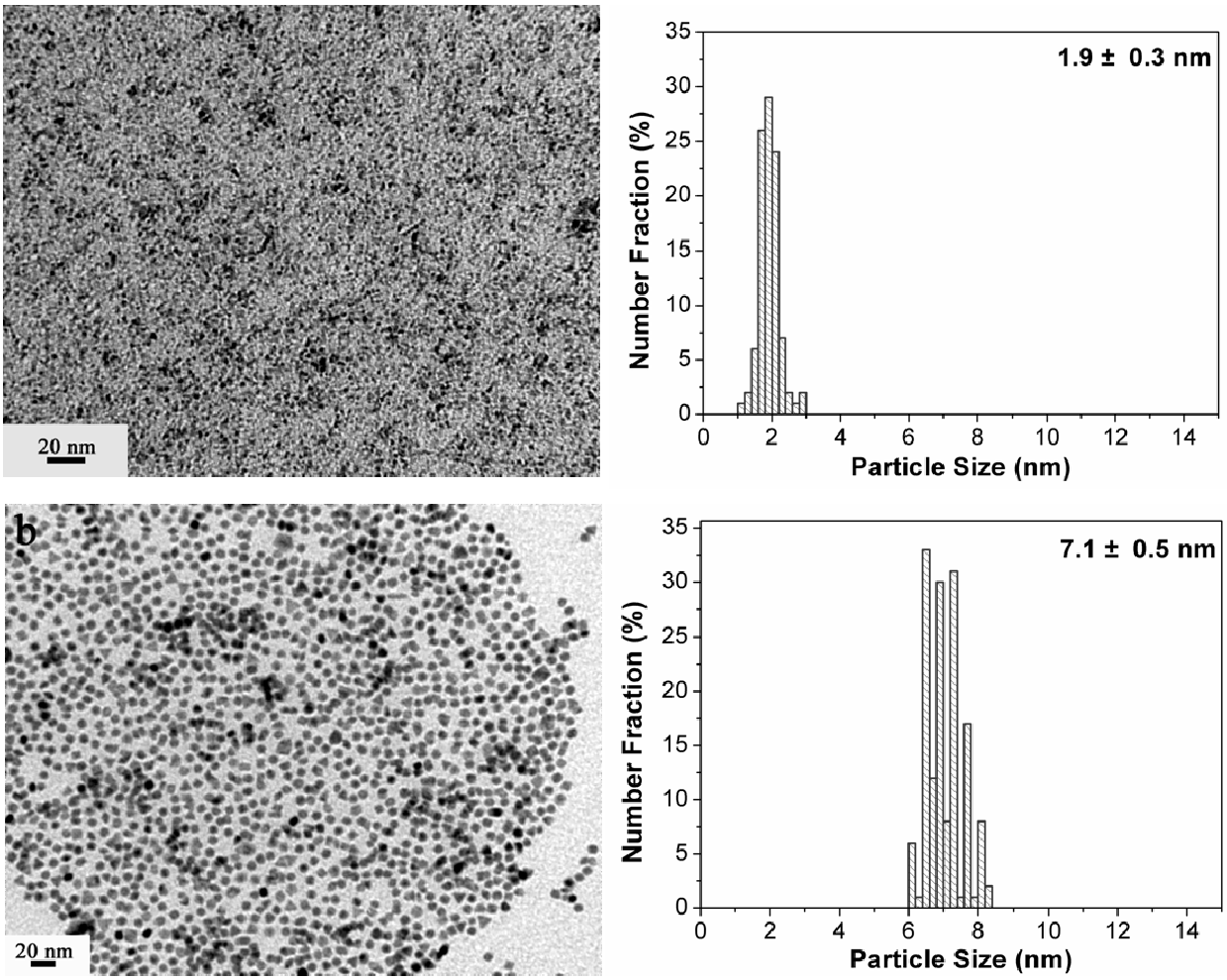

Figure 6.2 TEM images and particle size histograms of PVP capped 1.9 nm (top) and 7.1 nm (bottom) Rh particles.

The reactivity of the Rh nanoparticles for CO oxidation was found to have a strong size dependence. Figure 6.3 shows the reactivity at 200˚C, 50 Torr O_2, and 20 Torr CO relative to Rh foil (0.28 s^{-1}) and the activation energy of the Rh particles for the oxidation of CO to CO_2 over the range of temperatures from 150 to 225˚C. The catalytic activity increases as particle size decreases from 5.5 times that of the thin film for the 11 nm particles to 28 times for the 2 nm particles. This corresponds to a reduction in activation energy from 28 to 19 kcal mol^{-1}. The activity trends plotted in Figure 6.3 are fit with exponential curves.

The Rh nanoparticles did not deactivate when the reactions were run over multiple temperature cycles between 150 and 225˚C however at 250˚C the particles reduced in activity. SEM images of the particles revealed that the particles retained their original size distributions at 225˚C but sintered after the 250˚C reaction conditions. The deactivation was attributed to the increase in particle size and the corresponding decrease in surface area. The sintering was attributed to the decomposition of the PVP capping layer which stabilizes the particles and prevents aggregation.

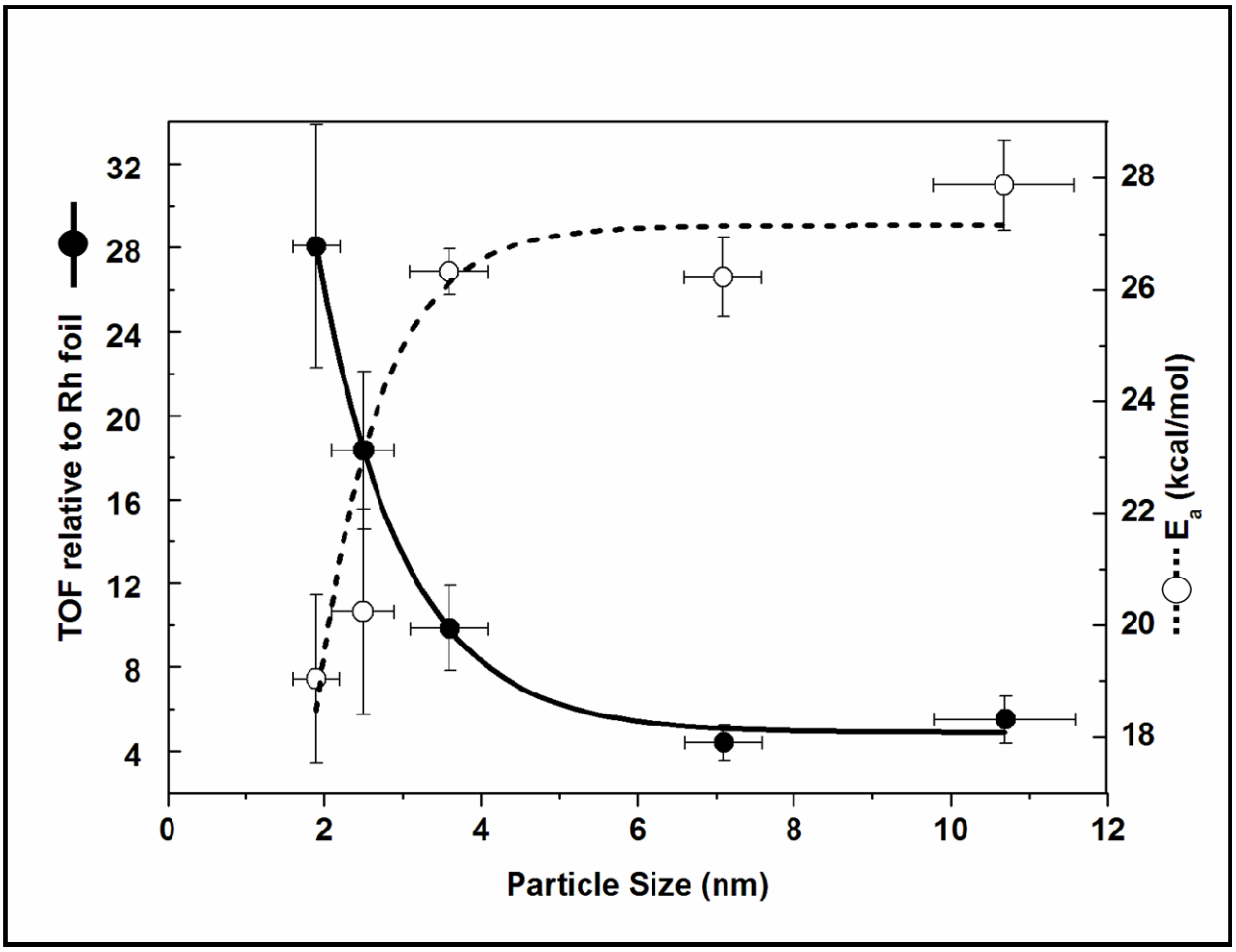

Figure 6.3 Turn over Frequency (TOF) relative to Rh foil (0.28 s^{-1}) at 200˚C, 50 Torr O_2, 20 Torr CO and Activation Energy (150-225˚C) for CO oxidation. TOF data plotted with solid black circles and solid black line. Activation Energy plotted with White circles and dashed line.

In order to gain insights into the size dependent activity of the Rh nanoparticles, *in-situ* studies were carried out on The PVP capped Rh nanoparticles deposited on silicon wafers using APXPS at beamline 11.0.2 at the Advanced Light Source at Lawrence Berkeley National Laboratory. In these experiments spectra were acquired when the samples were exposed to 200 mTorr CO at 25, 100, 150, and 200˚C. The samples were then cooled to room temperature and the chamber was evacuated to 10^{-8} Torr. The chamber was then filled with 500 mTorr O_2 and spectra were taken over the same temperature range. Lastly 500 mTorr O_2 and 200 mTorr CO was added to the chamber and the sample was heated. Due to the experimental design of the APXPS sample heater which uses narrow gauge bare Pt electrical leads, as current is delivered to the heater the leads are active for CO oxidation. Blank runs were conducted to quantify this effect and in the reactive mixture, the sample was found to be in the presence of equilibrium pressures of 20 mTorr CO, 180 mTorr CO_2, and 410 mTorr O_2.

The Rh 3d spectra contain multiple overlapping peaks from the different chemical species. In order to understand the contributions of these components, fittings were performed using the

XPS Peak 4.1 freeware package. The peak fitting parameters were first determined for the 7 nm Rh 3d spectra at 200˚C in the presence of CO, which was the most highly reduced experimental condition. The 3d spectra consisting of both the $3d_{5/2}$ and $3d_{3/2}$ was fit with a spin orbit splitting of 4.74 eV using the known area ratio of (3:2). The peaks were then adjusted allowing the program to optimize the binding energy, peak width, peak area, and Gaussian/Lorenzian mixing. An asymmetric peak shape was needed to accurately fit the spectra. The Gaussian/Lorenzian and peak asymmetry parameters were then kept constant for the remainder of the peak fittings. The reduced Rh(0) spectra was fit with a 30% Lorenzian peak with asymmetry parameters (TS = 0.155, TL = 180), a FWHM peak width of 0.91 eV ($3d_{5/2}$) and 1.29 eV ($3d_{3/2}$), and a $3d_{5/2}$ binding energy 307.51 eV. The Rh(0) fitting parameters were then constrained for the metallic component of the 2 nm Rh nanoparticles at 200˚C in 500 mTorr O_2. In order to accurately fit the spectra in oxidizing conditions two higher binding energy peaks were added using the same peak parameters as in the Rh(0) at +0.91 and +2.01 eV. The relative binding energies were then held constant but the total was allowed to shift up to 0.2 eV to compensate for errors in the absolute binding energy.

Figure 6.4 shows the changes in the Rh 3d spectra caused by the presence of CO for the 7 nm (left column) and the 2 nm (right column) Rh particles. In the top spectra, the particles are in UHV before the CO exposure. The 2 nm particles are significantly oxidized at the start of the experiment due to exposure to the air whereas the 7 nm particles are metallic. When CO is added to the chamber at 25˚C, the spectra are not significantly changed, however when the sample is heated to 100˚C, the XPS peaks become narrower. This is caused by a reduction of the capacitance between the particles and the support due to changes in the capping layer. When the temperature is raised to 150˚C in the presence of CO, the 2 nm sample begins to reduce with the Rh(0) metallic peak becoming the dominant surface species. At 200˚C, the particles reduce further but the 2 nm particles still show a small oxidized peak on the high binding energy side relative to the 7 nm sample.

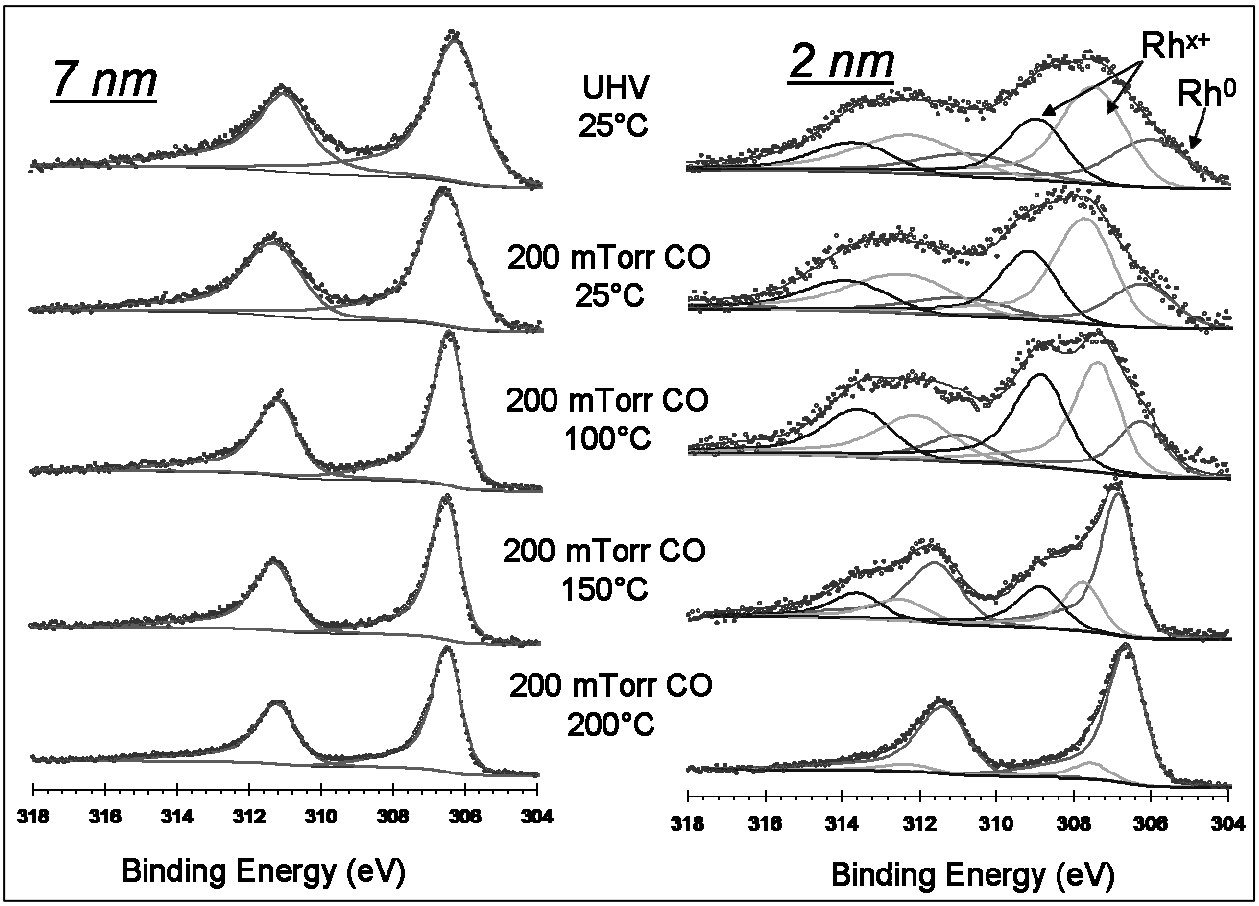

Figure 6.4 Rh 3d spectra of 7 (left) and 2 (right) nm particles at UHV and in the presence of 200 mTorr CO. As the temperature increases, the 2 nm samples, which were initially oxidized, become reduced.

After the samples were cooled and the CO was evacuated 500 mTorr O_2 was introduced. Figure 6.5 contains a series XPS spectra of the 7 nm (left column) and 2 nm (right column) particles in the presence of oxygen over the same range of temperatures from 25-200˚C. The 2 nm particles have clear oxide peaks at room temperature. As the samples are heated in the presence of oxygen, both particles develop an oxide layer however the contribution from the oxidized peak is larger on the smaller particles.

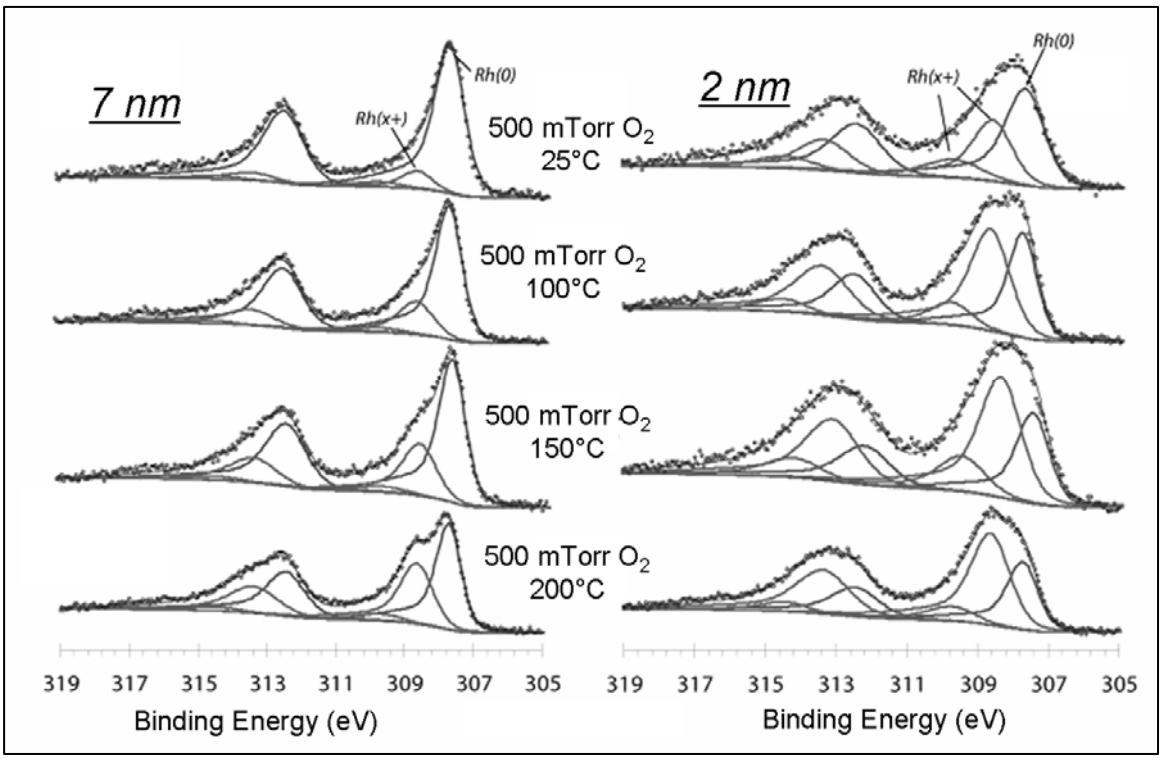

Figure 6.5 Rh 3d spectra of 7 (left) and 2 (right) nm particles at in the presence of 500 mTorr O_2. As the temperature increases, the Rh nanoparticle surface becomes in increasingly oxidized with the 2 nm particles oxidizing at a lower temperature.

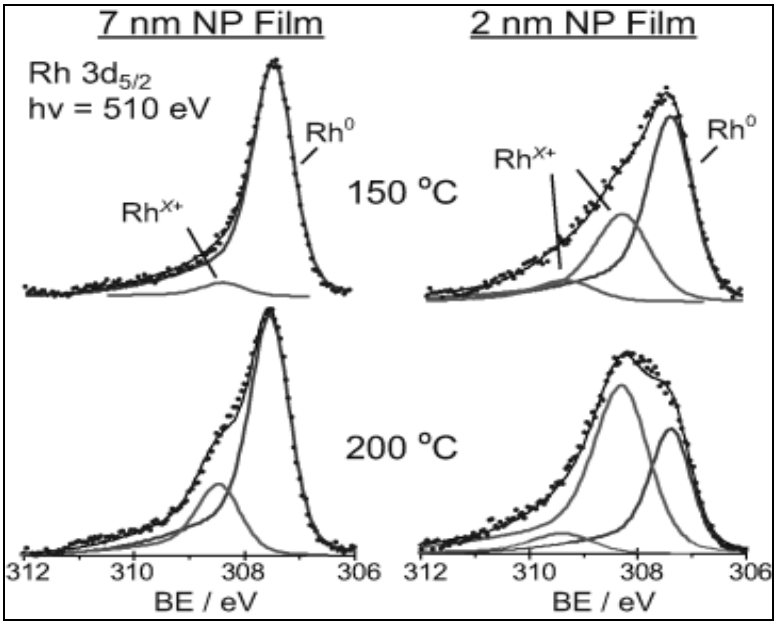

Figure 6.6 Rh $3d_{5/2}$ spectra in the reactive CO, O_2, and CO_2 gas mixture.The smaller particles have a larger contribution from the oxidized Rh species.

In the presence of the reaction mixture, the same trend holds. Figure 6.6 shows the Rh $3d_{5/2}$ spectra in the reaction mixture of 20 mTorr CO, 180 mTorr CO_2, and 410 mTorr O_2. The O1s spectra plotted in Figure 6.7 shows some interesting behavior. Panels A and B contain the O1s spectra for the 2 and 7 nm particles at 100 and 200˚C in the presence of 500 mTorr O_2. Panels C and D show the same particles in the reaction mixture of 20 mTorr CO, 180 mTorr CO_2, and 410 mTorr O_2. The peaks at 538 and 539 eV in all for panels are the gas phase O_2 doublet. At 537 eV a shoulder due to $CO_{(g)}$ can be seen on the $O_{2(g)}$ peaks in panels C and D, which also show a strong $CO_{2(g)}$ signal. The broad peak at 532 eV contains the various oxygen surface species including the oxide layer on the Si wafer, the polymer cap, and the surface species on the Rh nanoparticles themselves. Although the Rh3d spectra under reaction conditions (Figure 6.6) was consistent with the oxidation and reduction behavior in the CO and O_2 treatments (figures 6.4 and 6.5), the O1s spectra shows a shoulder at 529.5 eV that was not present in any of the CO or the O_2 treatments. This peak is attributed to a distinct surface oxide stabilized by the reactive conditions or reaction intermediate and is more pronounced on the 2 nm than in the 7 nm particles. The intensity of this peak decreases when the sample is cooled to room temperature indicating that it is related to the reactive conditions.

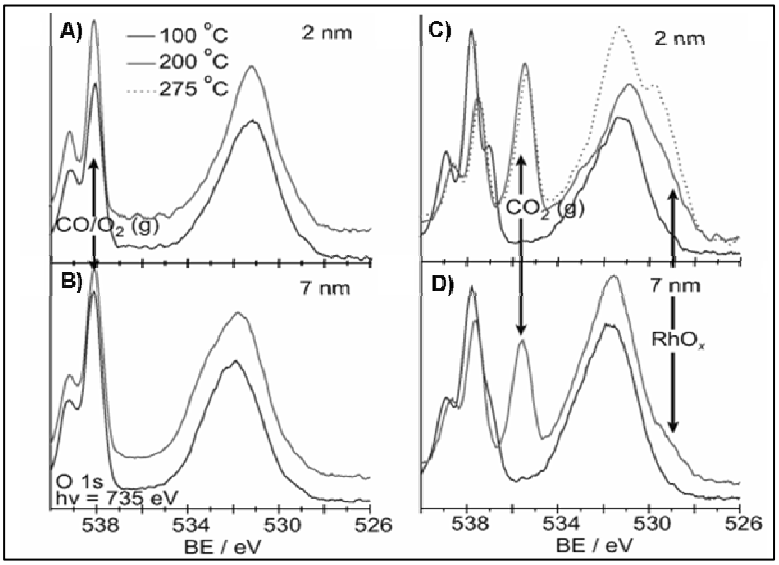

Figure 6.7 O1s XPS spectra taken in the presence of 500 mTorr O_2 on 2 nm (A) and 7 nm (B) samples and in the presence the reactive mixture (20 mTorr CO, 180 mTorr CO_2, and 410 mTorr O_2) for both the 2 nm (C) ad 7 nm (D) samples. During the reaction at high Temperature (C-D) the formation of a reaction stabilized oxide species grows in at 529.5 eV.

6.5 Conclusions

CO oxidation reactions performed on size controlled Rh nanoparticles revealed that the catalytic activity increases with decreasing particle size in the 2-11 nm size range. APXPS was used to characterize the catalyst surface layer *in-situ* and identified a reaction stabilized oxide species with a distinct O1s chemical shift from the oxide peak formed by heating in O_2 alone.

The XPS data also shows the formation of the oxidized Rh peaks occurs at lower temperatures for smaller Rh particles.

6.6 References

1. Watanabe, M., et al., *Hydrogen purification for fuel cells: selective oxidation of carbon monoxide on Pt-Fe/zeolite catalysts.* Applied Catalysis B: Environmental, 2003. **46**(3): p. 595-600.
2. Haruta, M., et al., *Low-Temperature Oxidation of CO over Gold Supported on TiO2, [alpha]-Fe2O3, and Co3O4.* Journal of Catalysis, 1993. **144**(1): p. 175-192.
3. Valden, M., X. Lai, and D.W. Goodman, *Onset of Catalytic Activity of Gold Clusters on Titania with the Appearance of Nonmetallic Properties.* Science, 1998. **281**(5383): p. 1647-1650.
4. Kunimatsu, K., et al., *Role of terrace/step edge sites in CO adsorption/oxidation on a polycrystalline Pt electrode studied by in situ ATR-FTIR method.* Electrochimica Acta, 2008. **53**(21): p. 6104-6110.
5. Wang, L. and Q. Ge, *Studies of rhodium nanoparticles using the first principles density functional theory calculations.* Chemical Physics Letters, 2002. **366**(3-4): p. 368-376.
6. Bluhm, H., et al., *Soft X-ray microscopy and spectroscopy at the molecular environmental science beamline at the Advanced Light Source.* Journal of Electron Spectroscopy and Related Phenomena, 2006. **150**(2-3): p. 86-104.
7. Beamson and D. Briggs, *High Resolution XPS of Organic Polymers: The Scienta ESCA300 Database*. 1992, New York: John Wiley & Sons.
8. Zhang, Y., et al., *One-step Polyol Synthesis and Langmuirâ˜Blodgett Monolayer Formation of Size-tunable Monodisperse Rhodium Nanocrystals with Catalytically Active (111) Surface Structures.* The Journal of Physical Chemistry C, 2007. **111**(33): p. 12243-12253.
9. Grass, M.E., et al., *A Reactive Oxide Overlayer on Rhodium Nanoparticles during CO Oxidation and Its Size Dependence Studied by In Situ Ambient-Pressure X-ray Photoelectron Spectroscopy13.* Angewandte Chemie International Edition, 2008. **47**(46): p. 8893-8896.

Chapter 7. *In-situ* APXPS Characterization of the Catalytic Reaction-Induced Surface Segregation of RhPd and PdPt Bimetallic Nanoparticle Catalysts

7.1 Abstract

The reaction-induced surface segregation behavior of bimetallic noble metal nanoparticles was observed with APXPS. Monodisperse 15 nm RhPd and PdPt nanoparticles were synthesized with well controlled Rh/Pd and Pd/Pt compositions. *In-situ* XPS studies showed that at 300 ˚C in the presence of and oxidizing environment (100 mTorr NO or O_2), the surface concentration of the more easily oxidized element (Rh in RhPd and Pd in PdPt) was increased. Switching the gas environment to more reducing conditions (100 mTorr NO and 100 mTorr CO) caused the surface enrichment of the element with the lowest surface energy in its metallic state. Using *in-situ* characterization, the redox chemistry and the surface composition of bimetallic nanoparticle samples were monitored in reactive conditions. The particle surfaces were shown to reversibly restructure in response to the gas environment at high temperature.

7.2 Introduction

Bimetallic catalysts are widely used in industry because by changing composition the surface properties of catalysts can be changed to improve catalytic activity [1]. These studies use *in-situ* surface characterization to monitor the restructuring of the catalyst surface in response to changing gas environments [2]. Although the catalytic activity of nanoparticles is widely studied, few techniques are capable of characterizing the chemical composition of the surface under reactive conditions. Ambient Pressure X-ray Photoelectron Spectroscopy (APXPS) was used to study the changes in surface composition of RhPd, PdPt, and RhPt bimetallic nanoparticle systems in the presence of gases.

Model systems allow the systematic study of bimetallic catalysts. Colloidal techniques can be used to synthesize nanoparticles with uniform size distribution and composition. Nanoparticles are synthesized through the reduction of metallic salts in the presence of a polymer capping agent used to prevent aggregation of the particles. The size of the particles is controlled by the concentration of the precursor and the kinetics of particle nucleation and growth in the presence of the solvent and surfactant molecules. In some cases, with the right reaction conditions, a bimetallic nanoparticle synthesis can be performed in a one pot synthesis where differences in reduction potentials allow the reduction to occur stepwise with one metal first forming particles with the second metal forming a shell on the outside of those particles. In this way, bimetallic particles are prepared with uniform and tunable concentrations of the two components.

7.3 Experiment

15 nm $Rh_{0.5}Pd_{0.5}$ nanopaticles were synthesized in solution under Argon. 0.05 mmol $Rh(acac)_3$, 0.05 mmol $Pd(acac)_2$, and 1 mmol PVP in 20 ml 1,4-butanediol was heated to 50 ˚C in a 50 ml three neck flask and evacuated for 20 min while stirring to remove water and oxygen resulting in a transparent orange-yellow solution. The solution was heated to 220 ˚C in Ar gas at 10 ˚C min^{-1} and maintained at 220 ˚C for 90 min. After the reaction the solution was washed in acetone forming a black suspension containing the product. The black precipitate was separated washed with acetone and dispersed in ethanol. $Pd_{0.5}Pt_{0.5}$ particles were synthesized similarly using 0.05 mmol $Pt(acac)_2$ and 0.05 mmol $Pd(acac)_2$ for the precursor and a reaction temperatire of 215 ˚C for 30 min. The syntheses produced 15 ± 2 nm particles which were characterized using SEM, TEM, XRD, and XPS. For SEM and XPS, a monolayer films of the particles were deposited on a Si wafer support using a Langmuir-Blodgett trough.

The bimetallic nanoparticle samples were studied using APXPS at beamline 9.3.2 at the Advanced Light Source (ALS) at Lawrence Berkeley National Laboratory. In APXPS, the sample is located in a UHV chamber that can be filled with high pressures of gases. A skimmer cone with a small diameter aperture (~0.5 mm) that separates the high pressure cell from the electron analyzer is brought within a distance of less than 1 mm from the sample surface. The analyzer is differentially pumped by a series of turbomolecular pumps that bring the analyzer pressure to UHV allowing the detection of the photoelectron signal without scattering from the gas phase. Additionally the photoelectron signal is increased using an electrostatic lens before reaching the analyzer [3, 4]. This allows the use of XPS from UHV up to a working gas pressure of ~1 Torr, with the upper limit caused by the loss of signal by gas phase scattering of the electrons.

7.4 Results and Discussion

XPS analysis in vacuum show that the metal composition of the 15 nm Rh_xPd_{1-x} and Pd_xPt_{1-x} particles is different at the surface than in the bulk. In XPS, the photoelectron kinetic energy is dependent on the photon energy. At the kinetic energies used in these experiments, the inelastic mean free path of the photoelectrons, which determines the sampling depth, increases with energy. Once corrections are made for the energy dependence of the photoionization cross section and any intensity changes in the X-ray source, the differences in spectra at multiple energies is due to changes in the sample composition as a function of depth. By obtaining XPS spectra over a range of energies, insights can be gained into the structure of the sample.

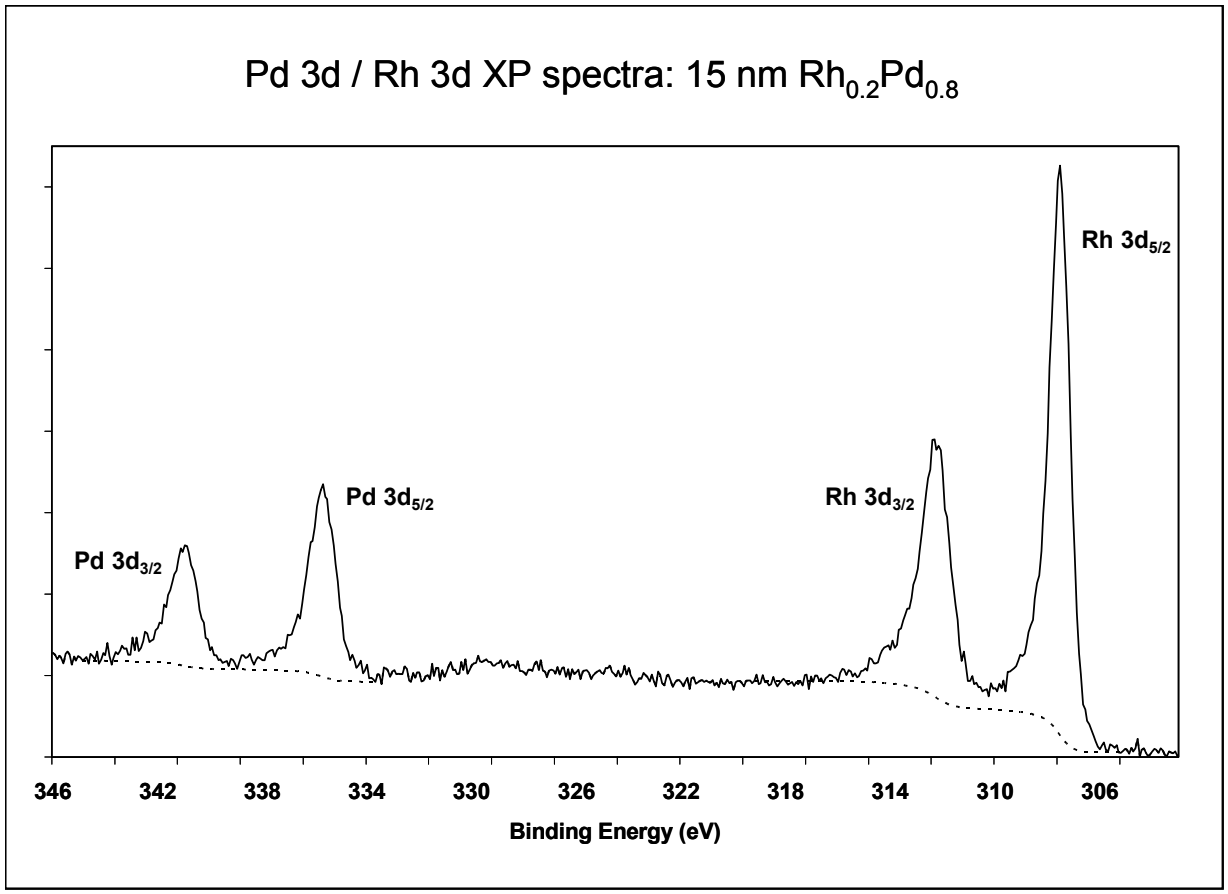

Figure 7.1 Pd 3d / Rh 3d spectra of $Rh_{0.2}Pd_{0.8}$ 15 nm particles in UHV.

Figure 7.1 shows the Pd 3d and Rh 3d spectra take of 15 nm $Rh_{0.2}Pd_{0.8}$ particles in UHV at a photon energy of 650 eV. The peaks were fit with Shirley backgrounds and the peak area was integrated to determine the composition of the particles. Figure 7.2 shows the elemental composition of three 15 nm Rh_xPd_{1-x} samples: $Rh_{0.2}Pd_{0.8}$, $Rh_{0.5}Pd_{0.5}$, and $Rh_{0.8}Pd_{0.2}$. The bottom axis is the kinetic energy of the photoelectrons and the y-axis is the atomic fraction of Rh and Pd in the spectra which was calculated from the integrated peak areas. The plots show data points from three kinetic energies: 335, 540, and 1180 eV. The 1180 eV photoelectron energy spectra were taken on a separate XPS instrument using an Al kα source because the experimental setup of beamline 9 could not reach this energy. The top axis gives the inelastic mean free path at the three photon energies. As the sampling depth increases, the Rh fraction decreases. This shows that the particles as synthesized are enriched with Rh at the surface.

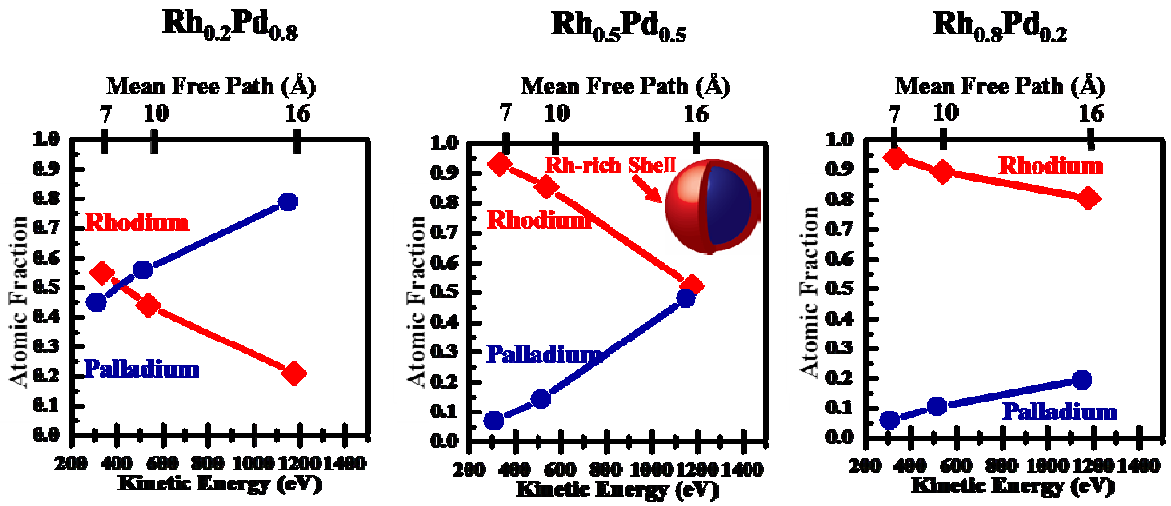

Figure 7.2 Atomic fraction of 15 nm $Rh_{0.2}Pd_{0.8}$, $Rh_{0.5}Pd_{0.5}$, and $Rh_{0.8}Pd_{0.2}$ particles as a function of photoelectron mean free path. The XPS data shows that the surface of the particles is Rh rich after synthesis.

The increased Rh concentration of the RhPd bimetallic particles is consistent with the particle synthesis. The particles are formed by the solution phase reduction of the metal precursors. Since the reduction potential of Rh^{3+} (0.76 V) is lower than that of Pd^{2+} (0.95 V), the Rh reduces second causing a higher proportion to be present on the surface. The other bimetallic combinations showed similar trends. Since the reduction potential of Pt (1.2 V) is larger than either Pd or Rh, after synthesis the PdPt particles were found to be surface enriched in Pd and the RhPt particles were found to be surface enriched in Rh.

When the $Rh_{0.5}Pd_{0.5}$ particles were heated to 300 ˚C in the presence of 100 mTorr NO the concentration of Rh atoms at the surface of the nanoparticles increased. When 100 mTorr CO was added to the NO, the Pd surface concentration increased. This effect was reversible bringing Rh back to the surface when the gas conditions were switched back to 100 mTorr NO. Although the structure of the particles was reversible, the concentration of surface Rh was not returned to the level in the initial NO treatment. The Pd was brought back to the surface in the presence of NO and CO followed by a 100 mTorr oxygen treatment that enriched the surface in Rh. The switching behavior of these gas treatments are plotted in Figure 7.3.

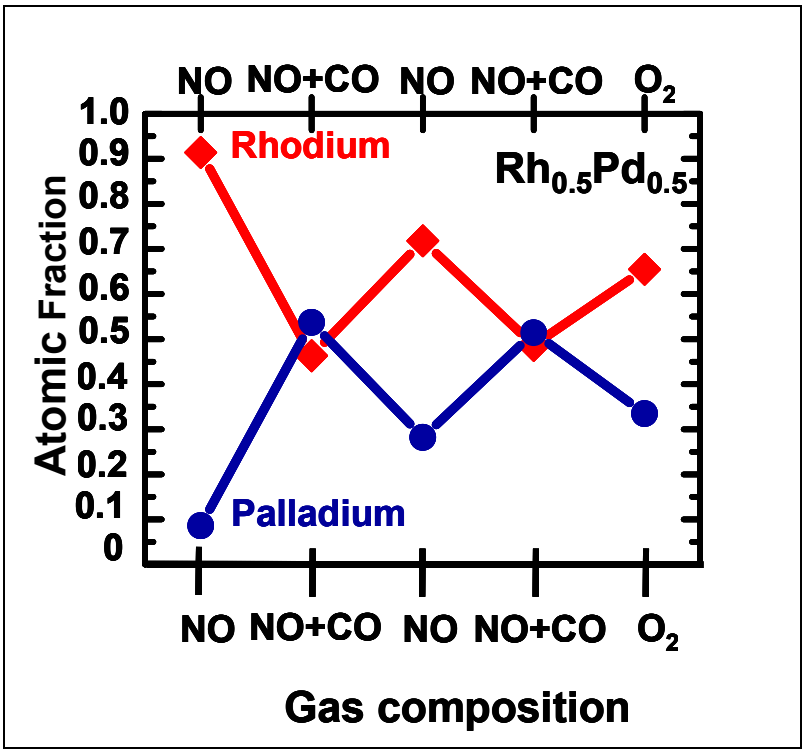

Figure 7.3 Surface composition of $Rh_{0.5}Pd_{0.5}$ in the presence of gases at 300 ˚C (all gases at 100 mTorr with reaction conditions 100 mTorr NO and 100 mTorr CO). The XPS data was obtained with a photon energy of 645 eV and a photoelectron mean free path of ~0.7 nm. The Rh composition increases in oxidizing conditions and decreases in reducing environment.

In the RhPd nanoparticle experiments, the Rh surface concentration increased in oxidizing conditions: NO, O_2, but decreased in the more reducing conditions: the CO/NO mixture. Pd could also be brought to the surface by CO and H_2 alone indicating that reducing conditions favor Pd surface enrichment. The surface energy of metallic Pd is 70% lower than metallic Rh [3] causing the metallic particle to be more stable when the Pd concentration increases on the surface. However in an oxidizing environment, Rh is more highly oxidized than Pd [4].

The Rh 3d and Pd 3d spectra at 300 ˚C in the series of alternating oxidizing and reactive gas environments is plotted in Figure 7.4. The spectra were taken at a photon energy of 645 eV corresponding to a photoelectron mean free path of ~0.7 nm. A Shirley background has been subtracted from the XPS spectra. The 3d spectra show the characteristic doublet splitting: Rh $3d_{5/2}$ (308 eV), Rh $3d_{3/2}$ (313 eV), Pd $3d_{5/2}$ (335.5 eV), and Pd $3d_{3/2}$ (341 eV). The spectra were fit for two components: a low binding energy metallic peak and a high binding energy oxidized peak. A (3:2) ratio was maintained for the peak areas of the $3d_{5/2}$ and $3d_{3/2}$ peaks and the spin orbit splitting was held constant at 4.67 and 5.26 eV for Rh and Pd respectively.

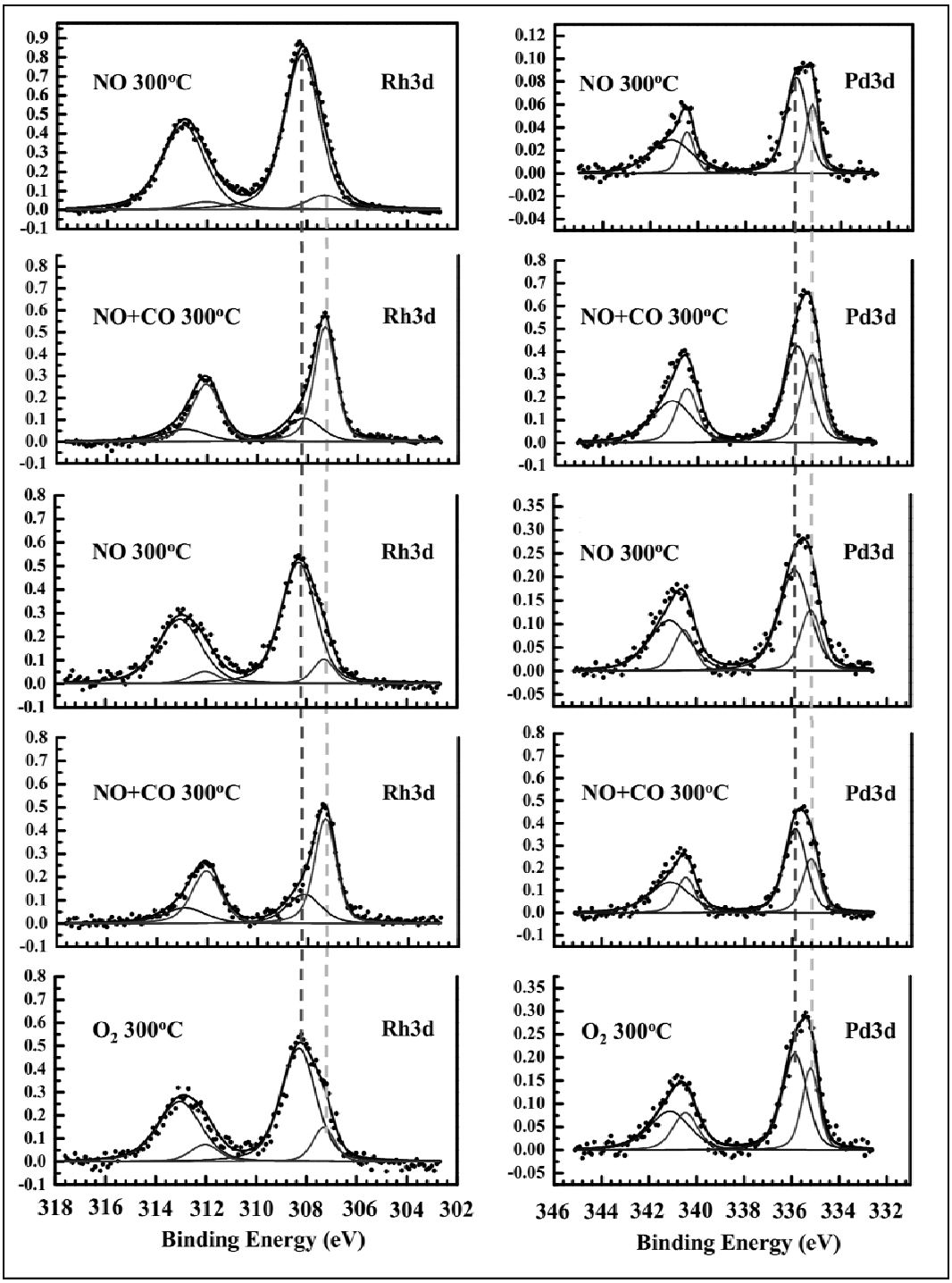

Figure 7.4 Background subtracted Rh 3d and Pd 3d spectra with peak fittings in alternating oxidizing and catalytically active conditions at 300 ˚C. Both the Rh 3d and Pd 3d are fit with a low binding energy metallic peak (Rh $3d_{5/2}$: 307 eV, Pd $3d_{5/2}$: 335 eV) and a high binding energy oxidized peak (RhO_y $3d_{5/2}$: 308 eV, PdO_y $3d_{5/2}$: 336 eV). The Rh 3d peak shows more pronounced oxidation and reduction behavior than the Pd 3d peak in the switching gas environments.

The changes in oxidation state as a function of gas environment at 300 ˚C are plotted in Figure 7.5. The vertical axes plot the integrated peak area of the oxidized peaks divided by the total peak area for both Rh (left, red) and pd (right, blue). In 100 mTorr NO the Rh is 90% oxidized with Pd 60% oxidized. When 100 mTorr CO is added to the 100 mTorr NO at 300 ˚C, the Rh is reduced with the oxidized peak now constituting 25% of the total Rh. As was discussed above and plotted in Figure 7.3, the reduction of Rh coincides with the formation of a Pd rich surface layer. By returning to an NO environment, the bimetallic nanoparticle surface became Rh rich again with 90% RhO_y. By comparison, the redox chemistry of Pd was very mild. The spectra in Figure 7.4 which are summarized in Figure 7.5, show that the Pd oxidation state is relatively constant at 60-70% PdO_y in the surface layer.

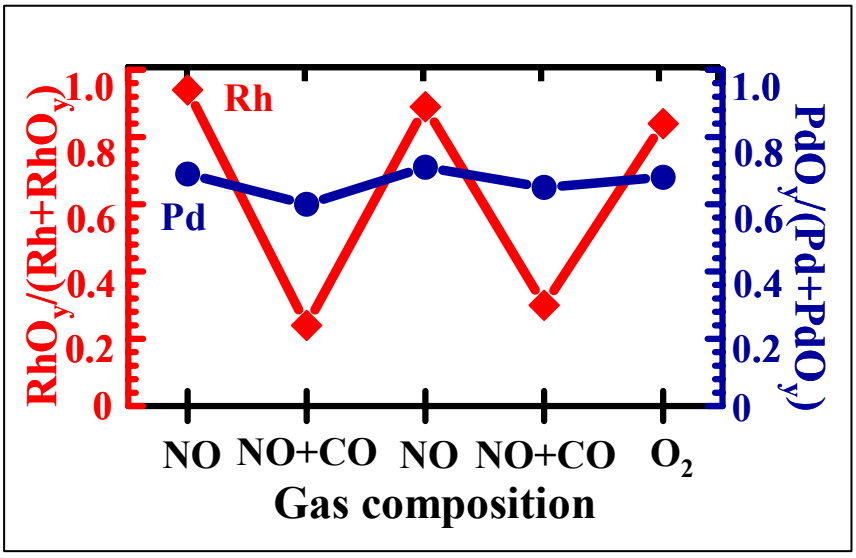

Figure 7.5 $Rh_{0.5}Pd_{0.5}$ surface oxidation formation as a function of gas composition at 300 ˚C. The y axes plot the percentage of the RhO_y (left, red) and PdO_y (right, blue) contributions to the total Rh 3d and Pd 3d XPS peak areas. The spectra were taken using a photoelectron mean free path of ~0.7 nm. The surface composition of Rh was show to be 80-95% surface oxide in 100 mTorr NO or O_2, but 20-30% surface oxide in the 100 mTorr NO, 100 mTorr CO reaction conditions. The oxidation chemistry of the Pd present in the surface layer was less dramatic.

At high temperature and pressure, the 15 nm particles were shown to undergo structural changes in surface composition. The $Rh_{0.5}Pd_{0.5}$ Particles were shown to reversibly restructure at 300 ˚C in response to changes in the gas composition. The *in-situ* APXPS results directly and unambiguously monitored the changes in the nanoparticle surface layer. The RhPd particles were synthesized with Rh rich surfaces. High temperature oxidizing conditions selectively oxidizes the Rh atoms. Since oxide formation lowers surface energy, the selective oxidation of the Rh is a driving factor in the increase of the Rh surface concentration. When CO is added to the NO, the surface Rh became reduced and Pd was brought to the surface. At this high temperature (300 ˚C) in the presence of gases the atoms have sufficient energy to rearrange through diffusion. In the more reducing reactive environment (NO/CO) the particle surface

becomes more reduced forming metallic Rh which selectively diffuses in to the bulk of the particle due to its higher surface energy.

The structure of 15 nm $Pd_{0.5}Pt_{0.5}$ particles was investigated at the same experimental conditions as the above $Rh_{0.5}Pd_{0.5}$ particles. In UHV, XPS spectra of the as-synthesized PdPt nanoparticles showed the particle surface to be enriched in Pd (Figure 7.6). The reduction potential of Pd (0.95 V) is lower than that of Pt (1.2 V) causing the reduction of the Pd precursor to precede that of the Pt precursor resulting in particles that show a Pd enriched surface [2].

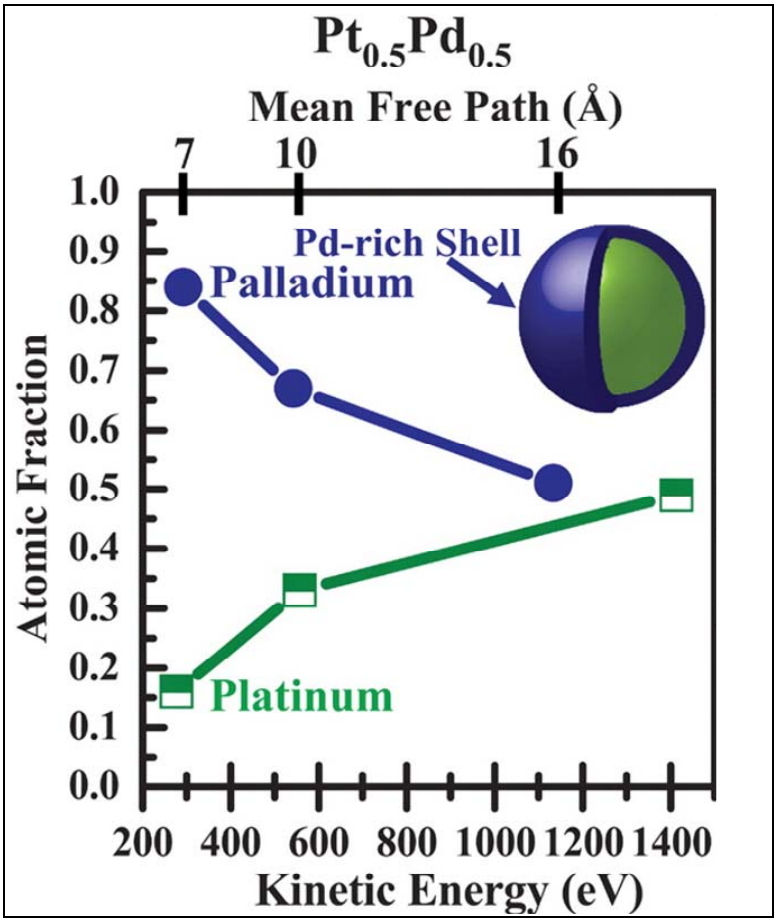

Figure 7.6 XPS analysis of 15 nm $Pd_{0.5}Pt_{0.5}$ particles in UHV. Spectra were taken with photoelectron mean free paths of ~7, 10, and 16 Å. The relative peak area of Pd and Pt are plotted as a function of photoelectron kinetic energy. The decrease in the atomic fraction of Pd as a function of surface probing depth shows that the as-synthesized particles have a Pd enriched surface structure.

When the PdPt particles were heated to 300 ˚C in the presence of 100 mTorr NO, the APXPS spectra, taken at a photoelectron mean free path of 0.7 nm, showed the particle surface to be Pd enriched (Figure 7.7). Using the same procedure as in the RhPd nanoparticle study, the Pd 3d spectra was fit with two peaks: metallic Pd and oxidized PdO_y. In NO, the surface Pd was found to be 85% oxidized. It should be noted that in the same conditions, the $Rh_{0.5}Pd_{0.5}$ particles showed only 70% PdO_y surface oxide (Figure 7.5). When 100 mTorr CO was added to the NO

environment, the surface concentration of Pd decreased slightly to 80% and the fraction of PdO_y decreased to 55% PdO_y, which is lower than the 60% PdO_y composition of $Rh_{0.5}Pd_{0.5}$ at the same reaction mixture and temperature. Switching the gas composition to 100 mTorr CO further reduced the PdO_y concentration, but resulted in a slightly increased Pd surface enrichment to 85% Pd.

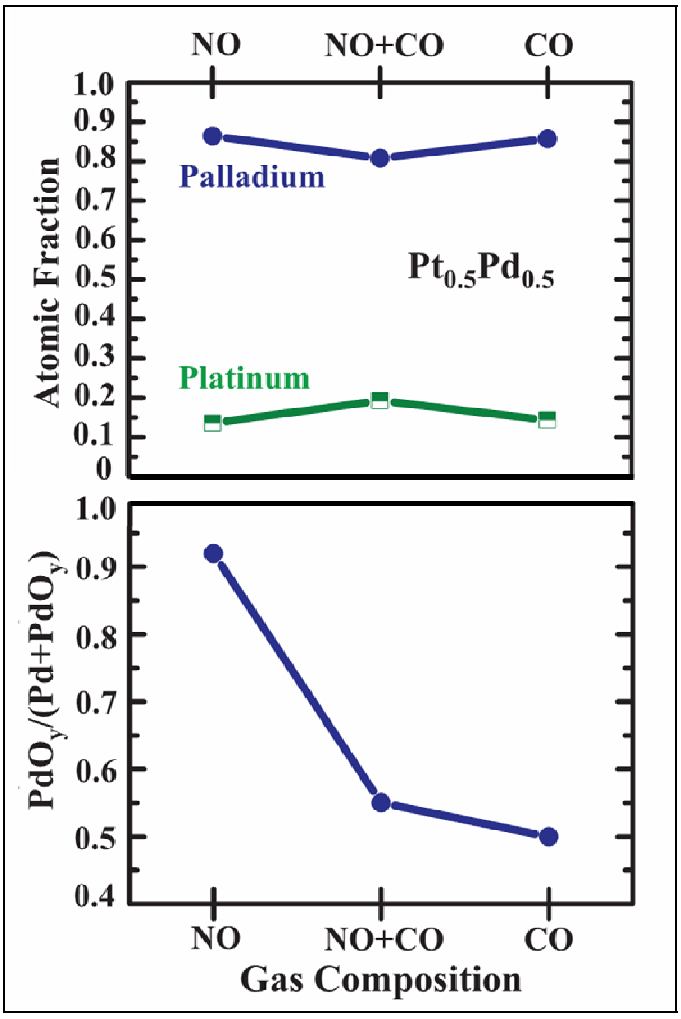

Figure 7.7 Integrated peak area of the Pd 3d and Pt 4f peaks of 15 nm $Pd_{0.5}Pt_{0.5}$ at 300 ˚C in the presence of 100 mTorr NO, 100 mTorr NO and 100 mTorr CO, and 100 mTorr CO (top panel). The Pd 3d spectra was fit with 2 peaks: a low binding energy metallic peak (Pd) and a high binding energy oxidized peak (PdO_y). The bottom panel is the fraction of PdO_y in the XPS spectra. The Pt 4f peak did not show any significant redox behavior. All spectra were taken with a photoelectron mean free path of ~0.7 nm.

The $Pd_{0.5}Pt_{0.5}$ and $Rh_{0.5}Pd_{0.5}$ particles were both initially shown to be surface enriched relative to the bulk composition of the lower reduction potential metal: Pd and Rh respectively. When placed in an oxidizing environment at 300 ˚C, the more easily oxidized element: Rh in the RhPd particles and Pd in the PdPt particles, was the majority species on the surface. Adding CO to the NO environment resulted in more reducing conditions and a decrease in the fraction on

surface oxide in both particles. This reduction caused the Rh surface concentration to significantly decrease in the RhPd particles, but had only a small effect on the PdPt particles. In reducing conditions at 300 ˚C, the bimetallic particles are surface enriched by the element with the lowest surface energy. This caused the RhPd particles to become Pd rich on the surface, but since Pd has a lower surface energy than Pt [3], the PdPt particles remained Pd rich on the surface. Changing the gas composition from oxidizing to reducing conditions caused large changes in the surface oxidation state of only one of the metals in both sets of particles: Rh in the RhPd sample and Pd in the PdPt sample. The change in the electronic structure in bimetallic systems caused different redox chemistry of the Pd atoms at the same experimental conditions. When incorporated in the RhPd system, the PdO_y fraction remained relatively constant within 10% with the majority of the redox chemistry. In the PdPt particles, the PdO_y fraction changed 40%, while no changes were seen in the Pt oxidation state.

The transformations in the surface structure and composition on the bimetallic nanoparticle systems reinforce the use of *in-situ* catalytic characterization. The accurate description of the active catalyst requires a detailed understanding of the surface layer. While the surface segregation of alloy constituents is widely known, the phase space in active conditions and on nanoparticle systems is largely unmapped. *In-situ* techniques allow for the direct measurement of the dynamic changes induced in the surface layer by high temperature and the presence of gases. The ability to control and predict this behavior could lead to the ability to engineer catalysts with useful properties. For example the surface segregation in reaction conditions could be exploited by choosing a bimetallic system with an expensive active component and a cheap spectator component. If the proper combination and conditions were found, the active, expensive component could be a minority species in the bulk composition yet the majority species on the active catalyst surface. The mass transport from surface to bulk that takes place during surface restructuring also suggests a disruptive surface changes that could be used to renew the surface and prevent catalytic deactivation due to active site blocking. The use of multi-component catalysts provides more parameters to adjust the activity to improve catalytic activity, lifetime, and cost effectiveness. These studies show how *in-situ* methods when applied to working catalysts can be used to study processes on the active surface that could not have been observed with *ex-situ* methods and may lead to improvements in the catalytic processes that are central to the energy and chemicals industries.

7.5 Conclusions

The surface restructuring of bimetallic nanoparticles was directly studied at high temperature in the presence of gases using APXPS. The systematic study of the bimetallic nanoparticle samples was made possible by the development of synthetic recipes to produce particles with a narrow size distribution and well controlled composition. Surface restructuring induced by the reactant gases at elevated temperature was observed on the nanoparticle systems. Oxidizing conditions pulled the more easily oxidized element to the surface while reducing conditions brought the metal with the lowest surface energy to the surface layer. These processes are governed by the reduction of the surface energy on the strained nanoparticle systems.

7.6 References

1. Jacobsen, C.J.H., et al., *Catalyst Design by Interpolation in the Periodic Table:â€‰ Bimetallic Ammonia Synthesis Catalysts.* Journal of the American Chemical Society, 2001. **123**(34): p. 8404-8405.
2. Tao, F., et al., *Reaction-Driven Restructuring of Rh-Pd and Pt-Pd Core-Shell Nanoparticles.* Science, 2008. **322**(5903): p. 932-934.
3. Skriver, H.L. and N.M. Rosengaard, *Surface energy and work function of elemental metals.* Physical Review B, 1992. **46**(11): p. 7157.
4. Reuter, K. and M. Scheffler, *Oxide formation at the surface of late 4d transition metals: insights from first-principles atomistic thermodynamics.* Applied Physics A: Materials Science & Processing, 2004. **78**(6): p. 793-798.

Chapter 8. *In-situ* Studies of the High Pressure Oxygen Induced Formation and Catalytic Removal of Subsurface Oxygen by CO on Pt(110) using AP-XPS and STM

8.1 Abstract

The oxidation behavior of the Pt(110) surface was studied using surface sensitive *in-situ* characterization by APXPS and STM. In the presence of 500 mTorr O_2 and temperatures between 25 and 200 ˚C, subsurface oxygen was detected in the surface layer. STM images show that these conditions were found to cause a roughened surface decorated with 1 nm islands. The formation of this surface oxide is a high pressure phenomenon and was not detected in 50 mTorr O_2. After forming the surface oxide at high pressure, its chemical activity was measured through the reaction with CO at low pressure while continuously monitoring the oxygen species with XPS. The subsurface oxygen was removed by CO oxidation at a comparable rate to the chemisorbed oxygen at 2 ˚C. Repeating the experiment at -3 ˚C reduced the reaction rate, but not the relative activity of the two chemical species indicating that neither species is significantly more active for the CO oxidation reaction.

8.2 Introduction

CO oxidation on transition metals has been widely studied due to its use in the catalytic converter, its fundamental importance as a model system in the understanding of oxidation reactions, and as a test reaction for catalyst activity. Pt is an important oxidation catalyst and despite the extensive study on this system, questions still remain about the chemical composition of the active surface layer at elevated pressure [1, 2].This study uses XPS and STM to study the onset of oxidation and the activity of oxygen species on the Pt(110) surface.

The low coordination number of surface atoms with respect to the bulk affects both the chemical activity and electronic structure. The (110) surface is the most open of the three low Miller index fcc surfaces. The high degree of strain on the (110) face causes the clean surface to form the missing row reconstruction producing a highly stepped surface consisting of (111) facets (Figure 8.1). *In-situ* STM studies have been used to study the adsorption of oxygen and CO on Pt(110) [3-5]. Hendriksen et al. studied the switching behavior of the Pt(110) surface as the gas phase conditions changed from oxidizing to reducing conditions [1]. The surface was found to contain steps and terraces in the CO dominated conditions. In an oxygen rich reactive environment the surface was found to be roughened. The CO treatments at 1 atm and 150 ˚C were shown to flatten the terraces through the removal of the lifted row reconstruction resulting in a (1x1) structure [3, 4]. The low coordination of the (110) surface results in a dynamic interface that readily reconstructs leading to the formation and removal of edge sites. In contrast the oxygen-induced roughening was attributed to a surface oxide phase [1], similar to that

characterized by Thostrup et al. [5]. The formation and catalytic activity of the surface oxide phase has received considerable attention [2]. In collaboration with Michael Grass, Funda Aksoy, Hendrik Bluhm, B. S. Mun, and Zhi Liu at the ALS, *in-situ* XPS studies were used to study the formation and catalytic properties of this high pressure surface species.

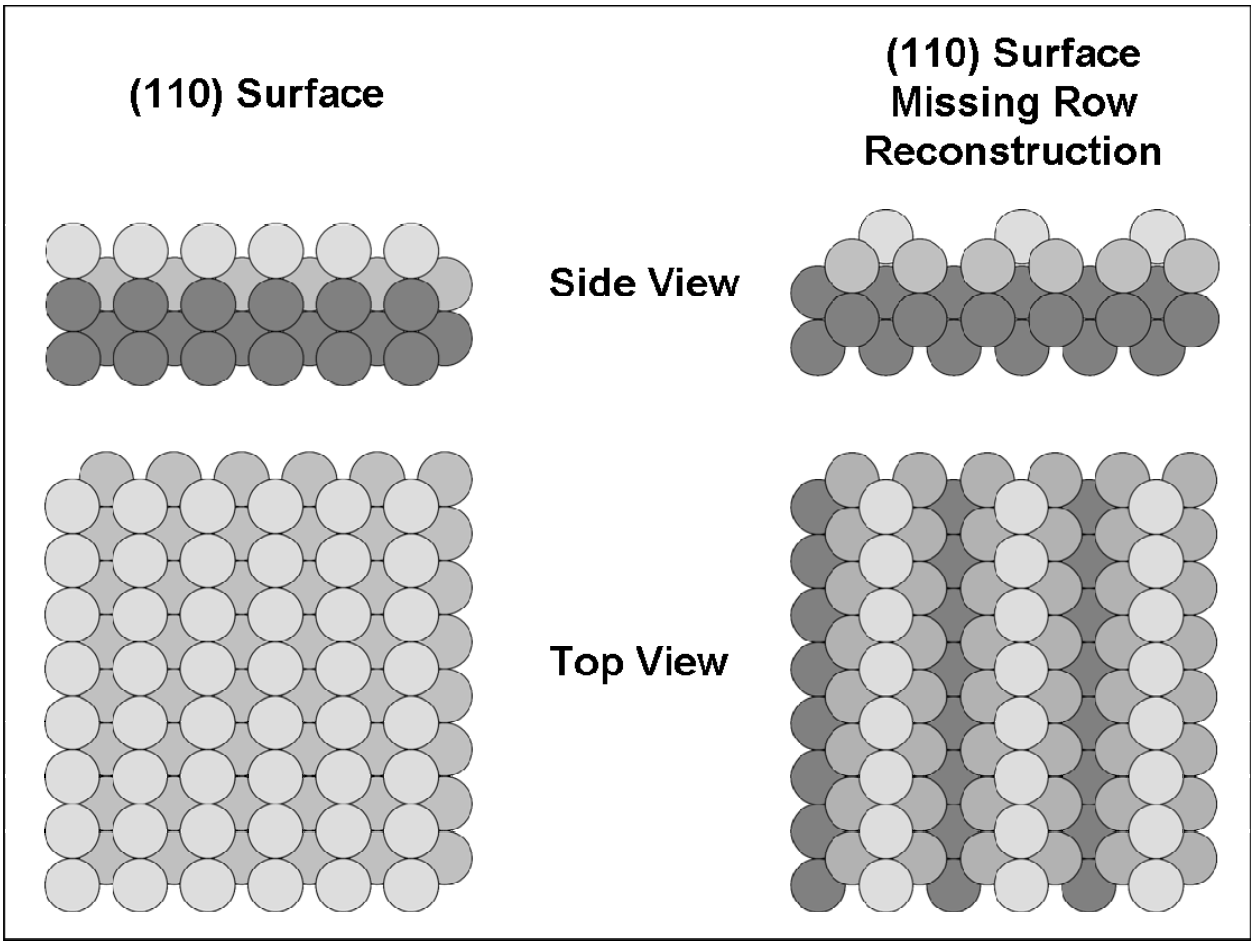

Figure 8.1 Schematic of the fcc(110) surface (left) and the (2x1) missing row reconstruction (right).

8.3 Experiment

The clean Pt(110) crystal was prepared with cycles of Ar^+ sputtering, annealing at 500 ˚C in 10^{-7} Torr O_2, and finally a 700 ˚C annealing step at 10^{-10} Torr UHV. The cleanliness of the surface was verified through XPS in UHV at the start of each experiment. The oxidation behavior of the Pt(110) surface was studied using APXPS, an *in-situ* technique which allows the direct characterization of the surface in the presence of gases. The experimental setup of the APXPS systems at beamlines 9.3.2 and 11.0.2 at the synchrotron source at the Lawrence Berkeley Lab allows experiments in both vacuum and at pressures up to the Torr regime [6, 7]. Additionally the synchrotron provides a tunable X-ray source which allows the photon energy to

be adjusted to control the sampling depth. This can be used to both ensure that spectra of elements with different binding energies are measured with consistent photoelectron kinetic energy and to compare spectra over a range of energies to measure differences in surface composition as a function of depth. Since the maximum pressure of the XPS experiments is limited to the Torr range due to photoelectron scattering from the gas phase, complimentary *in-situ* STM experiments were used to measure the changes in surface morphology in the Torr regime.

8.4 Results and Discussion

The Pt4f spectra of the clean Pt(110) surface taken with a photon energy of 230 eV is shown in the black (top) spectra in Figure 8.2. Two components are clearly visible in the UHV spectra: a bulk Pt peak at 71.2 ± 0.1 eV and a surface peak at 70.9 eV. The presence of the surface peak arising from the undercoordinated Pt atoms in the topmost atomic layer indicates that the surface was clean which was confirmed by the absence of peaks in the C1s and O1s spectra. In a separate experiment using the same single crystal, the clean surface was characterized using STM (Figure 8.2, upper spectrum). The image shows flat terraces separated by a single atom step. The terraces have parallel rows resulting from the (2x1) missing row reconstruction. There are also point defects on the surface which are likely to be oxygen atoms which often appear depressions in STM images [8].

In the presence 50 mTorr O_2, the Pt4f spectra show contributions from two chemical species: the bulk Pt peak at 71.2 eV and a chemisorbed oxygen (ChemO) peak at 71.9 eV (Figure 8.2 red/middle spectrum). The chemisorbed oxygen peak in the Pt4f spectra comes from the surface layer of Pt atoms that are directly bound to oxygen atoms and appears at the same binding energy as the chemisorbed species at low oxygen pressure. After increasing the oxygen pressure to 500 mTorr, ChemO peak increases relative to the bulk Pt peak and a third high binding energy peak is seen at 73.4 eV assigned as a surface oxide phase (Figure 8.2 blue/lower spectrum). In the 500 mTorr conditions, the two separate species are not resolved in the O1s spectra which show a single peak at 530.4 eV with a high binding energy tail in agreement with the low pressure spectra. The high pressure oxygen species has a binding energy that is lower than the literature values for PtO and PtO_2 [9]. The STM images at high pressure (200 mTorr) conditions show a roughened surface with 1 nm features 0.2 nm in height (Figure 8.2 bottom) which is in agreement with previous STM experiments up to an atmosphere of O_2 [1]. The surface oxide remains on the surface when the chamber is evacuated to UHV and can also be formed in *ex-situ* experiments where the surface is not exposed to the X-ray source and the consequent secondary electrons at high pressure.

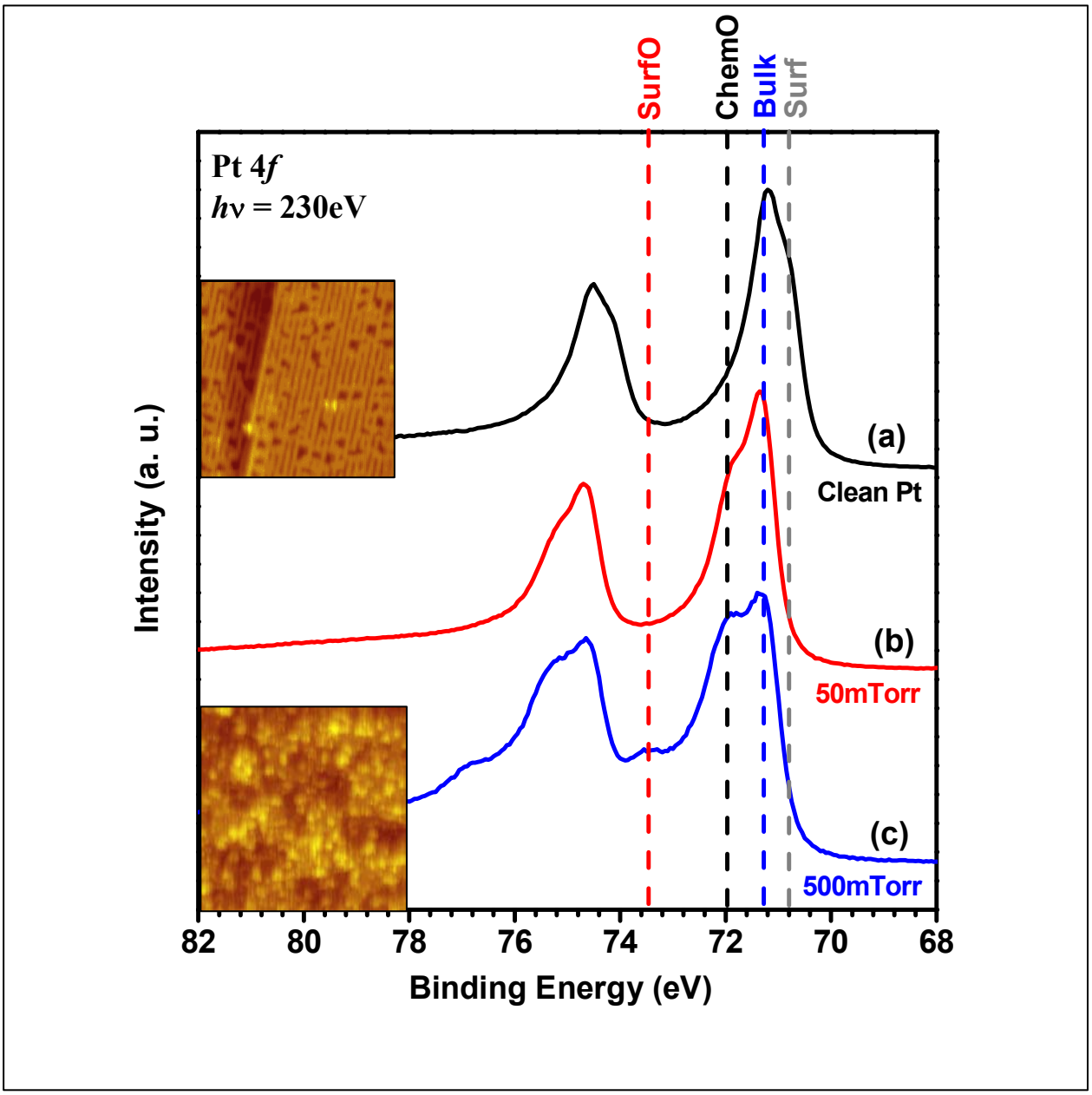

Figure 8.2 (a) Pt4f spectrum taken at after sputtering and annealing in UHV, a surface peak at lower binding energy can be clearly resolved. (b) Pt4f spectrum taken under 50mTorr O_2. The additional peak at the higher binding energy side of Pt4f bulk peak (blue) is chemisorbed oxygen induced peak. (c) Pt4f spectrum taken under 500mTorr O_2 . There are two oxygen induced peaks along with the Pt bulk peak (blue). They are from chemisorbed oxygen (black) and surface oxide (red). STM images taken under the similar conditions (clean surface & under 200mTorr O_2) are shown as inserts. It shows a roughened surface with islands of a few nanometers when the Pt(110) surface is exposed to high pressure of O_2.

In order to gain more information about the peak at 73.4 eV binding energy surface oxide peak, Pt4f spectra were collected at photon energies of 180, 340, and 475 eV in the presence of 500 mTorr O_2 (Figure 8.3). The photoelectron kinetic energy of a given species increases with the photon energy. Since the inelastic mean free path of photoelectrons increases with kinetic energy in the energy range of these experiments, decreasing the photon energy causes the spectra to be more sensitive to the topmost surface layer. The spectra in Figure 8.3 have had a Shirley background subtracted and were fit self-consistently with Doniac-Sunjic lineshapes with a 0.32 eV Lorentzian peak width and an asymmetry factor of 0.2. The spectra were fit with three doublet peaks: bulk Pt (71.2 eV, blue), chemisorbed oxygen (71.9 eV, black), and surface oxide (73.4 eV, red). Using photon energies 180, 340, and 475 eV to collect Pt4f spectra, the photoelectrons have inelastic mean free paths of 0.43, 0.57, and 0.72 nm respectively in bulk Pt [9]. As the photon energy was increased from 180 to 475 eV, the relative area of the chemisorbed oxygen bound Pt peak decreased with respect to the bulk Pt peak area while that of the surface oxide bound Pt remained constant. The relative areas are plotted in the graph at the bottom right of Figure 9.3. The decrease in the chemisorbed oxygen with increasing energy is expected since the species binds on top of the Pt surface atoms. As the photon energy is increased, the resultant spectra represent a deeper sampling of the surface so the contribution from species on the topmost outer layer decreases. The surface oxide peak does not decrease appreciably with photon energy indicating that those oxygen bound Pt atoms are in the subsurface. This information proves that the 73.4 eV peak results from a surface oxide species. The spectra were taken at 25, 100, and 200 ˚C and the surface oxide was found to be stable with increasing temperature while the coverage of the chemisorbed species decreased.

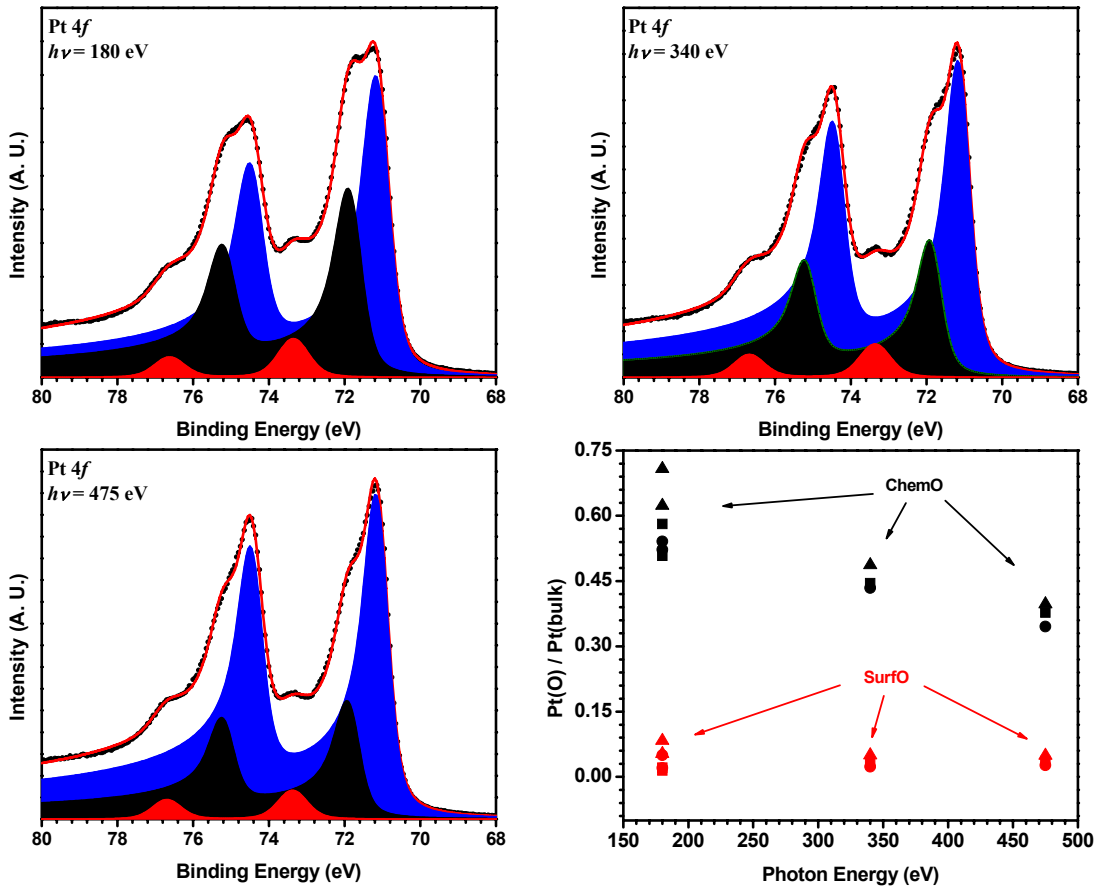

Figure 8.3 Pt4*f* spectra taken at 180, 340, and 475 eV under 500 mTorr O_2 in (a), (b), and (c) respectively. We fitted the spectra with two oxygen induced Pt 4*f* doublets: chemisorbed oxygen (black) and surface oxide (red) along with the Pt bulk one (blue). (d) The intensity ratios of Pt(ChemO)/Pt(bulk) and Pt(surfO)/Pt(bulk) are plotted with photon energies. The symbols: ■, ● and ▲ represent the data obtained at 25, 100, and 200 ˚C respectively. The Pt(ChemO) intensities decrease as the photon energy increases. This is consistent with the surface nature of chemisorbed oxygen. However, the intensities of Pt(SurfO) peak do not decrease significantly, implying a multilayer (≥2 Pt layers) nature of such an oxide.

In previous *in-situ* APXPS CO oxidation studies conducted at a maximum total pressure of 500 mTorr, the surface oxide was not detected/resolved in the presence of CO [6]. In order to test the relative stability and reactivity of the oxygen species on the Pt(110) surface, the prepared surface oxide was reacted away using low pressure CO titrations while monitoring with continuous XPS measurements. The Pt(110) surface containing both chemisorbed and surface oxide species was prepared by exposure to 500 mTorr O_2 at 200 ˚C. Although *ex-situ* experiments were conducted to confirm that the surface oxide was formed in the presence of elevated pressures (500 mTorr) O_2 and was not simply an artifact induced by the X-ray source, the coverage of the surface oxide phase could be increased by exposure to a high flux 230 eV X-rays in the presence of O_2. At beamline 11.0.2 the 230 eV X-rays are produced using the first harmonic of the diffraction grating causing the X-ray source at this energy range to be

significantly brighter than that which was used during the previous experiments. The surface oxidation induced by the X-ray source and the consequent secondary electrons is likely a result of the defect and kinetic restrictions to surface oxide formation described by Li *et al.* [10]. After the surface oxide had been prepared, the sample was cooled to the titration temperature and the O_2 was evacuated from the chamber to a base pressure of 10^{-9} Torr. The CO titrations were performed by dosing 10^{-6} Torr CO and continuously acquiring either Pt4f or O1s spectra at a rate of 6 and 13 sec per scan respectively. The Pt4f and O1s spectra were taken at photon energies of 340 and 800eV to ensure that the kinetic energy of the resulting photoelectrons and the sampling depths were comparable. CO titrations were conducted at 2˚C and -3˚C.

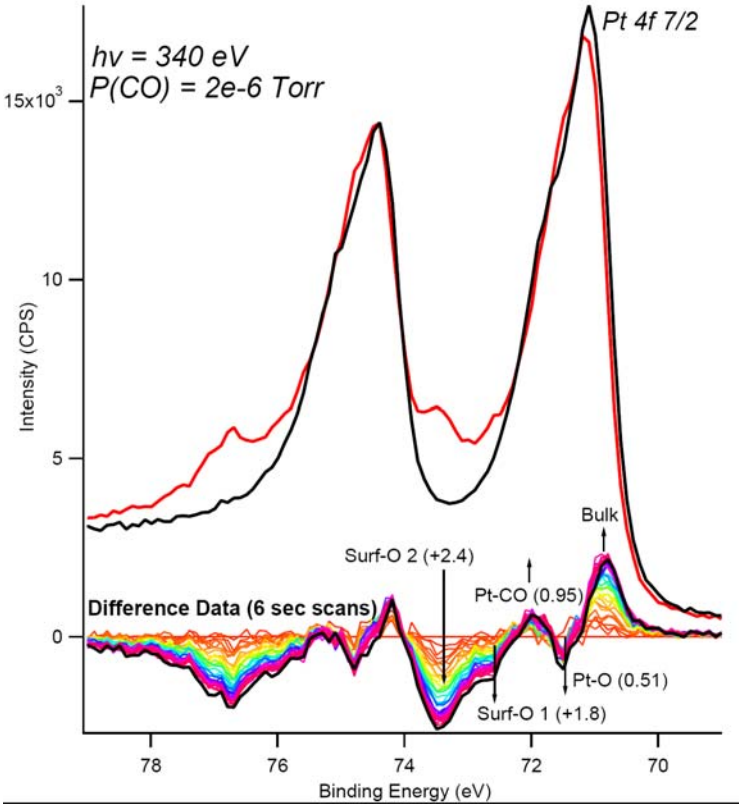

Figure 8.4 Pt4f spectra during CO titration of surface oxide at -3˚C showing the initial spectra (red), the final spectra (black), and the sequential difference spectra ending in the final (black) difference spectra.

Figure 8.4 shows the Pt4f spectra before (red spectra) and after (black spectra) the CO titration at -3 ˚C. The initial spectrum clearly contains a surface oxide peak. Upon exposure to 10^{-6} Torr CO at -3 ˚C, the surface oxide was removed through reaction with CO. The difference spectra in Figure 9.4 were taken at 6 second intervals and show an increase in the bulk Pt and decreases in the Pt-O and the Surf-O peaks as a function of time. The -3 ˚C CO titration was repeated monitoring the O1s spectra at 13 second intervals. The O1s titration spectra show a decrease in both chemisorbed O and the surface oxide as it reacted with CO. After 180 seconds, CO became the most abundant oxygen species (Figure 8.5). The experiments were then repeated

at 2˚C. The results of the fitted O1s spectra are plotted in Figure 8.5. At 2˚C the oxygen species reacted more quickly with CO becoming the highest concentration species after 95 seconds.

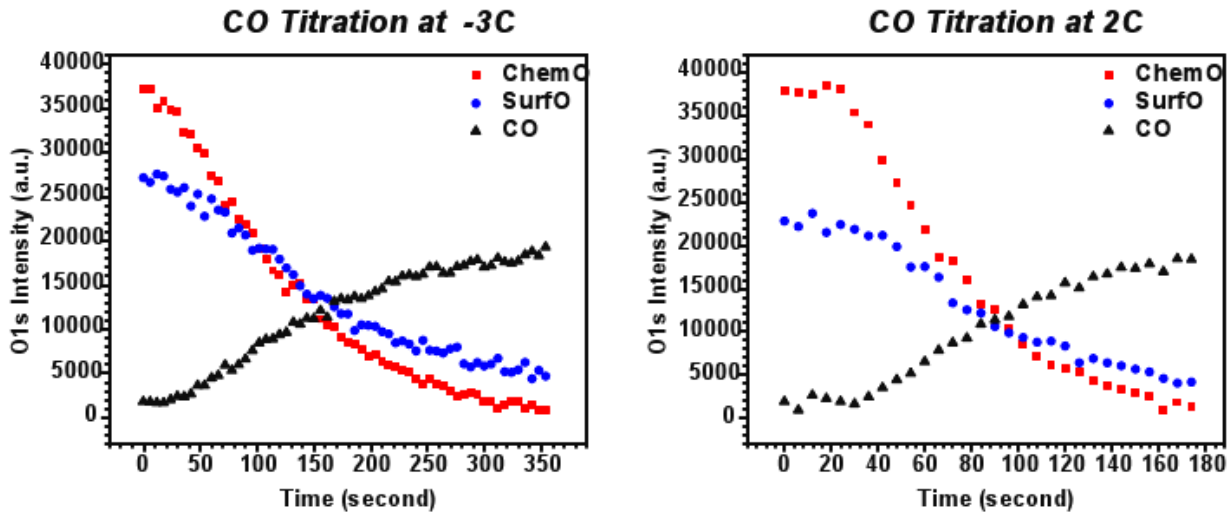

Figure 8.5 O1s spectra of CO titrations at -3 and 2˚C. When the prepared oxide surface is exposed to 10^{-6} Torr CO, the chemisorbed oxygen and surface oxide react with CO forming CO_2 and excess CO accumulates on the surface. CO becomes the majority species at 180 and 95 seconds at -3 and 2˚C respectively.

The XPS data monitoring the removal of surface oxygen by reaction with CO offers information about the relative activity of the species for the CO oxidation reaction. The two plots in Figure 8.5 are qualitatively similar although the time axes have different scales to accommodate for the increase in reaction rate at increased temperature. The chemisorbed oxygen and the surface oxide are simultaneously reacted off of the surface at both temperatures with similar depletion rates relative to one another. This indicates that either the two species have similar activity towards CO oxidation or that the removal of the two species is coupled. For example, if the subsurface oxygen was stabilized by chemisorbed oxygen, but quickly reacted with CO after the nearby chemisorbed oxygen was removed it would also be consistent with the titration data. However without some mechanism linking the activity of the two species, their activity for CO would have to be comparable to explain the similarities in the activity at the two temperatures, which could have implications for the active debate in the literature arising from high level *in-situ* studies on CO oxidation on Pt(110) surface under active high pressure conditions and the possible formation of a highly active surface oxide phase [1, 2]. Although the conditions in these studies were limited to lower pressures, our findings show, through low pressure CO titration experiments, that the surface oxide phase and the chemisorbed oxygen species are removed through reaction with CO at comparable rates.

8.5 Conclusions

In-situ APXPS measurements on Pt(110) were used to study the oxidation behavior of this open crystal face. In addition to chemisorbed oxygen, the XPS spectra show the formation of a surface oxide phase in 500 mTorr O_2 from room temperature up to 200 ˚C. XP spectra

collected over a range of energies definitively show that the surface oxide is a subsurface species which extends below the topmost atomic layer. The formation of the oxide was found to be defect dependent, forming more readily on surfaces prepared with a short final annealing step which increases the step edge density. The surface oxide coverage could also be increased through the exposure to a high intensity X-ray source in the presence of 500 mTorr O_2. Once formed, the subsurface oxygen was found to be stable in UHV and could be removed along with the chemisorbed oxygen through the low pressure reaction with CO forming CO_2. While the removal rate was found to be temperature dependent, both species reacted simultaneously at comparable rates indicating similar activity to CO oxidation or possibly a mechanistically linked activity whereby the removal of one species locally activates the other. *In-situ* STM studies showed that the same surface roughening that occurs at atmospheric pressure in oxygen rich environments occurs in the working pressure range (500 mTorr) of these APXPS experiments while the CO rich environment results in a surface characterized by steps and terraces.

8.6 References

1. Hendriksen, B.L.M. and J.W.M. Frenken, *CO Oxidation on Pt(110): Scanning Tunneling Microscopy Inside a High-Pressure Flow Reactor.* Physical Review Letters, 2002. **89**(4): p. 046101.
2. Gao, F., et al., *CO Oxidation on Pt-Group Metals from Ultrahigh Vacuum to Near Atmospheric Pressures. 2. Palladium and Platinum.* The Journal of Physical Chemistry C, 2008. **113**(1): p. 174-181.
3. McIntyre, B.J., M.B. Salmeron, and G.A. Somorjai, *A scanning tunneling microscope that operates at high pressures and high temperatures (430 K) and during catalytic reactions.* Catalysis Letters, 1992. **14**(3): p. 263-269.
4. Hendriksen, B.L.M., S.C. Bobaru, and J.W.M. Frenken, *Looking at heterogeneous catalysis at atmospheric pressure using tunnel vision.* Topics in Catalysis, 2005. **36**(1-4): p. 43-54.
5. Thostrup, P., et al., *CO-induced restructuring of Pt(110)-(1 x 2): Bridging the pressure gap with high-pressure scanning tunneling microscopy.* The Journal of Chemical Physics, 2003. **118**(8): p. 3724-3730.
6. Chung, J.-Y., et al., *In-situ study of the catalytic oxidation of CO on a Pt(1 1 0) surface using ambient pressure X-ray photoelectron spectroscopy.* Surface Science, 2009. **603**(5): p. L35-L38.
7. Bluhm, H., et al., *Soft X-ray microscopy and spectroscopy at the molecular environmental science beamline at the Advanced Light Source.* Journal of Electron Spectroscopy and Related Phenomena, 2006. **150**(2-3): p. 86-104.
8. Robert, V., *Electron Tunneling: A Scattering Problem and a Chemical Approach. Interpretation of STM O2 Image.* The Journal of Physical Chemistry A, 1999. **103**(34): p. 6805-6810.
9. Powell, C.J. and A. Jablonski, *NIST Electron Inelastic Mean Free Path Database, ed. 1.1*. 2000, National Institute of Standards and Tehnology, Gaithersburg MD.
10. Li, W.X., et al., *Oxidation of Pt(110).* Physical Review Letters, 2004. **93**(14): p. 146104.